A Study on Error Diffusion Method and Assessment Index Considering Material Appearance

August 2022

Donghui Li

Imaging Sciences
Creative Engineering
Graduate School of Science and Engineering
CHIBA UNIVERSITY

(Chiba University Doctoral Dissertation)

A Study on Error Diffusion Method and Assessment Index Considering Material Appearance

August 2022

Donghui Li

Imaging Sciences
Creative Engineering
Graduate School of Science and Engineering
CHIBA UNIVERSITY

ABSTRACT

Printing is an old technique for image production on paper or some other material surface. In the last decades the printing technology has been evolution due to the digital development which provides a better scheme of solutions for image printing reproduction. New solutions and automated process replace the traditional low-quality and low-efficiency printing process. With this rapid evolution, the image reproduction ability in hard support has essentially improved. Moreover, with the emergence of higher demand in the field of image reproduction, image appearance reproduction has gradually become the further goal of the printing industry. This leads to an issue for various techniques comparing according to reproduction quality. The reproduction quality in printing is an intuitive concept which is usually easy to understand by our human visual system (HVS). However, it is difficult to evaluate the reproduction quality of image appearance through measurable index. This research is also produced under the background of the increasing demand for higher reproduction printing quality and more intelligent image reproduction quality perception in industry. This research focuses on the concept of printing appearance reproduction and proposed assessment index based on image structure, standard deviation and skewness.

The first aim of this dissertation has been to consider and solve the problems, which called multi-level halftone. This can affect the output reproduction quality of digital halftone image, and then affect the final printing reproduction. To better improve the image reproduction effect in printing, the most used method is to increase the amount of ink in the printing process, that is, dots with different values need to be generated in the process of digital halftone. The simplest and most practical method of this process is to expand from binary halftone to multi-level halftone. However, this process will produce classical problems. First, binary halftone has good blue noise characteristics in the frequency domain. When extended to multi-level halftone, the characteristics of blue noise will be destroyed due to the appearance of gradient reproducibility, which will affect the quality of appearance reproduction in the final printed image. To solve this problem and maintain the quality of appearance reproduction, this research introduce effective edge detection and nonlinear technology in the process of halftone, to improve the appearance reproduction of multi-level halftone images. Second, halftone technology with stronger detail reproduction ability, such as error diffusion, is more prone to irregular artifacts in the process of binary halftone processing, because error diffusion halftone does not have a mask that can produce regular dot distribu-

tion like dithering algorithm. Therefore, to improve the effect of reproduction and reduce the generation of artifacts, the author adopt the idea of multiple halftones to process the non-linear images respectively, which not only eliminates the influence of artifacts on the appearance reproduction quality in the visual effect, but also retains the characteristics that binary halftones can better restore the appearance of image details.

The second aim of this research is to develop an assessment method that can evaluate the proposed method. To evaluate the appearance of halftone more effectively, the author use a dual strategy evaluation method closer to Human visual system (HVS). Since the appearance of image is the result of the joint action of multiple attributes, then a comprehensive score is given by HVS. Therefore, to reduce the complexity of image appearance evaluation, the author evaluate the most important and relatively complex gloss attributes and propose a color halftone image evaluation method based on structure and appearance measure (CSAM). The first strategy is based on the detection of structural information distortion, which is to quantitatively calculate the structural distortion. The second strategy is based on appearance distortion, which used is to calculate the appearance distortion.

Finally, in order to test the author's hypothesis, whether the presentation of texture is related to perceived gloss. Firstly, based on the proposed glossiness index , this research verify the proposed Multi-level texture-aware error diffusion (MTAED) algorithm by subjective and objective experiments based on 100 glossy and non-glossy images. The experimental results show that the proposed MTAED has advantages over other halftone algorithms, both subjective and objective experiments, and prove that the glossiness index can predict the texture presentation. Secondly, based on the above verification, in order to verify whether the presentation of texture can affect the gloss performance of objects. An objective verification experiment is carried out based on different databases to compare whether the proposed index has advantages in the image database containing glossy and non-glossy objects. The results show that the proposed MTAED with better texture reproduction shows greater advantages than other algorithms in glossiness index.

Chiba, August 2022

Contents

FOREWORD

This research has written based on the research that has been published in journals. These two papers are multi-level halftone based on texture perception and appearance based halftone image assessment, respectively. Based on a study of the entire printing process, the findings were also presented at international conferences.

Typically, halftone is a process of transforming continuous images into images with discrete dots. Therefore, digital halftoning introduces distortion, reducing the image visibility and destroy the structure in the original image. Eventually, these shortcomings will be revealed through the printing process, which will cause displeasure to the observer. In order to solve these shortcomings, many algorithms based on image perception have been designed and developed. For example, the simplest processing is to introduce image processing technologies such as edge detection in the process of halftone. However, in view of the higher requirements of customers for the appearance reproduction of printed images, these technologies obviously can not really achieve these goals. At the same time, different from the traditional image quality assessment methods, the assessment based on appearance reproduction becomes more difficult, because no index can give a complete evaluation of the appearance of image reproduction. Subjective evaluation relies too much on observers, and different observers often give different evaluation results.

This research consists of 6 chapters, which are based on two published journal papers, respectively.

- In Chapter 1, The history of traditional halftone technologies are briefly described. The model of digital printing system used in this dissertation is also briefly explained. Then the conventional halftone quality assessment is also have a briefly explained.

- In Chapter 2, An example of the study on the perception of texture and material is presented. A description of the texture editing method is described.

- In Chapter 3, This chapter proposes a multi-level texture error diffusion algorithm based on texture-aware halftone algorithm. In this algorithm, a step-by-step halftone method is introduced, that is, the method of using nonlinear transformation to process the halftone, then synthesize the halftone result.

- In Chapter 4, An index of perceived object gloss of halftone image is proposed. The index subjectively evaluates the perceived gloss of color

halftone image based on the structural similarity of image and the image attribute standard deviation and skewness related to gloss. At the same time, combined with the objective evaluation score, the consistency of the two is verified.

- In Chapter 5, Based on the error diffusion algorithm of texture perception proposed in Chapter 3 and the perceived gloss index proposed in Chapter 4, this Chapter verified whether the perceived texture halftone will affect the reproduction of gloss. At the same time, it also verifies that the perceived gloss index can evaluate the texture perceived halftone.
- In Chapter 6, The summary of each chapter related to this research and the possible research direction and content in the future are described.

In Appendix A, published papers and international conferences attended are listed. In Appendix B lists the experimental data used in this research.

Chapter 1

General Introduction

1.1 Background

Recently, with the significant improvement of computer hardware and display performance, ordinary non-professional users can also easily process high-definition images. In addition, with the explosive rise of smart phones and the high-performance of mobile devices, high-performance image editing software that used to run only on PC has gradually become the mainstream software on portable PC and smart tablet. This has further promoted the widespread popularity of multimedia information, because people can realize their ideas more freely and communicate more efficiently. This provides unprecedented potential and opportunities for people to edit images and generate final product images. In addition, thanks to the rapid development and specialization of these computer hardware and display devices, industries that rely more on simulated originals, such as advertising, newspapers and magazines, have also become more professional and liberalized. Because of the improvement of these technologies, the management and editing of relevant images such as originals become more convenient and simple. In these media, because images are an important way to convey information to consumers, it is necessary to use more expressive original images to convey information closer to the original goods. At some more professional levels, professional personnel are needed to edit the image. For the printing press, in order to achieve the purpose of efficient information transmission, it must have super image reproduction ability. Generally speaking, the reproduction ability of printed image is restricted by various factors, which can be divided into hardware and software. These factors together determine the reproduction effect of the final printed image. The software mainly preprocesses the image, while the hardware undertakes the task of realizing these processing. They cooperate with each other and jointly control the effect of the final printed matter.

In terms of hardware, with the improvement of the processing accuracy and control technology of the printing machine itself, it has become a reality to print high-resolution images at high speed. From the perspective of household inkjet printers, the printing resolution in the early 20th century was 360 DPI, which was due to the

highest printing resolution limited by hardware. Since entering the 21st century, the printing resolution has reached 5760 DPI in the paper feeding direction and 1440 DPI in the working direction of the print head [1]. In addition, modern printing machines can not only show the gray level composed of black and white dot, but also show a higher gray level by printing gray or more gray values, so as to realize a more fine printing method. Taking the ink-jet printer as an example, the method of changing the ink-jet amount in hardware [2], and in software, the image can be up sampled once, so as to realize the printing of more gray levels through the density pattern. In addition, in order to narrow the difference between the printing field and the color gamut of the display, that is, to expand the color gamut of printing, in addition to using general ink, manufacturers also use high chroma ink to improve the accuracy of color reproduction [3].

In addition to improving the printing performance through hardware, many software methods have also been applied to improve the image quality of printed images. For example, considering that the initial input image will also affect the final printing image quality, many technologies to improve the original image quality are applied to the image preprocessing program. This is based on the process of printing, which is a process of image quality deterioration. Therefore, preprocessing can be used to enhance the details and colors that may change in the image. Among them, through the sharpening of the image and the adjustment of the tone curve, there can be a very obvious change in the reproduction effect. Therefore, these technologies have been widely used in their own products by various manufacturers until now. In addition to preprocessing the original, the appearance of the final printed image can also be changed through the use of halftone algorithm. Halftone technology is a method of quantifying images, which can represent different gray levels of images through the dispersion and aggregation of dot points. This is an image processing method different from image preprocessing. Compared with the display, due to the limitations of the printing press, it cannot show as many gray levels as the display. Therefore, it is necessary to quantify the original through halftone, and then display the image by printing on paper and other materials. Generally speaking, most printers only use binary dot points, that is, black and white (inked and non inked) to express the gray level. In this process, halftone is used for image quantization. Therefore, the quality of halftone directly determines the appearance of the final printed image. Halftone algorithms include screening and dithering [4] [5], and density pattern methods, such as Direct Binary Search (DBS) [6]. Among many halftone algorithms, the dithering error diffusion algorithm [7] is widely used because of its strong detail performance. In comparison, the error diffusion is more reproducible in gray scale and resolution than the density pattern and screening algorithm. Compared with the amount of calculation of DBS, error diffusion has better advantages. It greatly shortens the time of image quantization processing, and has a reproduction effect comparable to DBS. The original error diffusion algorithm will contain more high-frequency components and lose the low-frequency components containing more image details. Therefore, the clarity of the reproduced image is greatly reduced. In order to overcome these short-

comings, the extended error diffusion method is widely used in the industry.

As mentioned above, various methods have been proposed to improve the image quality of printing and halftone images, but how to comprehensively and correctly evaluate these improved image quality is often a difficult problem. A variety of indicators based on image signal processing and image processing have been proposed, such as widely used PSNR, MSE, SSIM [8] and CIE-ΔE. For example, when evaluating the quantized image, it is often necessary to use various filters based on the principle of human vision to smooth it, such as [9] [10]. However, these image quality evaluation indicators are not necessarily consistent with the image appearance perceived by human beings, because in the actual printing scene, while confirming the quality of the printed matter, customers will subjectively evaluate these relevant factors according to the appearance of the whole image, that is, the parameters of these factors expressing the appearance will be adjusted independently under the control of human vision and brain.

Texture is the comprehensive expression of various attributes of image perceived by human visual system. Therefore, human subjective evaluation of image texture has been concerned for a long time. In order to reveal the mechanism of human perception of image texture, Fleming et al. used 9 clues such as gloss, color and contrast to explain the role of these clues in translucent perception [11]. Taking indoor billboards as an example, in many cases, it is necessary to show customers a variety of textures, such as the freshness of supermarket food, the reproduction of texture and color of classical paintings, etc. Therefore, it is necessary to edit the texture related attributes with the help of an image processing method, so as to make the reproduction of objects in advertisements infinitely close to the real object. However, in reality, due to different observation environments and observed objects, the perceived texture may change. In some studies of texture perception, Tanaka et al. [12] have confirmed that the texture evaluation may be different between the actual image and the reproduced image on the display. Therefore, similarly, due to the change in the appearance of the printed image caused by the color gamut of the printed reproduction is smaller than that of the display, it is likely that the appearance of the object displayed in the display cannot be observed in the printed image.

The purpose of this study is to design an error diffusion method considering the texture reproducibility of printed images. Therefore, subjective experiments evaluated texture related attributes. In the subjective evaluation experiment, the attributes related to the texture of the printed image are investigated, and then the influence of a texture editing process on the appearance of the printed image is confirmed. In addition, improving the texture of the printed image from the aspect of image processing, and propose an image quantization method for the purpose of multi-level error diffusion. This method can better maintain the texture of the original image. Through the actual output of the quantized image obtained by the proposed method by the inkjet printer, and combined with the obtained printed image, this dissertation conduct texture assessment experiments to verify the effectiveness of the proposed method. Finally, the experimental results show that the proposed image quantization error dif-

fusion algorithm combined with image processing method can significantly improve the reproducibility of printed image texture. At the same time, in order to explore whether the gloss of printed image reproduction is related to the reproduction of texture, this research propose and verify a gloss index, and verify it on the proposed error diffusion algorithm with texture perception. Experiments show that the index is highly consistent with the experimental results of subjective observers, which can verify the reproduction intensity of printed image gloss to a certain extent.

1.2 Modeling of Digital Image Printing Systems

In order to use the inkjet printer to output the results of the proposed method, dividing the flow of the digital image printing system from inputting the original digital image to obtaining the printed image into four steps in Figure 1.1: image processing, color separation, error halftone processing (image quantization) and printing. In the image processing step, the function of image processing is to improve the appearance of the printed image. For example, in this step, the actual printing operator will use image editing software such as Adobe Photoshop to process the original. In the color separation step, the image output from the image processing step is subjected to color separation processing by relying on the color description file used by the printer assuming that the printer can print with C, M, Y and K inks, in the process of printing color images, perform the following operations: first convert the image from RGB space to CMYK color space used for printing, and finally adjust the gray level by LUT to ensure that the output result is linear. In the printing step, color separation and halftone processing can be carried out at the same time according to different quantitative methods [13]. As shown in Figure 1.2, it is an actual printing process. However, in order to simplify the complexity of the system and realize more accurate control of the printing process, these two steps are processed in a separate way. In this study, the quantized image after error diffusion processing is input to the selected four-color CMYK printer, and finally the printing step of the image is completed.

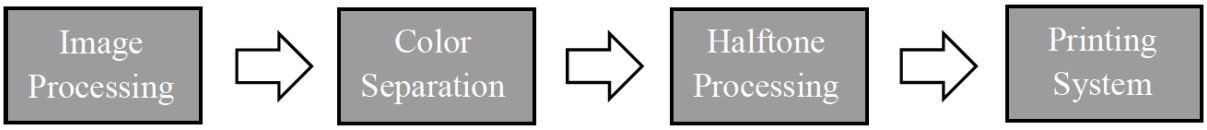

Figure 1.1 Modeling of digital image printing system

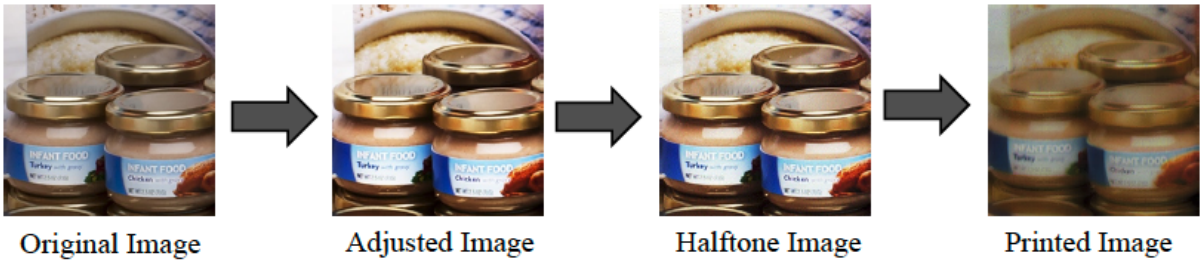

Figure 1.2 Printed image by printing system

1.3 Assessments for Texture-Aware Halftone Images

In order to verify whether the object gloss is related to the restoration of appearance perception in printed images, a gloss assessment method is proposed. This is a fully referenced image gloss index for printing image assessment. In this index, different from the single evaluation index, the proposed index uses two strategies to evaluate the distortion of halftone image. The first strategy is based on the evaluation of image structure information distortion, and the second is based on the evaluation of image appearance distortion. This research verify the index on the image database containing glossy and non glossy objects, The proposed gloss index has a strong correlation with the subjective experimental results, which can verify the reproduction of gloss of halftone image to a great extent. In order to verify whether the gloss is consistent with the appearance of the printed image, the proposed gloss index used to evaluate the reproduction appearance of the printed image. The experiment shows that the reproduction of gloss in the printed image is consistent with the reproduction of appearance.

Chapter 2

Error Diffusion Halftoning in Printing

This chapter mainly introduces two image editing methods used to halftone image, edge detection and texture editing.

2.1 Edge Detection

As we all know, when printing digital images, the quality of reproduced images will change due to various factors. Firstly, because the color gamut in the printing field is smaller than that of the display, and the process of image quantization itself is a process of reducing image quality. Therefore, the printing press leads to the decline of perceived image quality. In addition, when actually using the printer for image printing, there are various factors such as unstable output due to the thermal noise of the printer, ink splash, color gamut change caused by the combination of paper and ink, dot expansion, etc. To sum up, in the printing process, due to these phenomena, the color range, dynamic range and resolution of the image will be reduced. Finally, the image effect printed by the printer is very different from the image observed on the display, which cannot meet the requirements of printing.

Not only in the field of printing, as a method to improve image quality, digital image processing is widely used in various fields. In printing, the main operations used are image smoothing and sharpening, which belong to the most basic operations in image processing. Smoothing operation is helpful to remove the noise in the image and reduce the interference to the image content. Moving average filter and Gaussian filter are designed to smooth the image. Their design is very simple, but they also have disadvantages. These filters will reduce the definition of the image. Therefore, in order to overcome this shortcoming, researchers proposed bilateral filter [14], which cannot only smooth the image on the premise of ensuring image clarity, but also be easily extended to improve the efficiency of operation. In addition, the Guided filter [15] is also a smoothing filter that retains edge information. Different from the

bilateral filter, the filter also needs additional guide image. The guide image can be the image itself, which is used to smooth filter the image on the premise of ensuring the structure of the guide image.

Different from the principle of image smoothing, sharpening is a method to improve image clarity by enhancing the processing of image edges. Because the printing process is a process of image quality reduction, it is appropriate to use sharpening operation to enhance the edge of the image in the printing process, so this processing method is widely used in the preprocessing of the original. The simplest way to sharpen is to apply Laplacian filter. However, although Laplacian filter has high operation speed, it is also sensitive to noise and prone to artifacts. As sharpening filters with high performance, there are Gaussian quadratic differential filter (GD filter) and Gabor filter [16]. The filter is designed based on the mechanism of human visual system, so it has better sharpening performance [17] [18]. GD filter is a method to design the filter by using the second-order differential of Gaussian function. Once the filter is designed, the actual filter processing can be represented by convolution operation in image space. Therefore, to quickly and simply processing the image, as an example of the effect of typical image processing, the moving average filter 11×11 and bilateral filter 11×11, $\sigma_c = 20$, $\sigma_s = 20$, and GD (9×9). The results of sharpening according to $\sigma = 0.7$ are shown in Figure 2.1.

The basic idea of these sharpening algorithms is to improve the definition by detecting and emphasizing the edge of the image. Because the edge of the image carries the important information to be expressed by the image, the image processing method using edge detection is widely used in various fields of image processing. The most basic edge detection methods are Laplacian filter mentioned above and Sobel filter which can detect edges in any direction [19]. Because the processing of these filters is simple, the quality of detectable image edges is very low. This requires more refined edge detection so that higher quality edge information can be obtained. For example, Canny's method [20] is designed to achieve this goal. At the same time, there are also filters designed according to the filter shape, such as Susan's circular filter, which can also obtain high-quality edge information in the image [21].

In addition to using sharpening to improve the image quality of printed images, there are simpler and widely used methods. For example, adjust the hue curve of the image. After the image is printed on the material, the phenomenon of point gain will appear. If this process is not controlled, in the area with low image brightness, the amount and type of ink required for printing are more than those in the area with high brightness, so the phenomenon of point gain is more likely to occur, and it is easier to cause errors such as color and brightness, that is, the tone curve of the printed image is nonlinear. Its gamma value is mainly concentrated in the high gamma region. Assuming that the pixel value I of the input image is [0.0, 1.0], the gamma adjusted pixel value p can be expressed by Eq. 2.1. The parameter gamma represents the adjustment intensity of the tone curve. In order to show the contrast effect before and after gamma correction, Figure 2.2 shows their printing images respectively. The sample is printed at 600dpi, and the model of the printer is Thinklab

(a) The original image

(b) The move average filter used result

(c) The bilateral filter used result

(d) The GD filter used result

Figure 2.1 Image processing with different filters

inkjet printing. The results are shown in Figure 2.2.

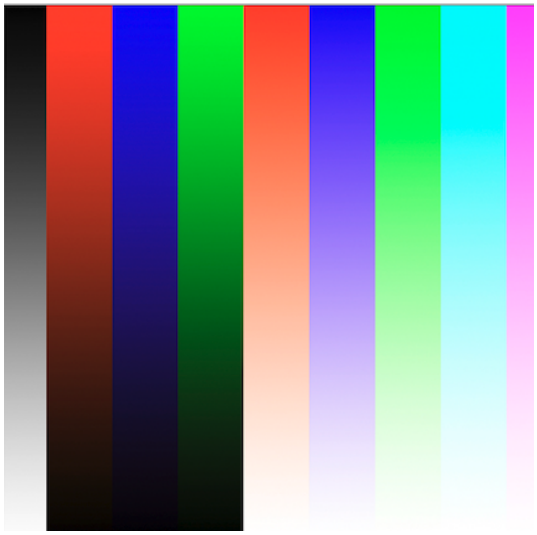

(a) The original image

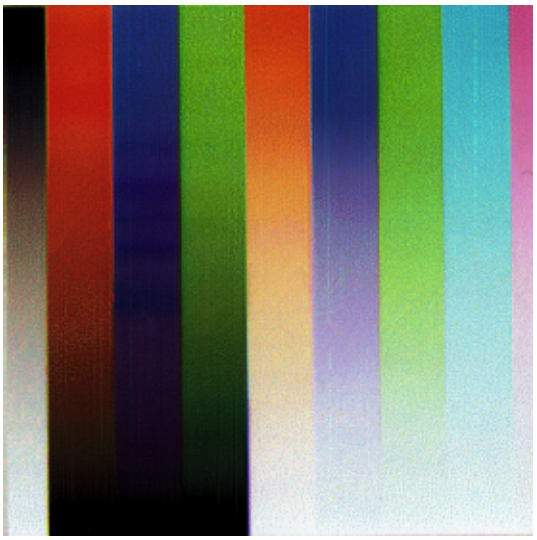

(b) gamma=1.0

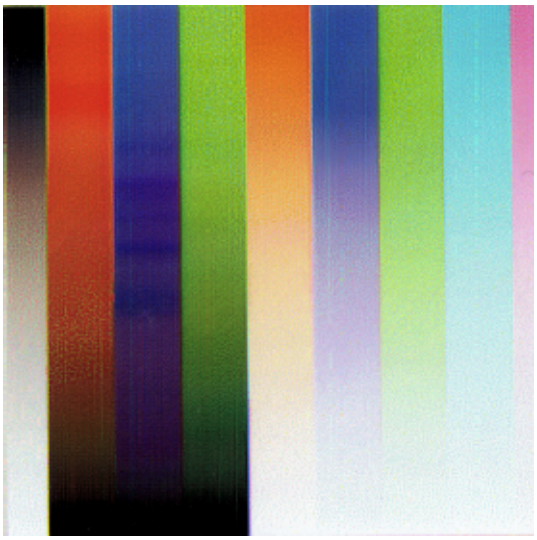

(c) gamma=3.0

Figure 2.2 The printed images with different gamma

In addition, in the printing of color images, sometimes different tone curves are used according to the different requirements of CMYK channel. For example, in the printing including skin, in order to make the printed skin show the skin closer to the blood color of human body, the printing staff can control the printing output result by adjusting the tone curve of cyan and yellow channels. In addition, by adjusting the tone curve of the image, the image contrast can be enhanced, and then some information of the image can be highlighted. Using Eq. (2.1) and Eq. (2.2), the tone curve of the image can be changed into S shape, which realizes the mapping operation of 8-bit

image. Where g represents the strength of the process, $S_{max} = F_s(255)$, $S_{min} = F_s(0)$. The color image is converted to YCbCr color space, and then the image is mapped using the above method for luminance Y. As shown in the Figure 2.3, by adjusting the tone curve, the gloss of the shiny object is enhanced, and the gloss effect perceived by human eyes is changed.

$$p = F_s^{'}(i,g) = \frac{255}{S_{max} - S_{min}} \times (F_s(i,g) - S_{min}) \tag{2.1}$$

$$F_s(x,g) = \frac{1}{1 + exp(-g) \times (x - 128)} \tag{2.2}$$

(a) The original image

(b) g=0.015

(c) g=0.0225

Figure 2.3 Tone curve adjusting in gloss image

2.2 Texture Editing

In recent years, people pay more and more attention to image quality. Research based on image material categories (metal, cloth, paper, etc.) has always been carried out. These studies not only include the establishment of material databases such as Sharan, but also the classification tasks represented by machine learning [22]. It also includes the technology of editing these materials. Khan et al. proposed the method of restoring normals from the image and editing materials [23] shown in Figure 2.4. In addition, Motoyoshi et al. studied the texture using nine attributes such as gloss and transparency, and the results confirmed the relationship between the perception of transparency and gloss and the image histogram [24]. In addition, in the research of Mantiuk et al., it was confirmed that when the hue mapping of HDR image is carried out, the contrast of the image is related to the perception of light [25].

(a) The original image (b) The edited image

Figure 2.4 Image editing sample [23]

2.3 Edge Detection Error Diffusion

Error diffusion halftone is one of the halftone methods proposed by Floyd et al. [26] [27], which is widely used even now because it can quickly obtain high-quality halftone quantized images. As shown in the formula, $X(i,j)$ represents the pixel value of the input image at position (i,j), and $Y(i,j)$ represents the pixel value of the halftone image at the corresponding position. In general error diffusion, each pixel of the image is accessed successively from the top left to the last pixel through raster scanning. The process is quantified according to the Eq. (2.3):

$$Y(i,j) \Leftarrow Q(X(i,j) + E(i,j)) \tag{2.3}$$

where $Q(x)$ represents the quantization function and E represents the cumulative error of surrounding pixels. The initialization value of cumulative error E at the beginning of processing is 0, and it is constantly updated during processing. In addition, the quantization function $Q(x)$ is a function of the available value after quantization and the set quantization level. In halftone, the following formula is generally used for quantization:

$$Q(x) = \begin{cases} 0 & x < 128 \\ 255 & x \geq 128 \end{cases} \tag{2.4}$$

After quantization, the quantization error needs to be spread to nearby pixels. First, the quantization error e is calculated by Eq. (2.5). Then, the quantization error e is diffused to the surrounding pixels according to the mask M. In Floyd's error diffusion, the above mask is multiplied by the error E of the corresponding position and added to each element of mask M. After the error is updated, the processing of the current pixel ends and the scanning of the next pixel continues. After scanning all pixels, $Y(i, j)$ is output as a quantized image. The function of diffuse (E, e, M) represents the error E, and the mask M is used to diffuse the quantized error e.

$$e \Leftarrow X(i, j) + E(i, j) - Y(i, j) \tag{2.5}$$

$$M := \begin{bmatrix} 0 & 0 & 0 \\ 0 & -16 & 7 \\ 3 & 5 & 1 \end{bmatrix} \tag{2.6}$$

The problem of error diffusion is that there will be a problem of worms and banding artifacts in the process of quantization. In order to solve the problem of bad patterns caused by image quantization, researchers have proposed many simple methods based on improved Floyd. By using the improved mask, Shiau et al. [28] not only improved the image quality of the quantized image, but also improved the processing speed of Floyd algorithm. Using only the same grating scanning direction is easy to cause error accumulation below the scanning direction, which is prone to directional point patterns. Therefore, in order to avoid this phenomenon, a method called snake scanning is often used [29] [30]. When the quantization value of the error diffusion image is near the threshold, the step difference pattern appears because the gradient process cannot be formed, which is called banding artifact. Sarailidis et al. proposed a special random number method called tie breaker to avoid this phenomenon [31]. Keotera et al. used a random number called "crossover random number" to reduce the occurrence of banding artifacts [32]. As shown in Figure 2.5, the effect of the original Floyd algorithm and the image quantization effect after introducing two random numbers are shown respectively.

In addition to the problem of point patterns such as "banding and worms", it is known that the error diffusion method has many high-frequency components, so the fine concave convex and the definition of contour are reduced. Figure 2.6 shows the original image and the image after Floyd quantization, as well as the distribution image of the respective DCT coefficients in Figure 2.7. In the frequency image,

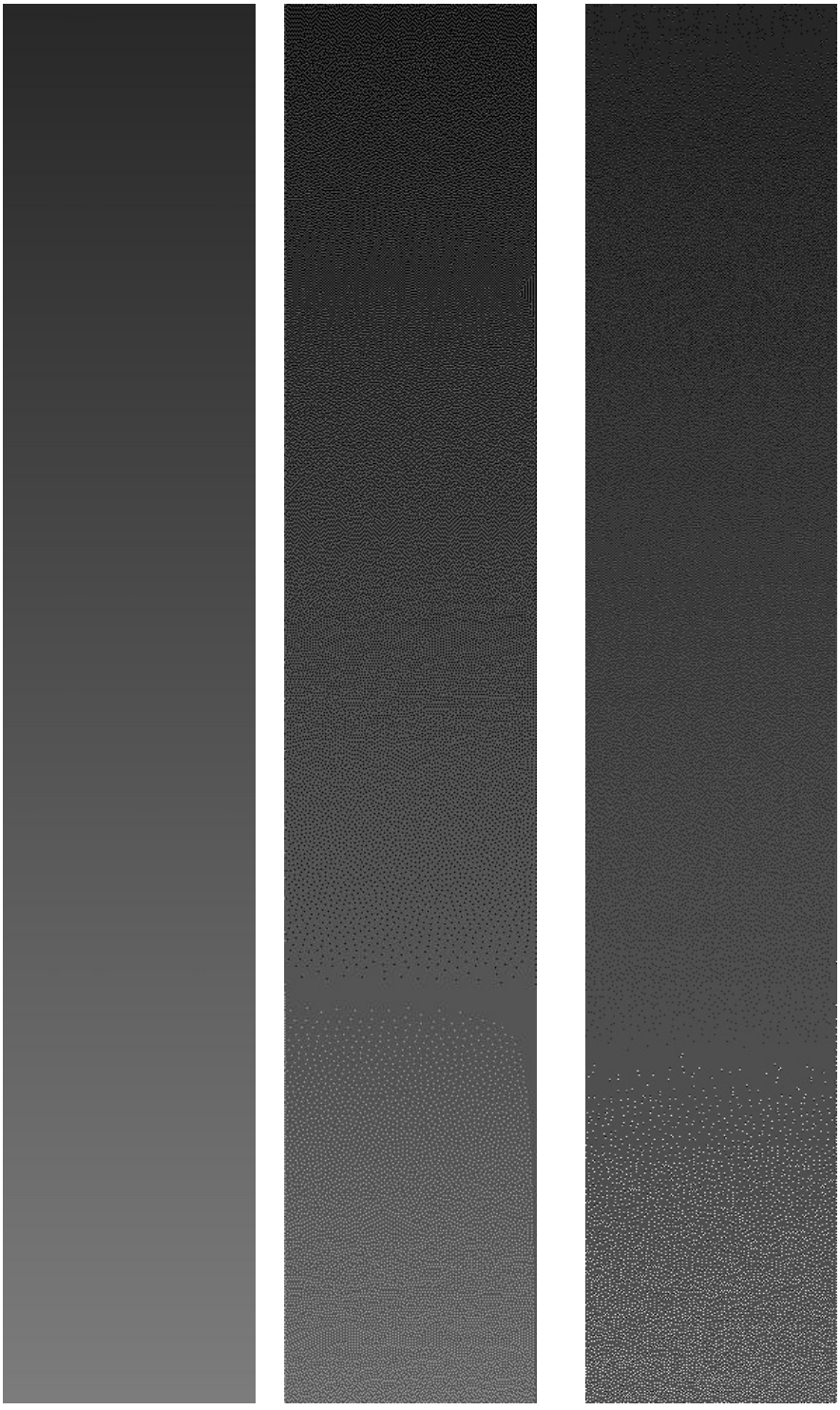

(a) (b) (c)

Figure 2.5 (a) The original ramp. (b) The ramp of Floyd. (c) The ramp with random number.

the lower left corner represents the low-frequency component of the image and the lower right corner represents the high-frequency component of the image. It can be seen that the image after error diffusion quantization introduces the high-frequency component. Therefore, the loss of low frequency represents less detail performance of the image, while the increase of high frequency represents more blur of the image. Therefore, it can be determined that the definition of the quantized image decreases as a whole.

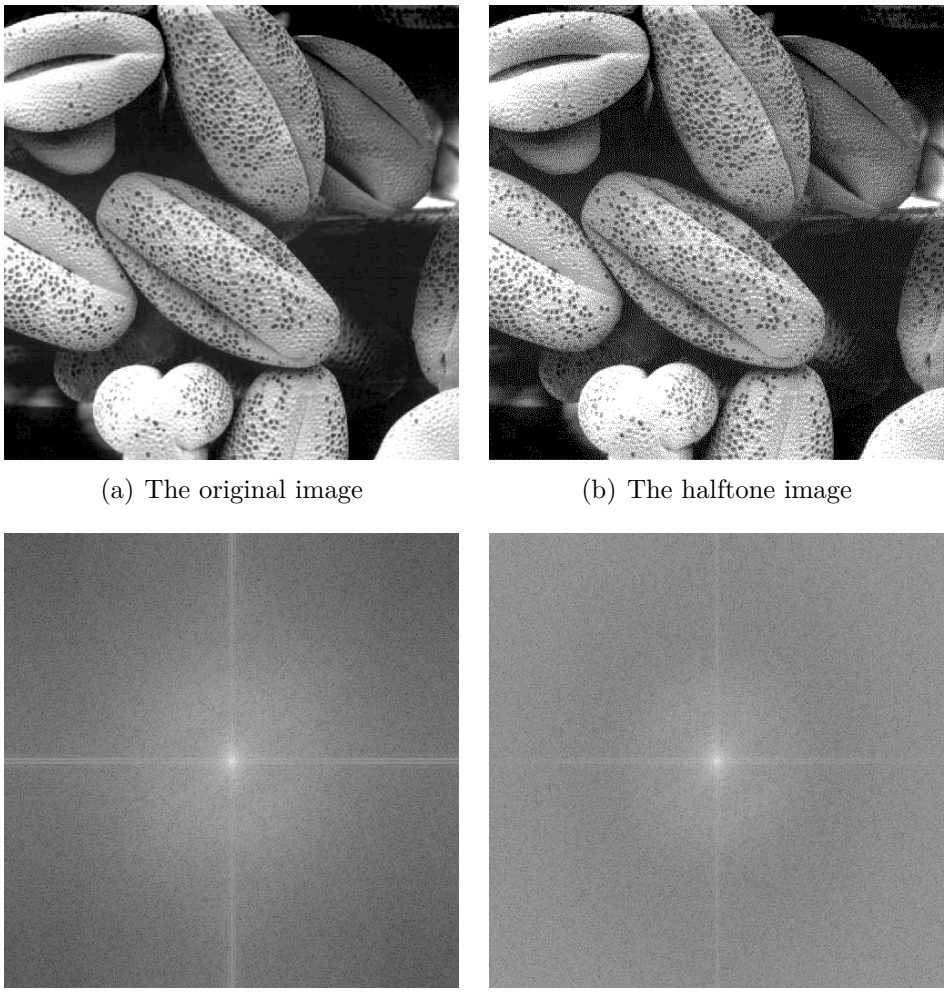

(a) The original image (b) The halftone image

(c) The spectrum of original image (d) The spectrum of halftone image

Figure 2.6 Spectrum comparison between original and halftone image

In order to solve the problem of image sharpness degradation caused by error diffusion, researchers proposed various edge information conservation error diffusion methods. Fung et al. Proposed a method to preserve the edge by dynamically changing the error diffusion mask by combining the error diffusion method and dithering method [33]. Li et al. successfully obtained the edge preserving quantized image ac-

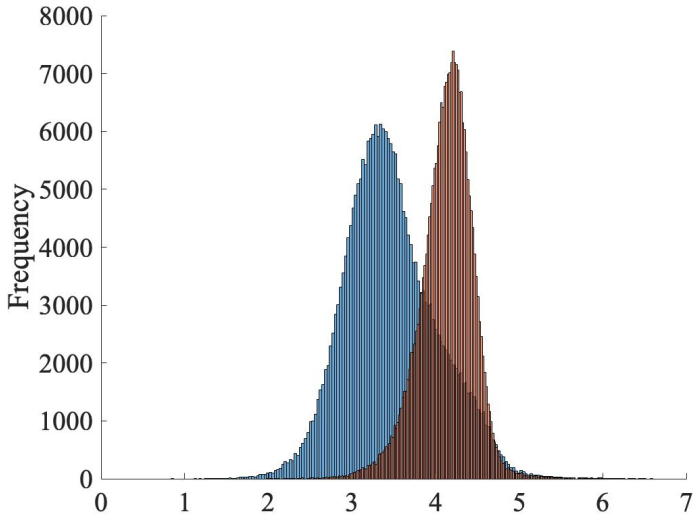

Figure 2.7 The spectrum histogram of original (left) and halftone (right) image.

cording to the edge information of the image [34]. Hwang proposed a method to change whether to consider the error accumulated during quantization or the next iteration according to the edge information [35]. Kwak et al. improved the method of Hwang et al. By introducing a simple visual model to obtain edge information to improve the accuracy [36]. In addition, Li et al. improved the contrast with surrounding pixels by quantization, rather than the edge of the image [37].

The quantization method proposed above only considers how to save the edge information of the image, but does not consider different edge types. For example, edge information can also be divided into the contour of the object in the image, the concave convex of the rough surface, the pattern and noise of the image and so on. For example, kiyotomo et al. proposed an error diffusion method for edge information preservation. In this method, only edge information such as the outline of rectangle and text contained in the image is extracted, so as to retain the clarity of rectangle and text in printing [38]. The error diffusion of structure preservation proposed by Pang et al [39]. Retains the texture information such as concavity and convexity of the object surface except the contour, but this method has a large amount of computation [40]. Laplacian based structure aware error diffusion (LBED) [41] by Lee et al. and visual difference based error diffusion (VDBED) [42] by Shi et al. are proposed based on different edge information preservation methods. As shown in the Figure 2.8, in order to compare different error diffusion algorithms that save edge information, the quantized images of Floyd, Lee and Shirley are listed. It can be seen that the surface roughness of the quantized image saved based on texture has higher reproducibility.

To sum up, the fine concave convex and pattern of the object surface in the quan-

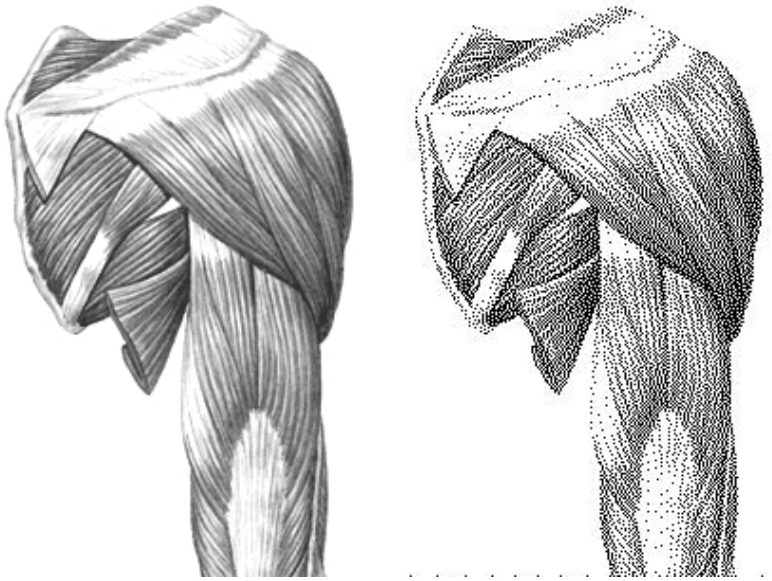

(a) The original image of arm (b) The result of Floyd

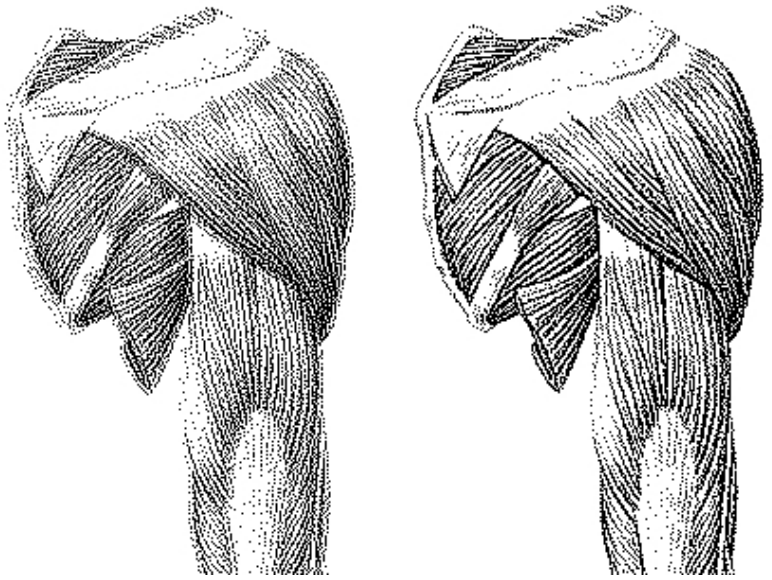

(c) The result of LBED (d) The result of VDBED

Figure 2.8 The quantized images of Floyd, LBED and VDBED

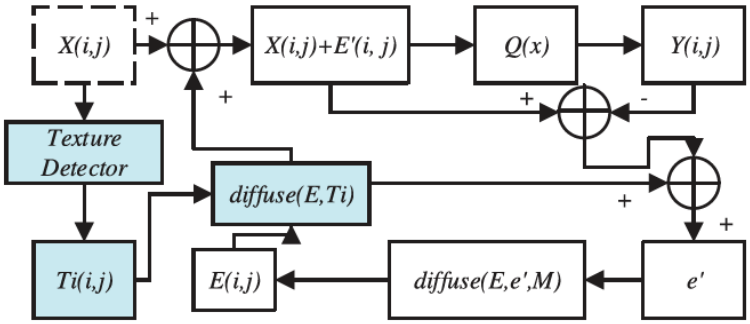

Figure 2.9 The flowchart of TAED.

titative image are considered to have a great impact on the texture of the perceived image. Therefore, based on the above considerations, an error diffusion algorithm based on texture perception proposed by kiyotomo et al [38].

2.4 Texture-Aware Error Diffusion

In this section, The error diffusion TAED based on texture preservation proposed by kiyotomo et al [38]. The processing flow of this method is shown in Figure 2.9. The purpose is to obtain quantitative images with high reproducibility such as concave convex on the object surface. This method detects the texture information from the image and uses the information as the image features saved during quantization. The texture information contains information about the concave convex and pattern of the object surface in the image. In addition, in the subsequent processing, according to the intensity of the texture information, the accumulated quantization error is not included in the pixel value at the time of quantization, but is allocated to the pixels not scanned later, so as to obtain the quantized image with the texture information saved.

Firstly, TAED detects texture information from the original image. The texture information refers to the edge information without noise and object contour. It is mainly composed of the concave convex and pattern information of the object surface in the image. In order not to contain noise from the detected texture information, a smoothing filter that saves the edge information or a band-pass filter considering the noise characteristics is used before edge detection. Using a method of increasing the core size of the edge detector, the information of the contour can be separated from the detected edge information. Lee et al. In the edge detected by Laplacian filter, the more scattered the edge of the surrounding area is, the more likely it is to represent the contour information of the image, and detected the texture information by dividing the edge intensity by the dispersion of the surrounding area. Threshold processed the edge information detected by Sobel filter using the scattered information of the surrounding area, and separated the contour information of the image from the

detected edge information [38]. The specific detection process is as follows. Firstly, Sobel filter is used to detect edge information. $X(i,j)$ represents the original image. If the Sobel edge detected in the horizontal direction is not $I_{Eh(i,j)}$, and the Sobel edge detected in the vertical direction is $I_{Ev}(i,j)$, the edge information of the detected image is $I_{Ehv}(i,j)$, which can be expressed as:

$$I_E(i,j) = \begin{cases} 1.0 & I_{Ehv}(i,j) > 1.0 \\ I_{Ehv}(i,j) & otherwise \end{cases} \tag{2.7}$$

$$I_{Ehv}(i,j) = \frac{\sqrt{I_{Eh}(i,j)^2 + I_{Ev}(i,j)^2}}{255} \tag{2.8}$$

Next, in order to separate the contour information from the detected edge information, first calculate the dispersion information $I_\sigma(i,j)^2$ of the surrounding pixels. The dispersion information of the image can be calculated using the following Eq. (2.9). The dispersion information of pixels in the image can be calculated by using the moving average filter F_k. k represents the filter size of the moving average filter, and its value is $k = 9$.

$$I_\sigma(i,j)^2 = F_k\Big(X(i,j)^2\Big) - F_k\Big(X(i,j)\Big)^2 \tag{2.9}$$

The texture information $I_T(i,j)$ is calculated according to the calculated edge information $I_E(i,j)$ and dispersion information $I_\sigma(i,j)^2$. The texture information is obtained by adding S-curve to the normalized dispersion information, threshold processing, and multiplying it by the edge information. In Eq. (2.10), it represents the derivation method of texture information $I_T(i,j)$. Max is the maximum value of $I_T(i,j)$, and g and θ are the parameters that determine the characteristics of S curve where $g = 16$, $\theta = 0.2$, the above is the texture detection method of gray image. If the color image is quantized, the color image needs to be converted to YCbCr space, then the texture information $I_T(i,j)$ is detected from the Y channel, and the texture information is used in the quantization process of each channel after color separation.

$$I_T(i,j)^2 = I_E(i,j) \times \left(1 - F_s\left(\frac{I_\sigma(i,j)}{\sigma_{max}}, g, \theta\right)\right) \tag{2.10}$$

$$\sigma_{max} = MAX(I_T(i,j)) \tag{2.11}$$

$$F_s(x,g,\theta) = \frac{1}{exp(-g \times (x - \theta))} \tag{2.12}$$

When quantifying the image, the general error diffusion method uses Eq. (2.3), but TAED uses the texture information $I_T(i,j)$ obtained first, and then uses Eq. (2.13) for quantization. Finally, the quantized image with texture clarity can be obtained.

$$Y(i,j) \Leftarrow Q(X(i,j) + E(i,j) \times I_T(i,j)) \tag{2.13}$$

$$carry \Leftarrow (1 - I_T(i,j)) \times E(i,j) \tag{2.14}$$

$$e \Leftarrow X(i,j) + I_T(i,j) \times E(i,j) - Y(i,j) \tag{2.15}$$

$$E \Leftarrow E + (carry + e) \times M \tag{2.16}$$

An example in which the image is quantized using TAED is shown in Figure 2.10. It is confirmed that the degree of softness of the contour improves the reproducibility of the surface unevenness, the mottled pattern, and the thin tube while keeping the same impression as the conventional error diffusion method.

2.5 Digital Printing System

This section introduces the printing system used for subjective assessment, and constructs an image printing system using an actual printer. The printing process used in this research is shown in Figure 1.1, and the four processes of the process are modeled. The image processing module is introduced in section 2.3 and section 2.4. The Chapter 3 introduces the image quantization module. In this section, the remaining plate splitting process and printing process will be introduced, and the setting of this research will be described. Finally, the printing system composed of these four projects is built using the printing machine shown in Figure 2.11.

2.5.1 Batch Process

Among the four steps of printing, the batch process is responsible for the CMYK conversion of the color image. Only the K channel is output in the case of the grayscale image, and the adjustment of each channel is made according to the setting of the printing. In general, the process called color management is also taken into account.

It is assumed that the input image is represented by sRGB, and the converted color ICC profile is used by the Japanese color coded 2001. The conversion of the color profile is made by the Adobe Photoshop CS3, and the matching method is set to the method to preserve the absolute color gamut. The tone curve of each channel after CMYK is adjusted by gamma correction.

In the general color management system, the color conversion is realized by actually printing the representative color by the printing machine, and making the LUT of the representative color from the result of the measurement, and interpolation of the remaining part. Therefore, the combination of representative colors and data interpolation technology are used, this performance is determined by the professional of printing technology such as the manufacturer of the printing machine.

The purpose of this research is the evaluation of the quantization method and the image processing method, and it is not evaluation of the color management system, and this research is aimed at the general user rather than the printing professional. The general user considers the printing of the poster, such as poster and pamphlet to the printer. In case of color printing, there are many cases where the data which is

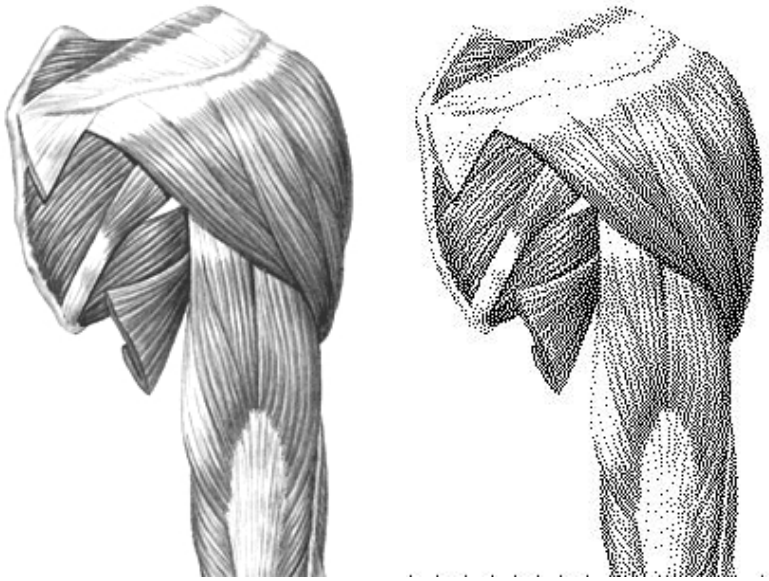

(a) The original image (b) The result of Floyd

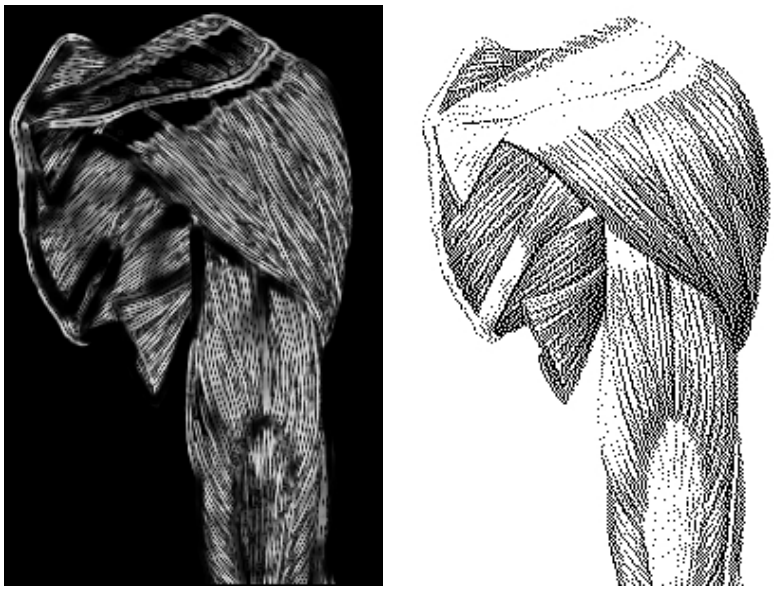

(c) The detected texture (d) The result of TAED

Figure 2.10 The quantized image of Floyd and TAED

Figure 2.11 FXIJ type 1000 FullAuto.

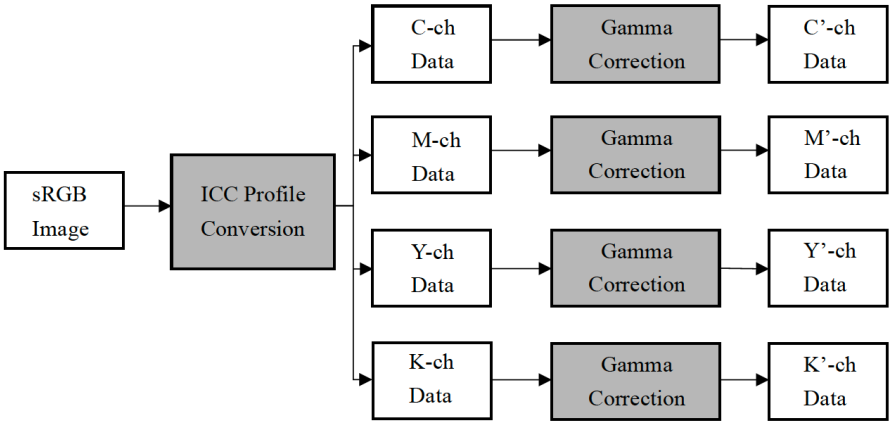

Figure 2.12 Outline of batch process.

divided into CMYK is often required. In this case, it is possible to adjust the result of the trial printing by confirming the result of the trial printing beforehand by carrying out the CMYK conversion and the adjustment of the data by the user's own hand, then printing by the printer. In this study, it is considered that if the output of printing is linear enough to some extent in the present study, the tone curve of each channel is adjusted by gamma correction. The Figure 2.12 shows the outline of this process.

2.5.2 Printing Process

In the printing process, the process of outputting the quantized data to the actual paper by the printing machine is in charge of printing by FXIJ's ink-jet printer, as shown in Figure 2.11.

Chapter 3

Multilevel Texture Aware Error Diffusion (MTAED)

This chapter is based upon the published journal paper of [A1] in AppendixA "Texture-Aware Error Diffusion Algorithm for Multi-Level Digital Halftoning" and [A3]the proceedings of "Society for Imaging Science and Technology 2020" - The Twenty-eight Color and Imaging Conference (CIC28) 4-19 November 2020.

3.1 Introduction

Some studies have been conducted with a focus on the quality loss at edges due to the ED algorithm. Fung and Chan [33] and Li et al. [34] used algorithms that focused on edges and led to edge-preserving ED techniques. In these studies, edge information was directly used. In other approaches for improving the quality of quantized images using edge information, Pang et al. [39], Lee et al. [41], Shi and Li [42], and Kiyotomo et al. [38] focused on weak textures vanishing in the quantization process and proposed halftoning algorithms to preserve these weak textures using edges. The objective of their methods was to emphasize edges that disappeared in the printing process.

Multi-toning is a halftoning method that adopts more than two tone levels for improving the similarity between the original and halftone images. The simplest method for this process is to increase the number of threshold values in the error diffussion process. Recently, the representation of the "texture" of an image, which includes properties such as its glossiness, transparency, and roughness, has become important for reproducing images on display devices.However, the texture of objects is often lost in images reproduced using conventional error diffusion algorithms based on the signal processing theory, and there has been limited discussion regarding the reproduction of texture in printing. Multi-level algorithms were developed by Sarailidis and Katsavounidis [31], Guo et al. [43], and Fung and Chan [33], who modified the halftoning ED algorithm to include multi-toning. However, in these previous studies,

actual printed images were not evaluated and the adverse effect of the expansion of black areas due to machine noise was not considered. There are some half-level algorithms using printer models. Pappas et al. [44], Lee et al. [45], and Lai et al. [46] proposed halftoning algorithms that focused on dot gain and overlap of ink. Yampolskiy et al. [47] proposed a special halftoning algorithm based on the genetic algorithm. Their methods were proposed for natural images and mainly improved reproduction in factors such as color and unwanted patterns. Therefore, their goals were different from ours. This section focus on the reproduction of the texture of objects.

In this section, a texture-aware ED algorithm proposed to improve the quality of texture in multi-level halftone images. In the proposed algorithm, multiple mapped images with different brightness levels are generated through nonlinear transformation. For each mapped image, a texture-aware binary ED method used to obtain multiple halftone images. Finally, generating a multi-level halftone image from the binary halftone images, this section compare the results of the proposed algorithm with those of the Floyd [26], Shiau [28], and classical algorithms and verify its feasibility.

3.2 Multilevel Texture Aware Error Diffusion (MTAED)

3.2.1 Error Diffusion for Binary Image

Assuming that the texture of the proposed algorithm is highly dependent on the texture representation of the image content. Therefore, a texture preserving approach considered to effectively preserve the texture of objects. The different weights for the error distribution between the texture and other regions to permit stable detection of texture pixels. A novel function used to implement the proposed texture-aware ED algorithm to detect pixels related to the texture of the image. Figure 3.1 and Figure 3.2 shows the original image and the detected edge information.

3.2.2 Multilevel Texture Aware Error Diffusion

Based on the algorithm described in the previous section, it is extended to multi-level ED. Figure 3.3 shows the flowchart of the proposed method. The extension method is a nonlinear transformation based on tone mapping. Because the result of nonlinear correction can highlight the level of the image, these levels often have different gray levels. These different levels are then halftoned and finally synthesized, thereby avoiding the artifacts caused by the classical algorithm. Thus, for a grayscale image, first performing multiple nonlinear transformations and generate multiple mapped images with different brightness levels. Next, performing binary ED processing on the results of the nonlinear transformation. Finally, utilizing a certain strategy, the results generated in the previous step used to synthesize the results of multi-level ED.

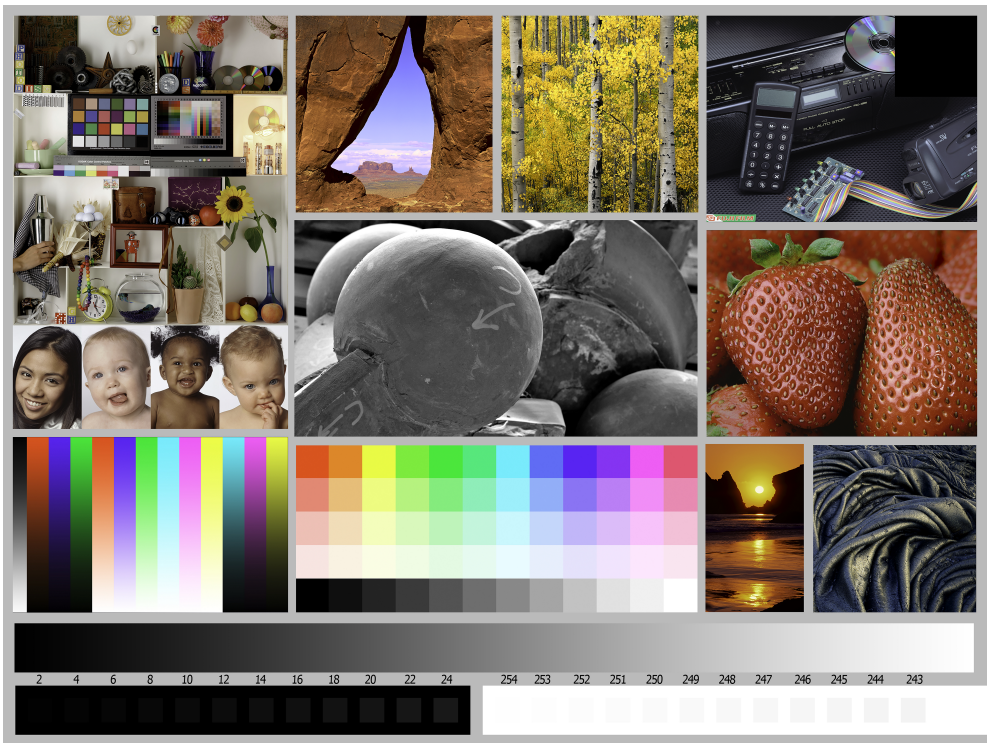

Figure 3.1 Test color image.

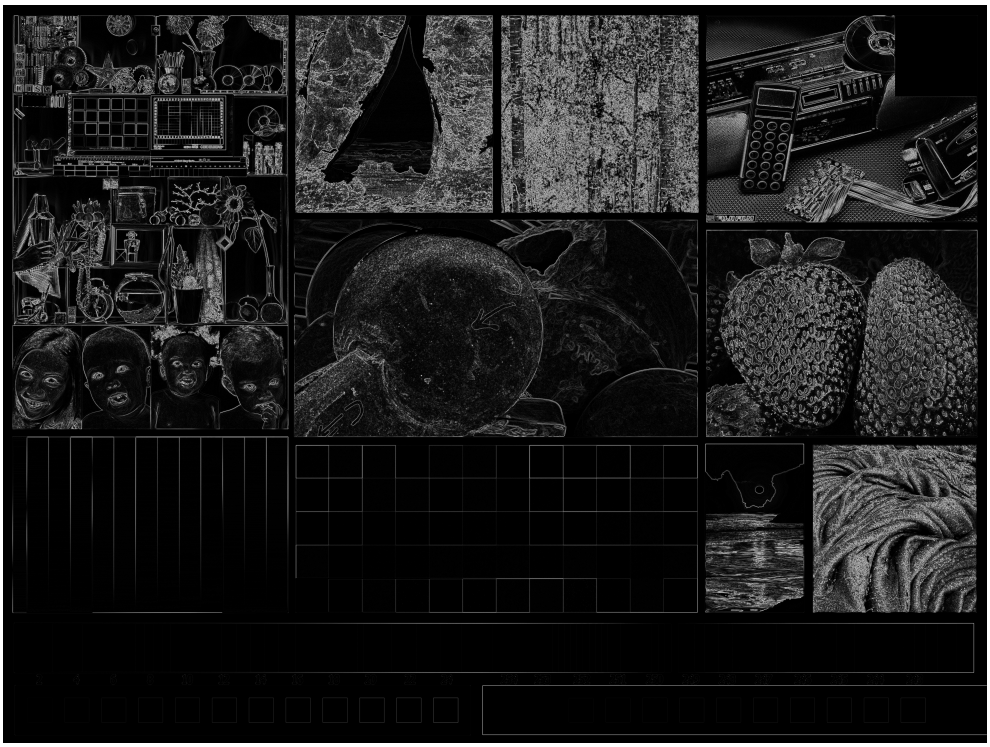

Figure 3.2 Detected texture.

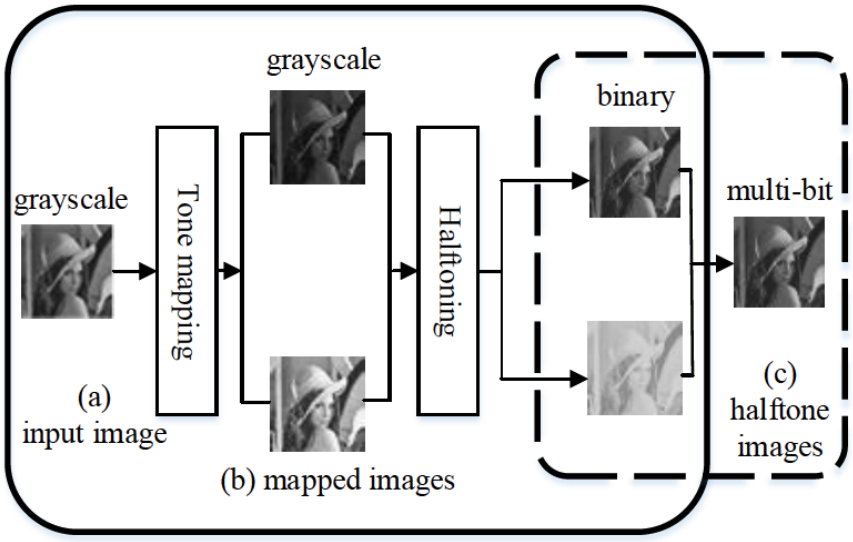

Figure 3.3 Process flow of multi-level ED.

For multi-level halftoning that is directly extended from binary halftoning, a "contour" artifact often appears in gray transition areas. In these areas, there is less error diffusion, resulting in no change in the pixel value after halftoning; then a continuous contour is produced. To discretize the continuous gray value area, an exponential function was selected for image transformation based on the idea of expanding and compressing the image gray value. This is because the exponential function can expand the high gray level of the image and compress the low gray level of the image.

As an example, Figure 3.4 show a 2-bit digital halftoning. The $X'(i,j)$ can be defined as

$$X'(i,j) = \begin{cases} (X(i,j))^{\frac{1+m}{2-m}} & if\ m \leq 0.5 \\ 1-(1-X(i,j))^{\frac{1+m}{2-m}} & otherwise \end{cases} \tag{3.1}$$

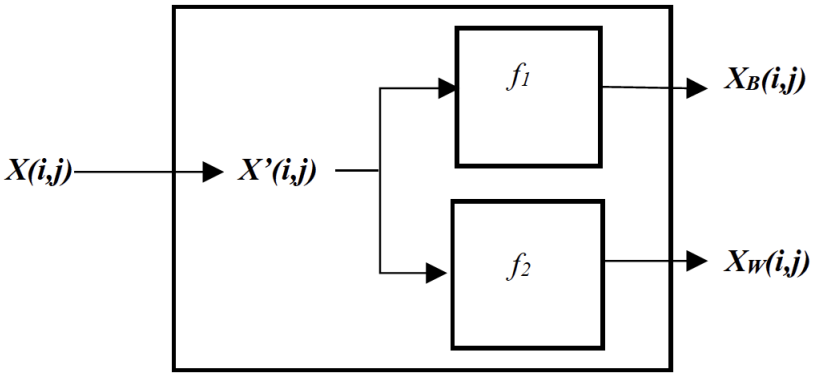

Figure 3.4 Tone Mapping.

where m is the intermediate level determined to minimize the root-mean-square errors of the multi-level halftone and original images.

Two mapped images X_B and X_W with different brightness levels are calculated using functions f_1 and f_2:

$$f_1 : X_B(i,j) = (X'(i,j))^2 \tag{3.2}$$

$$f_2 : X_W(i,j) = 1 - (1 - X'(i,j))^2 \tag{3.3}$$

To maintain good dot distribution characteristics of the binary ED algorithm, the white pixels of X'_W (the binary halftone result from X_W) are mapped to the corresponding positions of the X'_B image; that is, the pixel values of the corresponding positions on X'_B are replaced by the pixel values of the corresponding positions on X'_W. X'_B is the image after the pixels are replaced as follows:

$$X'_B(i,j) = \begin{cases} 255 & X'_W = 255 \\ X_B(i,j) & X'_W \neq 255 \end{cases} \tag{3.4}$$

Through such a substitution operation, the dot distribution characteristics of output X_B of the binary error algorithm are transmitted to X'_B.

Finally, the result of the multi-level ED is determined by X'_B, X'_W, and the input grayscale image $X(i,j)$. In the case of 2-bit (4-level) ED, the multi-level output can be represented as:

$$Y(i,j) = \begin{cases} 0 & if\ X(i,j) \leq T \\ 85 & if\ X'_B = 0\ and\ X'_W = 0 \\ 170 & if\ X'_B = 255\ and\ X'_W = 0 \\ 170 & if\ X'_B = 0\ and\ X'_W = 255 \\ 255 & if\ X'_B = 255\ and\ X'_W = 255 \end{cases} \tag{3.5}$$

where T denotes the threshold value. It is important to set pixels close to black in the original image (i.e., Y(i,j)=0). The remaining three levels are determined by the black and white combination of the two nonlinearly transformed images. In the two binary gray-scale images obtained by nonlinear mapping, to reduce the appearance of artifacts in the middle grayscale, the nonlinear transformation shifts the middle gray-scale value to two ends, that is, if the boundary is 128, the gray-scale values at both ends are compressed. For example, for a 2-bit halftone image, the values are 0, 85, 170 and 255 respectively, and the pixels with pixel values around 85 become quantized to 0. Therefore, it is necessary to set 0 and 0 to 85.

Through the aforementioned transformation, pixel replacement, and pixel comparison operations, finally obtain the final multi-level halftone image. This process only performs the most basic transformations in the field of image processing. Therefore, it will not significantly increase the original binary operation time of the halftone algorithm. The results of the TAED (2bit) and MTAED (2bit) algorithms proposed in this section are compared as shown in the Figure 3.5.

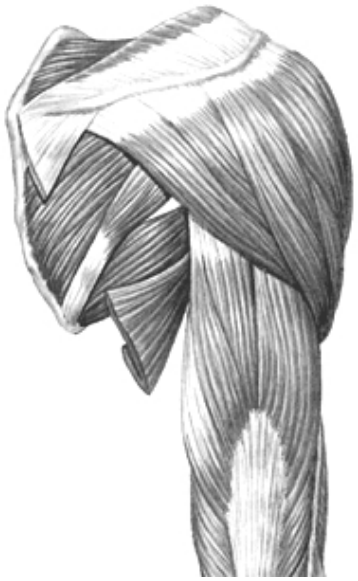

(a) The original image

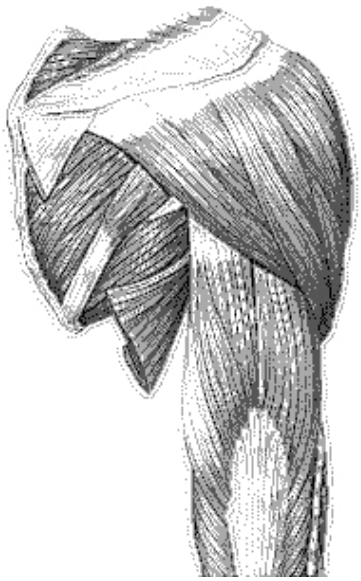

(b) The result of TAED(2 bit)

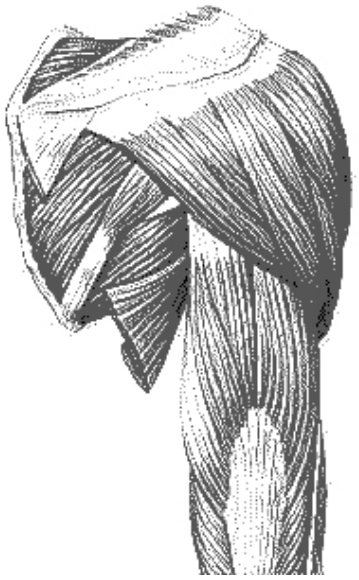

(c) The result of MTAED(2 bit)

Figure 3.5 The quantized image of TAED(2 bit) and MTAED(2 bit)

3.3 Experimental Results

This section introduces the subjective and objective evaluation experiments based on the proposed multi-level halftone algorithm.

3.3.1 Objective Evaluation

Here verified the physical performance of the proposed method by quantizing continuous-tone test images into halftone images and comparing the results to those of the conventional methods proposed by Floyd [26] and Shiau [28]. Figure 3.7 shows the test images used, and Figure 3.6 presents an example of quantized images, illustrating the effect of the proposed algorithm. Figure 3.6(a) and Figure 3.6(b) show a continuous gray image and the detected texture image, respectively, using the proposed algorithm. Figure 3.6(c), Figure 3.6(d), and Figure 3.6(e) show the halftone image after halftoning using the algorithms of Floyd, Shiau and the proposed ED algorithm, respectively. By comparing the halftone results, it is clearly observe that our algorithm can generate halftone images with good texture.

Similarity is a measure of resemblance between source and printed images as observed by humans. For this purpose, using an image-quality metric that considers the characteristics of the human visual system (HVS). This objective evaluation selected the sparse feature fidelity (SFF) function [48] to compare the images and obtain a value between 0 and 1. This value represents the similarity between reference and distorted images. Thus, the SFF function indicates the extent of similarity. The SFF function reflects the chromatic properties of the HVS, and it is considerably effective for color-image-quality assessments. It is based on the color components of red, green and blue (RGB) and can detect color distortion in a perceptual manner. To achieve this purpose, the digital halftone image was converted from cyan, magenta, yellow and black to RGB before applying the SFF function. In this evaluation, the distorted image was replaced by a halftone image processed by a Gaussian filter to facilitate the experiment. The size of the Gaussian filter was 5×5, and the σ of Gaussian filter was set to 1.5.

Observing the halftone results in Figurue 3.6, this experiment focus on the surface of the apple in each halftone image. Similarly to the real apple, the red skin of the apple in the original image is inlaid with many white spots. The areas of the spots on the apple surface in the original image are scattered and clear. After comparison, the closest to the distribution and sharpness of these spots is the halftone image generated by proposed algorithm as shown in the upper right region of the apple surface in Figurue 3.6(c) and Figurue 3.6(d). It is not clearly observe the white spots. The reasons for this texture are the following: the white spots embedded in the apple skin and the surrounding red areas belong to the area of pixel value transitions; the Floyd and Shiau algorithms, which only changed the threshold value, transition in grayscale; the "contour" artifacts in the area affect the visual effect in the halftone image. The proposed algorithm has dealt with the problem of "contour" artifacts and can present

(a)

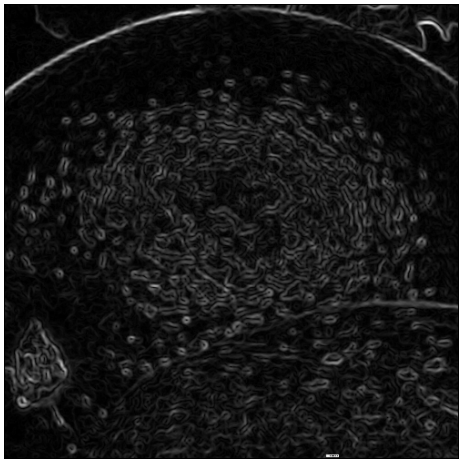

(b)

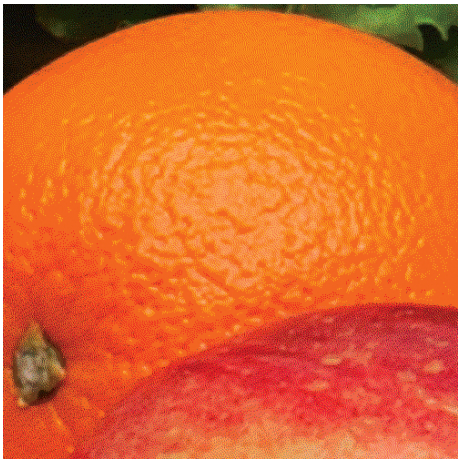

(c)

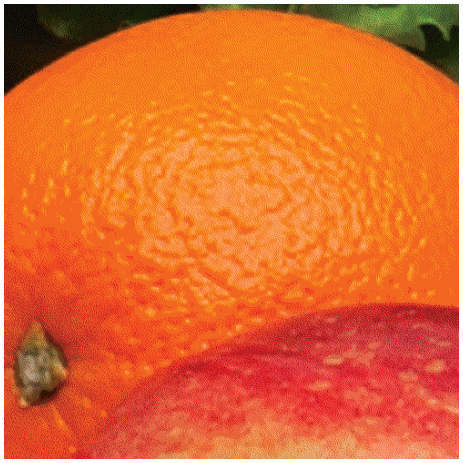

(d)

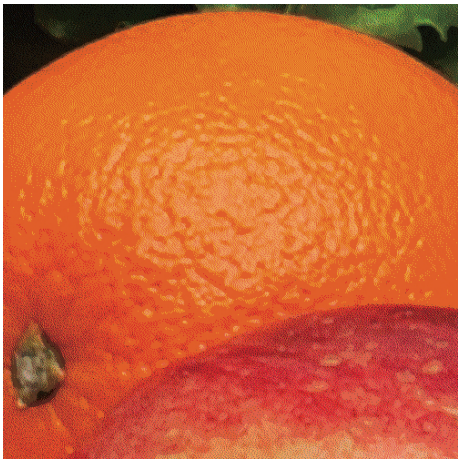

(e)

Figure 3.6 Experimental result of halftoning. (a) Original color image, (b) Texture information, (c) Floyd's ED result, (d) Shiau's ED result, (e) Proposed ED result.

Table 3.1 SFF of the algorithms of Floyd and Shiau, and the proposed algorithm.

Method	**(a)**	**(b)**	**(c)**	**(d)**	**(e)**	**(f)**	**Avg.**
Floyd	0.861	0.857	0.858	0.845	0.832	0.820	0.844
Shiau	0.856	0.853	0.848	0.840	0.826	0.830	0.847
This work	0.856	0.858	0.855	0.848	0.837	0.831	0.848

such white spots similar to those in the original image in terms of quantity, size, and distribution. Therefore, although observers cannot see a significant difference in the "reflection" area in the images of oranges, the proposed algorithm has advantage around this area.

To compare the objective data of the selected test images, this experiment compared the SFF values of the Floyd and Shiau algorithms and the proposed algorithm. These three algorithms used to process the six test images and then used the Gaussian filter to process the halftone images. Finally, the average value of the SFF as shown in Table 3.1. The table shows that the SFF value of the proposed algorithm is higher than that of the Floyd and Shiau algorithms. The selected image regions from (a) to (f) that expressed different physical properties. For images (b) and (f), the proposed algorithm performed best on objects such as plastics, glass, etc. These results showed that proposed halftone result is the most similar to the original image. However, from the result of (a), the performance of proposed algorithm was lower than that of Floyd, and proposed algorithm was inferior to the Floyd algorithm in representing the roughness. This is due to the limited edge information detected on a rough and single-color surface.

3.3.2 Subjective Evaluation

To subjectively evaluate the effectiveness of the proposed algorithm, its printing results compared with those of a raster image processor (RIP), Harlequin RIP®, developed by Global Graphics. The printed the entire selected image with 600 dpi using a four-color printer.

Six pairs of test images were prepared for the evaluation as shown in Figure 3.8. The images were scanned using Brother DCP-J152N with 600 dpi. In each pair, one image was printed using the proposed method and the other using the RIP software. Figure 3.10 shows that each observer is required to score the left and right images after comparing them. The figure presents the scoring rules. There are 16 questions, each one regards the attributes of the printed image. The total score of these questions is used as the standard for determining the quality of the printed image. For example, if the score of a certain test image is positive, this means that the quality of the left image is higher than that of the right image. The selection of questions in the questionnaire ensures that each question is independent of each other as much

(a) (b) (c) (d) (e) (f)

Figure 3.7 Test images used for subjective evaluation.

Table 3.2 Observers (stu1-stu7) internal consistency reliability Cronbach's alpha.

	stu1	**stu2**	**stu3**	**stu4**	**stu5**	**stu6**	**stu7**
(a)	0.8381	0.7103	0.8313	0.7884	0.8168	0.8962	0.7842
(b)	0.7143	0.7406	0.7711	0.8501	0.8046	0.8908	0.9254
(c)	0.7563	0.8558	0.8787	0.8873	0.8072	0.8546	0.9102
(d)	0.7848	0.8756	0.7453	0.7195	0.7735	0.7909	0.8320
(e)	0.8971	0.8555	0.8648	0.9231	0.8220	0.8948	0.8494
(f)	0.7037	0.8082	0.8342	0.8862	0.8226	0.8279	0.8235
Avg.	0.7824	0.8077	0.8209	0.8424	0.8077	0.8592	0.8541

Table 3.3 Average score of each test pair corresponding to seven observers.

	(a)	**(b)**	**(c)**	**(d)**	**(e)**	**(f)**
Score	+12.86	+10.71	+11.86	+9.86	+9.43	+10.14

as possible, so that a fair score can be given for the comprehensive evaluation of the image from different aspects. Conversely, if the score of the test image is negative, the quality of the right image is higher than that of the left image. Thus, the higher the absolute value of the score, the higher the image quality. Finally, to ensure fairness in the experiment, the average score was calculated of seven observers for each test image and used it as the actual score. Figure 3.11 shows the inter-subject standard deviation for the 16 items.

Seven observers with normal vision participated in the experiment. They evaluated a pair of printed images under simulated outdoor lighting environment. The viewing distance was set as 20 cm. As shown in the Figure 3.12, it is the environmental setting of the subjective experiment. Table 3.2 show the internal consistency reliability Cronbach's alpha for each observer of each image, and the average internal consistency reliability for each observer of all test images is calculated. If the value of Cronbach's alpha is greater than 0.6, the data is valid. Table 3.3 shows the average score of each test image. As shown in the table, for all the test pairs, the proposed methods obtained higher scores from the observers.

3.3.3 Physical Performance

Computation time. A comparison of the performance of several algorithms with regard to the average computation time for test images is provided as follows. The algorithms are presented in order from the fastest to the slowest.

PangFloyd > proposed ED > LeeShi

Peak signal-to-noise ratio (PSNR). The performance of several algorithms with

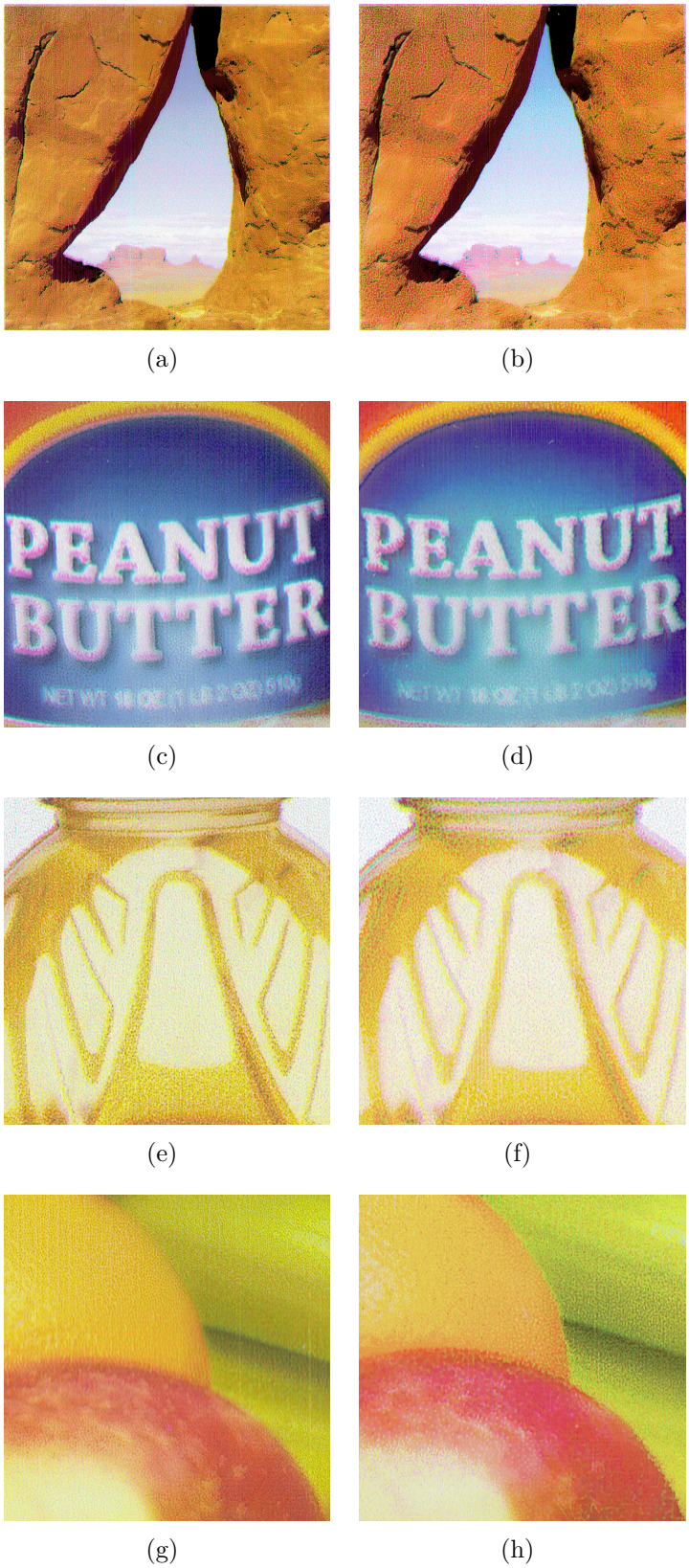

(a) (b)

(c) (d)

(e) (f)

(g) (h)

Figure 3.8 Printed images for subjective evaluation. (Left) Proposed algorithm. (Right) Current RIP software.

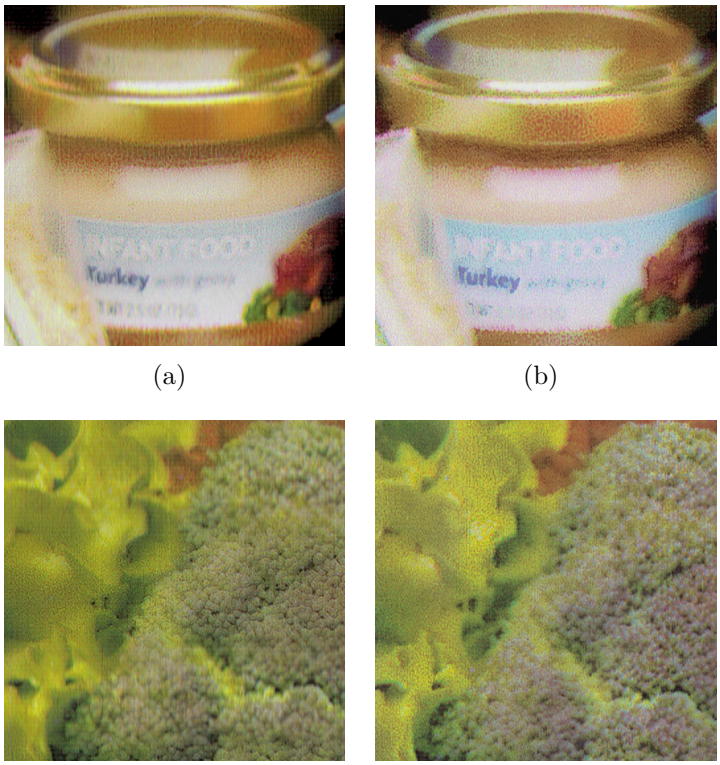

(a) (b)

(c) (d)

Figure 3.9 Printed images for subjective evaluation. (Left) Proposed algorithm. (Right) Current RIP software.

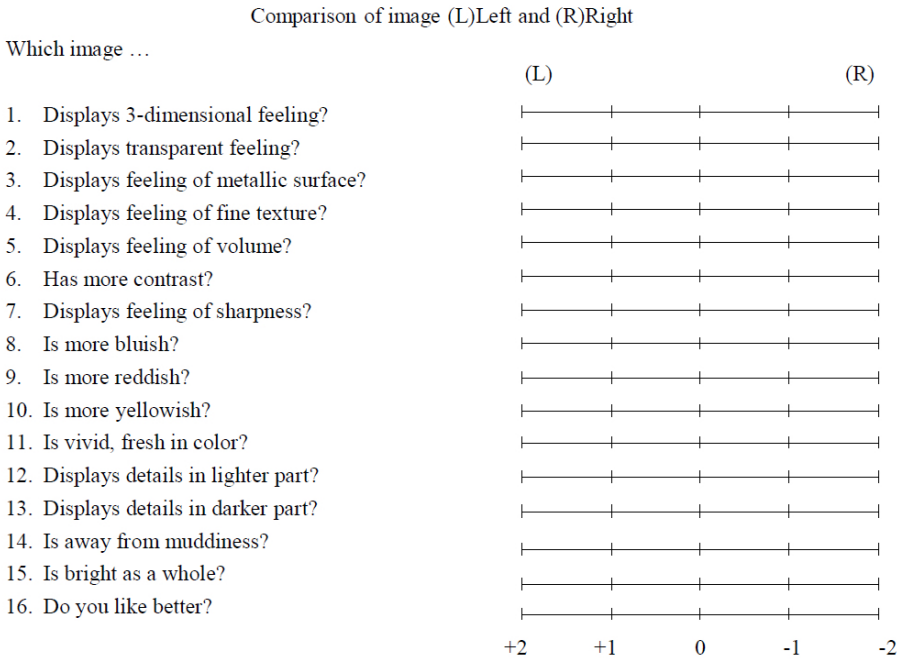

Figure 3.10 16 Test questionnaire for subjective evaluation.

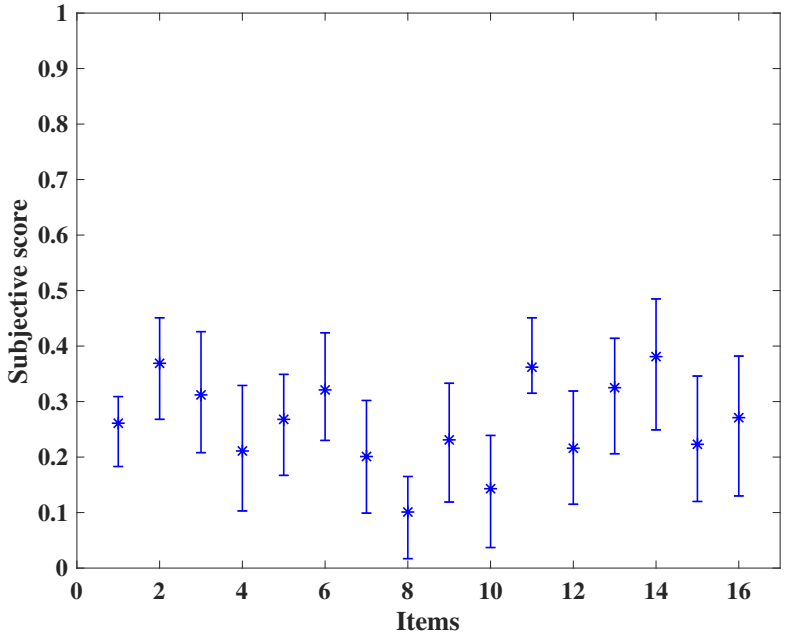

Figure 3.11 The inter-subject standard deviation for the 16 items.

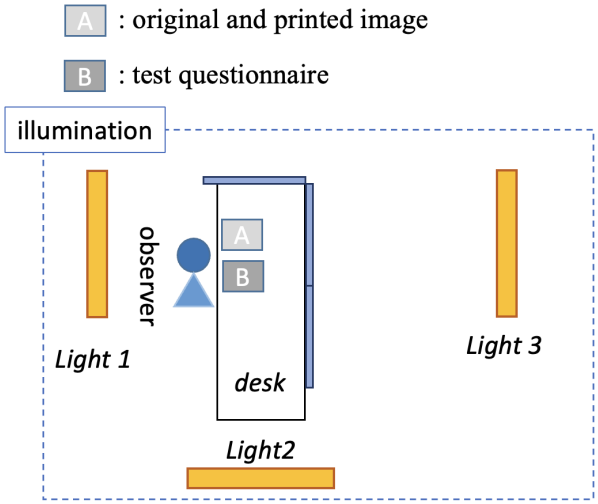

Figure 3.12 Subjective experiment environment.

regard to the average PSNR for all test images is compared below in order from the highest to the lowest value.

proposed ED > Floyd > Pang > Lee'Shi

Mean structural similarity (M-SSIM). The performance of the algorithms in terms of the average M-SSIM for all test images in order from the highest to the lowest value is as follows.

Pang > proposed ED > FloydShi > Lee

3.4 Conclusion

This chapter proposed a multi-level method that improves the texture representation of printed images through nonlinear transformation and binary texture-preserving ED. First, the nonlinear transformation was used to map the grayscale image to obtain two images with different brightness levels, process the images with binary halftone, and obtain the multi-value halftone result by synthesizing binary halftone results. Next, using an edge-preserving ED algorithm, which improved the sharpness, reduced the loss of image quality caused by machine noise, and reduced the loss of white area caused by printer noise, the proposed methods was applied to color packaging images from a website and confirmed their effectiveness. A current RIP was used to print the halftone image and compared it with the proposed algorithm printing. Consequently, the proposed method produced texture-aware images and reduced contouring artifacts in the transition region.

In future works, the research will continue to explore more effective nonlinear transformation functions to further enhance the effect of nonlinearly transformed halftone images for presenting higher texture characteristics.

Chapter 4

Glossiness Assessment of Halftone Color Images Based on Structure and Appearance Measure (CSAM)

This chapter is based upon the published journal paper of "Glossiness Index of Objects in Halftone Color Images Based on Structure and Appearance Distortion" in Appendix A [A2].

This chapter proposes an objective glossiness index for objects in halftone color images. In the proposed index, the characteristics of the human visual system (HVS) was considered and associate the image's structure distortion and statistical information. According to the difference in the number of strategies adopted by the HVS in judging the difference between images, it is divided into single and multi-strategy modeling. In this study, the multiple strategies were advocated to determine glossy or non-glossy quality. Assuming that HVS used different visual mechanisms to evaluate glossy and non-glossy objects. For non-glossy images, the image structure dominated, so the HVS tried to use structural information to judge distortion (a strategy based on structural distortion detection). For glossy images, the glossy appearance dominated; thus, the HVS tried to search for the glossiness difference (an appearance-based strategy). Herein, an index for glossiness assessment that attempts to explicitly model the structural dissimilarity and appearance distortion was proposed. Using the contrast sensitivity function to account for the mechanism of halftone images when viewed by the human eye. Estimating the structure distortion for the first strategy by using local luminance and contrast masking; meanwhile, local statistics changing in the spatial frequency components for skewness and standard deviation were used to estimate the appearance distortion for the second strategy. Experimental results showed that these two mixed-distortion measurement strategies performed well in consistency with the subjective ratings of glossiness in halftone color images.

4.1 Introduction

The halftoning technique is commonly used in the printing industry to reproduce the tone of an image with limited colors; e.g., black and white. During this process, the printed image inevitably loses both the original color and minute details. Since its introduction in 1975 by Floyd and Steinberg [26] [27], the error diffusion (ED) algorithm has attracted considerable attention in the graphics community. The main advantage of the initial version of the algorithm was its simplicity, combined with the good overall visual quality of the produced binary images and fast calculation speed [49]. However, early ED algorithms had problems with distortion, reduced visibility, worms and false textures, as well as additional noise. To overcome these shortcomings, researchers proposed many digital halftone algorithms. For examples using variable thresholds [50] and variable filter weights [51]. A halftoning technique based on optimization that preserves the similarities of tone and structure between the original and the halftone images has been proposed [39]. Existing algorithms always lose color and details when processing color images with binary dot patterns using dithering. To overcome these shortcomings, Xia et al. [52] developed two convolutional neural networks (CNNs) to learn the halftone scheme by using a nontrivial self-supervision formulation. Thus, improvements to the ED algorithm were implemented with the goal of improving "image quality".

Recently, the representation of the "texture" of objects in an image, which includes properties such as its glossiness, transparency, and roughness, has become important for reproducing images on display devices [53], [54]. However, the texture of the object is often lost in images reproduced using conventional ED algorithms based on signal processing theory, and there has been limited discussion regarding the reproduction of the texture in printing. In [55], the authors proposed a texture-aware ED algorithm to improve the quality of texture in multilevel halftone images. This led to the demand for halftone images to be evaluated not only for their "image quality" but also for the reproducibility of the texture of objects in the image. Here, this section focus on the evaluation of glossiness among textures represented in halftone images.

Most image glossiness assessment studies [56] are all device-based; i.e., based on photometer measurement, and these methods are not suitable for halftone image assessment. In the study of gloss perception in an image, it is currently debated whether the perception of gloss is linked to the statistical parameters of the retinal image [54] [57] [58]. Wiebel et al. [57] analyzed many images of natural surfaces to search for potential statistical correlations of perceived gloss. Anderson and Kim [54] found that skewness correlated with gloss when using rendered stimuli; however, the standard deviation, a measure of contrast, correlated better with perceived gloss when using photographs of natural surfaces. Finally, the study verified the key role of contrast by manipulating the skewness and contrast within images. However, these assessments did not apply to halftone images.

In the past few decades, a variety of proposed full-reference image quality assessment (IQA) methods have provided a better account of human perception than

the mean squared error, and the structural similarity (SSIM) index [8] has become a standard in the image processing field. In contrast to the above methods of using a single strategy for IQA, [59], [60], [61] used multiple strategies for IQA. These authors suggested that a single strategy may not be sufficient for IQA; on the contrary, the human visual system (HVS) determined the image quality through the interaction of multiple strategies. However, although the proposed methods simulated the HVS as much as possible, owing to their limitations, these methods could not be applied to the assessment of halftone images.

To evaluate the glossiness of objects in halftone images, the isolated dots in halftone images should be processed first. The dot process is a proposed method for material printing [62] [63]. However, the method only searches for the inter-dot relationship measurement, spectral characteristics between dots, and the image spatial characteristics. Lee and Horiuchi [64] proposed an innovative halftone IQA approach for color images. HVS characteristics were applied to the proposed method, which used color spatial HVS filters for luminance, red-green, and blue-yellow components. This model effectively measured color distortion consistent with that of a human observer. However, the index evaluated "image quality" and could not be used to evaluate the gloss of an object.

Here, this chapter present a fully referenced image glossiness index for halftone color images. Instead of treating image distortions in the same way, the proposed method assume that they are decoupled into two groups: structural dissimilarity (SDSIM) and appearance perception, which would be correlated in diverse ways with visual non-glossiness and glossiness perception.

4.2 Halftone Image Assessment Methods

Given a distorted image, humans can easily rate image quality. To eliminate the shortcomings of evaluation due to human observers, many researchers have focused on the assessment of computational models based on HVS [65] [66] [67]. The image quality metrics developed for traditional images are usually meant for multi-level (8-bit) images; hence, they cannot be applied directly to 1- or 2-bit discrete images. To overcome this issue, it is necessary to devise a process (e.g., a visual filter) to increase gradation.

To the best of our knowledge, the earliest halftone assessment index was proposed by Näsänen [68]. Näsänen's method used an exponential function for the luminance component to evaluate a dithering halftone image. Later, Lee et al. proposed a new exponential function for evaluating halftone color images [64]. To consider the visual color characteristics, they performed a new function for each luminance, red-green, and blue-yellow components. Then, the color SSIM was applied to the reference and distorted images for the purpose of localized structural difference assessment. The index in [64] is useful for non-gloss images because their approach is based on SSIM, so it is effective for non-gloss objects with rich structural information. If there is

an object like a mirror, for single strategy index, they work well on all parts of the glossy object that reflect the environment surrounding it. However, for gloss objects, the proposed methods would fail because the glossy part contains little structural information. Therefore, to realize the correct assessment of an image, which contains glossy and non-glossy parts objectively, a single assessment strategy could not meet this demand.

In contrast to single-strategy image assessment methods, studies in Refs. [59] [60] [61] used a variety of strategies to simulate HVS closely for image assessment. In [69], instead of treating the image distortions equally, they proposed treating distortions as linear frequency distortions and additive noise degradations. However, this algorithm only focused on the halftone artifacts. Also, the methods proposed in [60] did not solve the problem of combining the separated distortion measurement. Based on [69], they proposed two simple quality measures; i.e., the detail loss measure and the additive impairment measure, and developed a method of adaptively merging two strategies. In [59], it was assumed that the HVS determined the image quality by performing different strategies and modeled them together using trained parameters. To solve the texture resampling low tolerance problem for the image assessment index. Ding et al. designed a monotonous and differentiable function using a CNN. Through this function, the image was transformed into a multi-scale representation [61]. Then, IQA metric that mixed correlations of texture similarity and correlations of structure similarity was developed.

Inspired by these strategies, this study develops an image glossiness index for halftone color images based on structure and appearance distortion.

4.2.1 Structural Similarity Measure (SSIM)

Z.Wang et al. proposed the image quality assessment index SSIM [8]. The index is designed based on the HVS hypothesis which is that the HSV highly depends on the extracted structure information when processing the information from image. The SSIM compares the normalized pixel intensities between the reference image and the distorted image, which are derived from local brightness and contrast. The brightness of the surface of the observed object comes from the product of reflection and illumination, but the structure of the object has no corresponding relationship with the illumination in the scene. Since the distribution of luminance and contrast of objects may be uneven in the whole scene, SSIM uses the concepts of local luminance and local contrast considering that the whole scene will affect the calculation results. Let x and y represent the reference image and the distorted image respectively, and the two images have been aligned. Let μ_x, μ_y, σ_x^2, σ_y^2 and σ_{xy} be the mean of signal x, the mean of signal y, the variance of signal x, the variance of signal y, and the

covariance of signal x and signal y.

$$\mu_x = \frac{1}{N}\sum_{i=1}^{N} x_i \tag{4.1}$$

$$\mu_y = \frac{1}{N}\sum_{i=1}^{N} y_i \tag{4.2}$$

$$\sigma_x = \left(\frac{1}{N-1}\sum_{i=1}^{N}(x_i - \mu_x)^2\right)^{\frac{1}{2}} \tag{4.3}$$

$$\sigma_y = \left(\frac{1}{N-1}\sum_{i=1}^{N}(y_i - \mu_y)^2\right)^{\frac{1}{2}} \tag{4.4}$$

$$\sigma_{xy} = \frac{1}{N-1}\sum_{i=1}^{N}(x_i - \mu_x)(y_i - \mu_y) \tag{4.5}$$

where x_i, y_i are mean the pixels from reference image x and distorted image y, respectively. Here, the mean and standard deviation of a signal are roughly regarded as the estimated values of signal luminance and contrast. Covariance can be considered as measuring the degree of nonlinear change between one signal and another signal being compared. The definition of luminance, contrast and structure similarity measures can be defined as [8]:

$$l(x,y) = \frac{2\mu_x\mu_y + C_1}{\mu_x^2 + \mu_y^2 + C_1} \tag{4.6}$$

$$c(x,y) = \frac{2\sigma_x\sigma_y + C_2}{\mu_x^2 + \mu_y^2 + C_2} \tag{4.7}$$

$$s(x,y) = \frac{\sigma_{xy} + C_3}{\sigma_x\sigma_y + C_3} \tag{4.8}$$

C_1 and C_2 represent two constants, which are defined by C_1=$(K_1R)^2$, C_2=$(K_2R)^2$ and C_3=$C_2/2$ where R is the dynamic range of a pixel, and constants K_1=0.01 and K_2=0.03 must be small so that C_1 and C_2 will start to work only when (μ_x^2+μ_y^2) or (σ_x^2+σ_y^2) is small enough. When (μ_x^2+μ_y^2+C_1)(σ_x^2+σ_y^2+C_2)$\neq$ 0 is satisfied, the measured similarity between x and y is given as follows:

$$SSIM(\boldsymbol{x},\boldsymbol{y}) = [l(\boldsymbol{x},\boldsymbol{y})]^{\alpha} \cdot [c(\boldsymbol{x},\boldsymbol{y})]^{\beta} \cdot [s(\boldsymbol{x},\boldsymbol{y})]^{\gamma} \tag{4.9}$$

where $\alpha \geq 0$,$\beta \geq 0$ and $\gamma \geq 0$ are parameters used to adjust the relative importance of the three components. To simplify, in this case, $\alpha = \beta = \gamma$ is set to 1. Finally, the SSIM index specific form is defined as [8]:

$$SSIM(\boldsymbol{x},\boldsymbol{y}) = \frac{(2\mu_x\mu_y + C_1)(2\sigma_{xy} + C_2)}{(\mu_x^2 + \mu_y^2 + C_1)(\sigma_x^2 + \sigma_y^2 + C_2)} \tag{4.10}$$

The SSIM index meets the following conditions:

1. Symmetry: $SSIM(x, y) = SSIM(y, x)$
2. Roundedness: $SSIM(x, y) \leq 1$
3. Unique maximum: $SSIM(x, y) = 1$ if and only if $x = y$ (if it is a discrete scene, $x_i = y_i$ for all pixel indices $i = 1, 2, \ldots, N$).

the SSIM indexing method is applied for quality assessment of image using a sliding window approach. The window size is fixed to be 8×8 pixels. The Gaussian weight (11×11, $\sigma = 1.5$) within the window is applied to the image in the spatial domain. The SSIM indices are calculated within the sliding window, which moves pixel by pixel from the top-left to the bottom-right corner of image. The overall quality value, *Mean SSIM* (MSSIM), is defined as follows [8]:

$$MSSIM(\boldsymbol{x}, \boldsymbol{y}) = \frac{1}{M} \sum_{k=1}^{M} SSIM(x_k^{window}, y_k^{window}) \tag{4.11}$$

where x and y are defined as the reference and the distorted image. x_k^{window}, y_k^{window} are the contents of image at the position of kth local window. M is the local windows number of the image.

4.2.2 Most Appearance Distortion Measure (MAD)

The most apparent distortion (MAD) method was proposed by Larson [59]. In this paper, the author uses two strategies for distortion detection: the first strategy is based on high-quality image detection strategy, which uses the mean squared error (MSE) to calculate the distortion of visibility. The MSE is the simplest and most widely used full-reference quality metric, which is computed by averaging the squared intensity differences of distorted and reference image pixels. The second detection strategy is based on appearance distortion. The strategy uses standard deviation, skewness and kurtosis to calculate the distortion of low-quality images.

High Quality Images: Detection-Based Strategy

When HVS processes high-quality images, it is assumed that HVS is trying to find the distortion in the image to judge the image quality. In order to simulate the detection characteristics of the visual system, the distortion in this case is modeled. In this process, in order to simulate the perceived distortion, the local mean square error (MSE) is calculated in the lightness domain. In order to simulate the distortion perceived by the visual system, it is also combined with the spatial domain model of local masking.

The low-level psychophysical characteristics of human visual system, such as spatial contrast sensitivity function, nonlinear perception of brightness and brightness

and contrast masking, are used to calculate the position of visible distortion map. Next, the visibility map is used to calculate the visibility weighted local MSE map. Finally, the distortion perceived by the visual system is estimated by superimposing the visibility weighted local MSE map. The perceived distortion is defined as:

$$d_{detect} = \left\{ \frac{1}{P} \sum_{p} [\xi(p) \times D(p)]^2 \right\}^{\frac{1}{2}} \tag{4.12}$$

the summation means all the blocks of an image and P is the total blocks of an image. The local distortion map $\xi(p)$ is calculated by local contrast maps.$D(p)$ is defined as the local MSE for each block, the size of each block is set to 16×16.

Low Quality Images: Appearance-Based Strategy

When HVS processes low-quality images, visual masking is assumed to be less important in the quality of perceived images, that is, HVS uses a different way from the perception mechanism of high-quality images. That is, the degree of image appearance can be reduced by quantifying distortion, and the perceived distortion can be better simulated. Therefore, HVS changes from the strategy of detecting distortion in high-quality areas to the strategy of judging image appearance in low-quality image.

4.2.3 Perceived Texture Assessment of Halftone Image

Although SSIM and MAD have great advantages in the assessment of general images, but they cannot be directly used in the evaluation of color halftone images. Therefore, if we want to make full use of their advantages, we need to fuse and improve them. At the same time, in order to consider the influence of color on perceived texture, the proposed algorithm models the appearance distortion perceived by the visual system after fully considering the visual characteristics of HVS, combined with structural similarity and appearance assessment strategy. The proposed algorithm considers the influence of the distortion of color, structure information and appearance, and more realistically simulates the evaluation process of human observers on halftone images.

4.3 Color Image Similarity and Appearance Measure (CSAM)

4.3.1 Visual Perceptual Model

Color Space Conversion

The RGB images were transformed to CIEXYZ, and then to CIELab color space, which is a special set of tristimulus values used for transforming between XYZ and

RGB. Define L^*, a^* and b^* as Y_y, C_x and C_z for the convenience of the equation, respectively. X_n, Y_n and Z_n are tristimulus values with the D65 white point.

$$Y_y = L^* = \begin{cases} 116 \cdot (\frac{Y}{Y_n})^{\frac{1}{3}} - 16 & for \quad Y/Y_n > 0.008856 \\ 903.3 \cdot (\frac{Y}{Y_n}) & otherwise \end{cases} \tag{4.13}$$

$$C_x = a^* = 500 \cdot \left(f\left(\frac{X}{X_n}\right) - f\left(\frac{Y}{Y_n}\right)\right) \tag{4.14}$$

$$C_z = b^* = 200 \cdot \left(f\left(\frac{Y}{Y_n}\right) - f\left(\frac{Z}{Z_n}\right)\right) \tag{4.15}$$

$$where \quad f(t) = \begin{cases} t^{\frac{1}{3}} & for \quad t > 0.008856 \\ 7.787 \cdot t + \frac{16}{116} & otherwise \end{cases} \tag{4.16}$$

Color Space Conversion: Linearized Uniform Color Space

The nonlinear transformation from CIEXYZ tristimulus value to CIELAB value is cascaded with the linear transformation from RGB image coordinates to CIEXYZ tristimulus value, which will not retain the spatial average tone of the image, so it is not desirable in halftone color reproduction. Therefore, Flohr et al. [70] linearized the CIELab color space of the reference stimulus (X_n, Y_n, Z_n). The linearized CIELab color space is obtained by linearizing the CIELAB space around the D65 white point as:

$$Y_y = 116 \cdot \frac{Y}{Y_n} - 16 \tag{4.17}$$

$$C_x = 500 \cdot \left(\frac{X}{X_n} - \frac{Y}{Y_n}\right) \tag{4.18}$$

$$C_z = 200 \cdot \left(\frac{Y}{Y_n} - \frac{Z}{Z_n}\right) \tag{4.19}$$

The component Y_y is proportional to the luminance. The components C_x and C_z are similar to the components R-G and B-Y opponent color chrominance [71]. The original transformation from CIEXYZ to CIELAB is nonlinear. The nonlinearity in CIELAB transform will distort the spatial average tone of the image, resulting in halftone with incorrect average value [70]. The linearized color space overcomes this and has the additional advantage that it decouples the effects of incremental changes in (Y_y,C_x,C_z) at the white point on the value of (L,a,b):

$$\nabla_{(Y_y,C_x,C_z)}(L_*, a_*, b_*) \mid_{D65} = \frac{1}{3} I \tag{4.20}$$

where I is the identity matrix.

Contrast Sensitivity Function

The following exponential function was used for the luminance contrast sensitivity function.

$$W_{(Y_y)}(\widetilde{\rho}) = K(L)e^{-\alpha(L)\widetilde{\rho}} \tag{4.21}$$

$$K(L) = aL^b \tag{4.22}$$

$$\alpha(L) = \frac{1}{c\ln(L) + d} \tag{4.23}$$

the luminance for an image was represented by $L[cd/m^2]$, ρ (cycles/degree) was the spatial frequency, and a = 131.6, b = 0.3188, c = 0.525, d = 3.91. In contrast to Näsänen's model, $\widetilde{\rho}$ was defined as the weighted magnitude of $\rho = (u, v)$:

$$\rho = \sqrt{u^2 + v^2} \tag{4.24}$$

$$\phi = \arctan\left(\frac{v}{u}\right) \tag{4.25}$$

$$s(\phi) = \frac{1-\omega}{2}\cos 4\phi + \frac{1+\omega}{2} \tag{4.26}$$

$$\widetilde{\rho} = \frac{\rho}{s(\phi)} \tag{4.27}$$

the value of ω was set to 0.7. $s(\phi)$ is a weight function. At odd multiples of 45°, this function reduced the contrast sensitivity to the components of the spatial frequency. Comparing the sensitivity of human observers to spatial variations in luminance and to spatial variations in chromaticity, it was found that the latter decreased faster as the spatial frequency increased. The HVS chrominance model used here was based on Mullen's [71]. The chromaticity CSF function was approximated by the following exponential function:

$$W_{(C_x,C_y)}(\rho) = Ae^{-\alpha\rho} \tag{4.28}$$

the parameters α and A were set to 0.419 and 100 for the chrominance component.

Using a chromaticity response model that was different from the above luminance resulted in low-frequency chromaticity errors, which were difficult to perceive by the HVS. Figure 4.1 shows two different frequency response models, which represent the luminance and chromaticity response models.

4.3.2 Color Image Similarity and Appearance Measure (CSAM)

Based on the idea of MAD algorithm, the proposed algorithm also evaluates the gloss of the image through two strategies. In the first strategy, removing the HVS processing in the first strategy of MAD, and use SDSIM replace MSE to calculate the distortion of visibility. In the second strategy, only use the standard deviation and skewness related to gloss perception to calculate the appearance distortion. In addition, a new HVS filter used to preprocess the image. Finally, the adaptive method

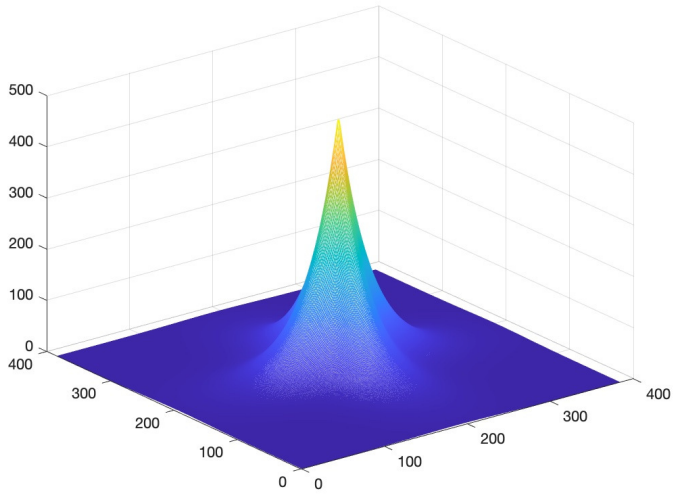

(a)

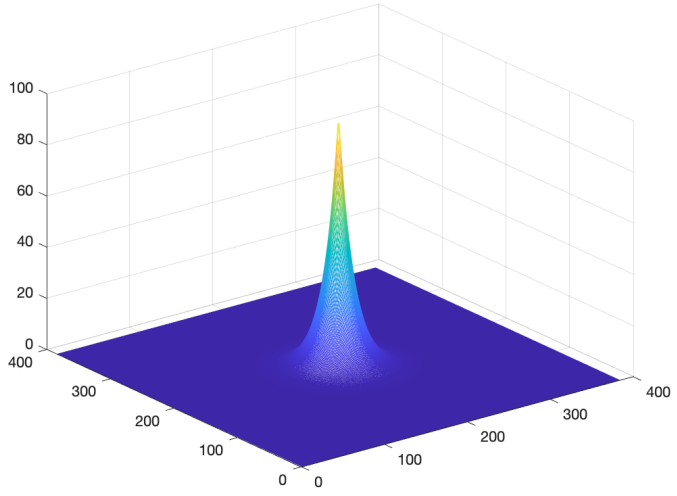

(b)

Figure 4.1 (a)luminance frequency response model. (b) chrominance frequency response model.

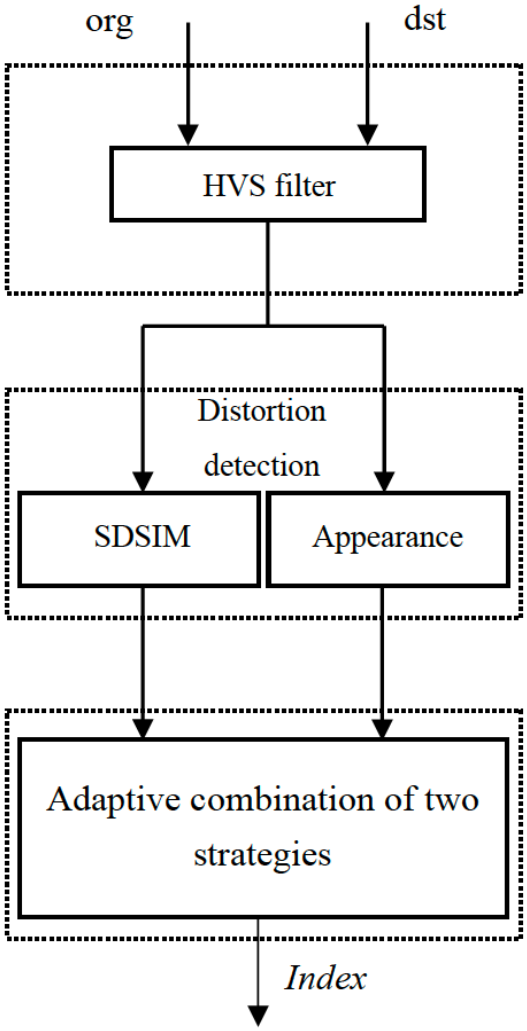

Figure 4.2 Flowchart of the proposed CSAM

proposed in MAD is used to merge two strategies. The details are presented in the following subsections. First, this section explain the near-threshold distortions using a method for quantifying perceived distortion, which was used to model the HVS detection. Second, the suprathreshold distortion, which was used to model HVS statistical characteristics. Third, using a parametric method to combine the two modeled perceptual distortions; thereby, achieving a single perception of overall distortion. Figure 4.2 presents a flowchart of the proposed algorithm.

A color HVS model takes into account the correlation among color planes. The HVS model is based on a transformation to the linearized uniform CIELab color space and exploits the spatial frequency sensitivity variation of the luminance and chrominance channels. Finally, the SSIM process without Gaussian spatial filtering (11×11, $\sigma = 1.5$) is carried out to assess the color halftone image.

Structural dissimilarity Measure for Color Image

Using the visible distortion location calculation method proposed in the MAD, except not to conduct the CSF filter. Only using perceived luminance and contrast masking methods in the high-quality assessment of MAD. Calculation of the locations of visible distortion

Let I_{org} and I_{dst} represent the reference and halftone images, respectively, both of which were processed by the HVS filter.

Perceived luminance: The reference and distorted images were transformed to luminance images via:

$$L = (b + kI)^{\gamma} \tag{4.29}$$

where L represents the luminance image and the parameters b = 0, k = 0.02874, and $\gamma = 2.2$. L_{org} and L_{dst} were calculated using the above equation. To consider the HVS nonlinear response to luminance, L_{org} and L_{dst} were transformed to luminance perception images $\hat{L}_{org}$ and $\hat{L}_{dst}$ via:

$$\hat{L} = \sqrt[3]{L} \tag{4.30}$$

$\hat{L}_{err} = \hat{L}_{org} - \hat{L}_{dst}$ is defined as the error image.

Contrast masking: This masking explained the fact that image presence reduced the distortion detectability. First, the original image was divided into several 16×16 blocks; The change in the block size changed the average contrast of each block. The local contrast map corresponding to each block was calculated. Second, calculating the root mean square (RMS) contrast for each block. The RMS contrast for block p of I_{org} was calculated as:

$$C_{org}(p) = \widetilde{\sigma}_{org}(p)/\mu_{org}(p) \tag{4.31}$$

where the mean value of block p is $\mu_{org}(p)$, and $\widetilde{\sigma}_{org}(p)$ is calculated from the standard deviations of the four sub-blocks of p. $C_{org}(p)$ represented the local RMS contrast measurement of the original image, which was separated from the distortion of the image. Then, a local contrast map was calculated for the error image, which explained the distorted spatial distribution of the distorted image. In addition, I_{err} was divided into 16×16 blocks, corresponding to the original image I_{org}. Each block's RMS contrast $C_{err}(p)$ was calculated via:

$$C_{err}(p) = \begin{cases} \sigma_{err}(p)/\mu_{org}(p) & if \quad \mu_{org}(p) > 0.5 \\ 0 & otherwise \end{cases} \tag{4.32}$$

where $\sigma_{org}(p)$ represents the standard of block p in I_{err}. The lightness threshold of 0.5, which explained why the HVS is insensitive to variations in dark regions. Finally, $C_{org}(p)$ and $C_{err}(p)$ are used to calculate the local distortion visibility map $\xi(p)$:

$$\xi(p) = \begin{cases} \ln C_{err}(p) - \ln C_{org}(p) & \text{if} \quad \ln C_{err}(p) > \ln C_{org}(p) > \delta \\ \ln C_{err}(p) - \delta & \text{if} \quad \ln C_{err}(p) > \delta > \ln C_{org}(p) \\ 0 \quad otherwise \end{cases} \tag{4.33}$$

specifically, $\xi(p)$ reflected the amount by which the contrast of the error was larger than the contrast of the original image, if their contrast was greater than the threshold ($\delta = -5$).

The combination of local structure errors and visibility map. After calculating the visible location map, using visibility-weighted local $SDSIM$, which is used in the lightness domain to obtain the distortion of the perceived structure. The $MSSIMMap$ is the $MSSIM$ distribution map of one image, $SD(p)$ is calculated from the $MSSIM$ mapping as follows:

$$SD(p) = \frac{1}{16^2} \sum_{i,j \in N_p} MSSIMMap^2 \tag{4.34}$$

where quantity $SD(p)$ represents the local $SDSIM$ calculated for each 16×16 block p. N_p is the set of pixels inside block p, i and j is the position of the pixel (i, j) in block p. $MSSIM$ is the mean of $SSIM$, which proposed in [8]:

$$MSSIM(m, n) = \frac{1}{M} \sum_{j=1}^{M} SSIM(x_j, y_j) \tag{4.35}$$

where m and n represent the original and halftone images. x_j and y_j are the image contents at the local window of jth; and M is the total number of local windows. Therefore, the perceived distortion d_{sdsim} was computed by:

$$d_{sdsim} = \left\{ \frac{1}{P} \sum_{p} [\xi(p) \times SD(p)]^2 \right\}^{\frac{1}{2}} \tag{4.36}$$

Eq. 4.36 represents a single value calculated from the visibility-weighted local $SDSIM$ by using the L_2 norm, which represented the sum of the visual structure of image distortion. $d_{sdsim} = 0$ meant that the distortion in the distorted image would not be perceived by the visual system; i.e., it was not visible. The larger the value of d_{sdsim}, the greater the distortion perceived. Figure 4.3 shows the images of the maps involved in the d_{sdsim} computation for a halftone image. Figure 4.3(a) and Figure 4.3(b) show the original and halftone images, respectively.

These figures showed the calculated visibility map, local $SDSIM$ map, and visibility-weighted local $SDSIM$ map. In Figure 4.3(c), the visibility map captured visible artifacts. In Figure 4.3(d), the local $SDSIM$ indicated that the greatest distortions appeared in the regions of greatest energy, so the distortions in these regions were invisible. As Figure 4.3(e) shows, the visibility-weighted local $SDSIM$ map had a better performance in predicting the locations and perceived visible intensities of distortions.

Appearance Distortion Measure for Color Image

When an image is of low quality, visual masking is less important for image quality judgment; on the contrary, when the image distortion exceeds the threshold, the degree of quantification of the distortion to reduce the appearance of the image subject

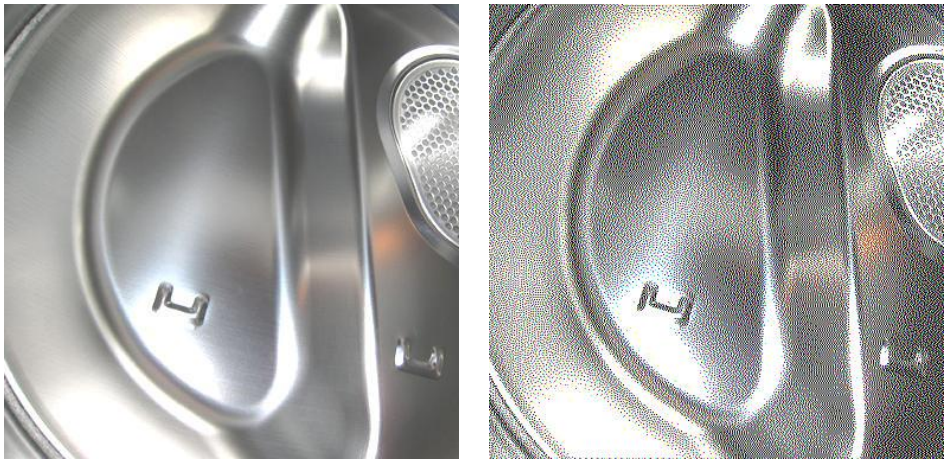

(a)

(b)

(c)

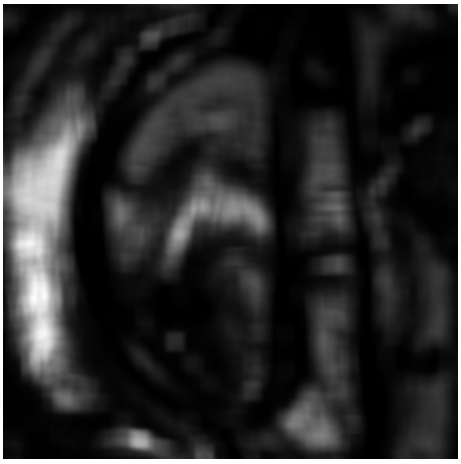

(d)

(e)

Figure 4.3 (a) original image, (b) Floyd, (c) visible map, (d) SDSIM, (e) perceived distortion.

can better simulate the visual system perceived distortion. Therefore, in this type of distortion, the HVS's judgment on the image was switched to a judgment based on the appearance of the image.

To model this appearance perception mechanism of the visual system, a method based on local statistics was developed, which used a multiscale log-Gabor filter response for statistical calculation. The use of this type of statistical model to capture the appearance of texture has been used in various image processing studies. In addition, existing research showed that log-Gabors better simulated and model simple cells in the primary visual cortex. In the processing of texture, the change in pixel-based statistics was less obvious than that in the log-Gabor filter response-based statistics.

Both original and halftone images are first transformed into a set of sub-bands using a log-Gabor filter bank. By calculating the inverse DFT of the product of the image DFT and the following two-dimensional frequency response, filtering for obtaining sub-bands are performed in the frequency domain.
The original image and the halftone image are decomposed by log-Gabor by multiplication in the frequency domain. $\{\acute{c}_{s,o}\}$ represents the set of log-Gabor sub-bands calculated for either the original or halftone image; here, each sub-band $\acute{c}_{s,o} \in \mathbb{R}_{M\times N}$ has the size of the images. The log-Gabor decomposition is calculated using five scales $s = 1, ..., 5$, and 4 orientations $o = 1, ..., 4$; thus, each image has 20 sub-bands. This decomposition is applied to both filtered original image I_{org} and the halftone image I_{dst} to obtain the sub-band sets $\{\acute{c}^{org}_{s,o}\}$ and $\{\acute{c}^{dst}_{s,o}\}$.

By comparing the local sub-band statistics of the original image with the corresponding local sub-band statistics of the distorted image, the local statistical difference map $\eta(p)$ was computed. For each 16×16 block, the difference in standard deviation and skewness of the corresponding sub-band coefficients of the block were calculated as:

$$\eta(p) = \sum_{s=1}^{5}\sum_{o=1}^{4} w_s[|\sigma^{org}_{s,o}(p) - \sigma^{dst}_{s,o}(p)| + |\varsigma^{org}_{s,o}(p) - \varsigma^{dst}_{s,o}(p)|] \tag{4.37}$$

where $\sigma_{s,o}(p)$ and $\varsigma_{s,o}(p)$ represent the standard deviation and skewness of the 16×16 sub-band coefficients corresponding to scale s and orientation o, respectively, and corresponded to block p at a certain location. The fixed scale weights $w_s = 0.5, 0.75, 1, 5$, and 6 are used to explain that the HVS preferred coarse scales rather than fine scales. The final scalar value of the perceived distortion is given as:

$$d_{appearance} = \left[\frac{1}{P}\sum_{p}\eta(p)^2\right]^{\frac{1}{2}} \tag{4.38}$$

where the summation is for all blocks and P represents the total number of blocks. $d_{appearance} = 0$ meant no distortion perceived, and an increase in the $d_{appearance}$ value indicates an increase in perceived distortion, which reduces visual quality.

Adaptive Combination of Two Strategies

The adaptive combination method is based on the study in [59] that the observer intends to interactively judge low-quality and high-quality images. To realize the interaction between the two strategies, the weighted geometric mean is used for operation. Here, the proposed index d_{sdsim} and $d_{appearance}$, given by:

$$Index = (d_{sdsim})^{\alpha}(d_{appearance})^{1-\alpha} \tag{4.39}$$

here, α is computed via:

$$\alpha = \frac{1}{1 + \beta_1(d_{sdsim})^{\beta_2}} \tag{4.40}$$

the parameters β_1 and β_2 were provided in [59], they found that selecting α according to d_{sdsim} can have a good result. For the database of A57 image database [72], the optimization values of these parameters through training are $\beta_1 = 0.467$ and $\beta_2 = 0.130$.

4.4 Experimental Results & Discussion

The proposed algorithms were implemented using MATLAB (R2021a) running on the Mac OS. The experiments were conducted using 100 images from the Flickr Material Database [73]. The selected images included not only pure glossy and non-glossy images, but also images that contained both glossy and non-glossy parts, such as images containing textured leaves and water drops. Figure 4.4 to Figure 4.7 shows the partial glossy and non-glossy images. Based on the above images, subjective and objective experiments were conducted, respectively. Then, calculating the correlation between them. To verify the correlation between them, ranking the observers' scores from high to low, and the corresponding objective scores were automatically ranked. Then, the 50 data pairs with the highest subjective score as the score of the non-glossy image, and the other 50 data pairs as the score of gloss images.

For comparison, selecting several halftone algorithms to process selected 100 images. These algorithms included three different halftone algorithms: dithering [28], Floyd [26], and direct binary search (DBS) [74]. These different processing data were treated as three diverse types of distorted images. Different halftone technologies often produced different halftone effects. Processing the color image by using color separation where a RGB image is divided into separate R, G and B components with sRGB. After being processed by the halftone algorithm the components are finally synthesized into an RGB image. In this process, the RGB color space is used. It was believed that the ED halftone reproduced more details of the original image than the dithering algorithm. Therefore, the distortion effect of the ED algorithm was less than that of the dithering halftone algorithm. Figure 4.8 and 4.9 shows an example of the application of each algorithm to the enlarged images. The size of the images is 384 $\times$ 384 pixels. The error diffusion and dithering halftone dots occupy 1 pixel

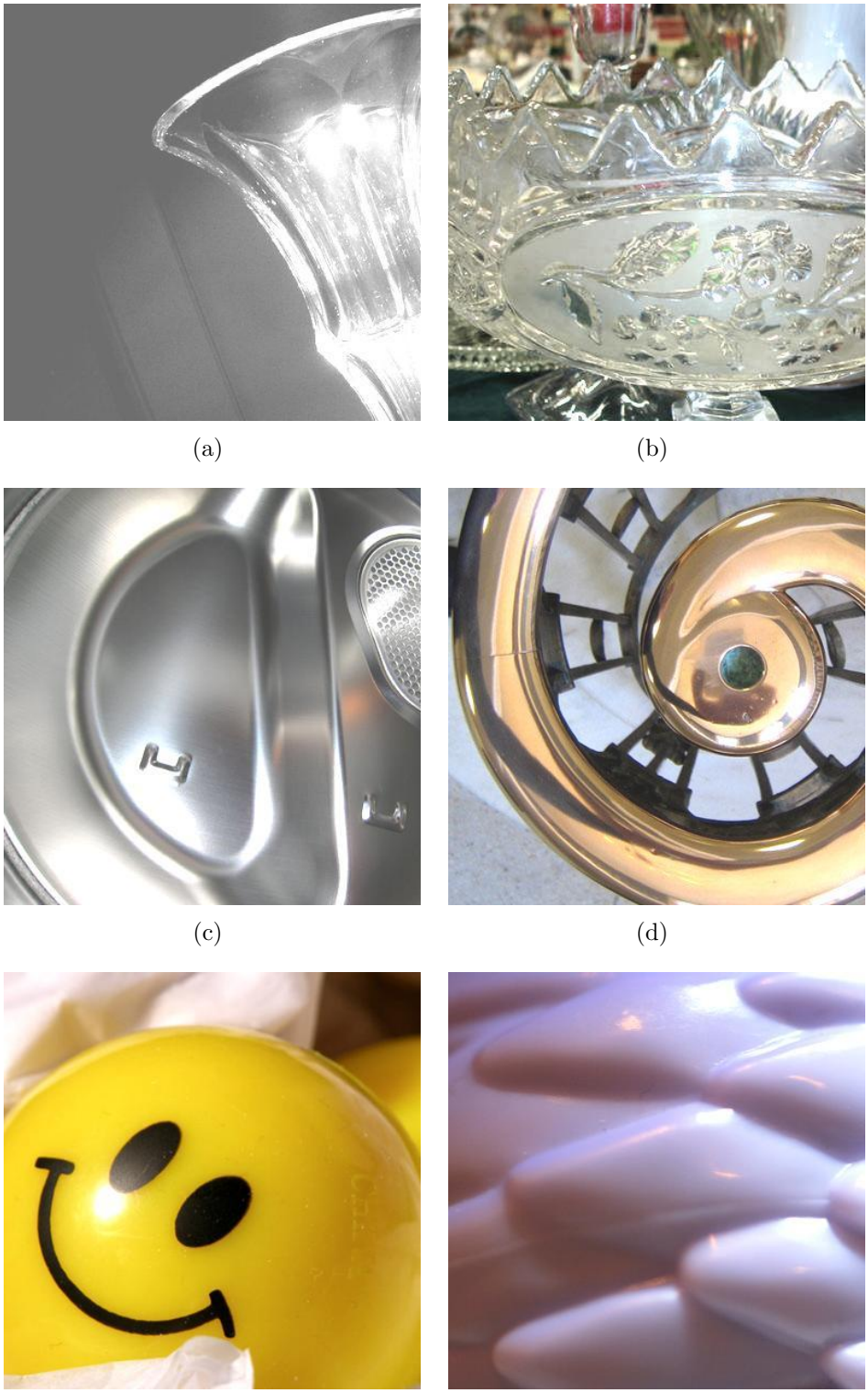

(a) (b)

(c) (d)

(e) (f)

Figure 4.4 Gloss images.

(a) (b)

Figure 4.5 Gloss images.

and 4 × 4 pixels respectively. In dither halftoning the dot size determines the image quality of halftone, and final affects the printed image. Too large dot size will cause the image losing too many details, and also affect the output effect of printer. Too small dot size will appear regular fence phenomenon, reducing the image quality.

In the actual printing process, various effects (e.g., dot gain) occur, depending on the characteristics of the paper. They can be perceived differently depending on lighting effects. Therefore, it is difficult to isolate how these effects impact the subjective evaluation of the printed material. Therefore, this research evaluated the digital data presented on the display device. The original image and the halftone image were displayed simultaneously, and the observer scored them. Observers were asked to assign a score from 0 to 100 for each test image pair. The viewing distance was designed to be equivalent to the retinal image of a 600 dpi at 24 cm. Five observers participated in a subjective observer experiment with normal vision.

4.4.1 Subjective Assessment

There are five students (three males and two females; age 27.2 ± 6.65) participated in the experiment. One student (the author) had significant experience with the subjective assessment of printing image quality. The other 4 students were all non-experts in printing and image quality assessment. All students were screened prior to participation for normal, or corrected to normal, visual acuity and normal color vision. Image pairs were presented on the display for a duration of 10s. A reference image and a halftone image are placed on the left and right respectively. Observers were given instructions to judge the reproduction of objects' glossiness in images and to provide corresponding scores. After observing an image pair, observers were asked to provide corresponding scores to the image pair using a continues horizontal scale as

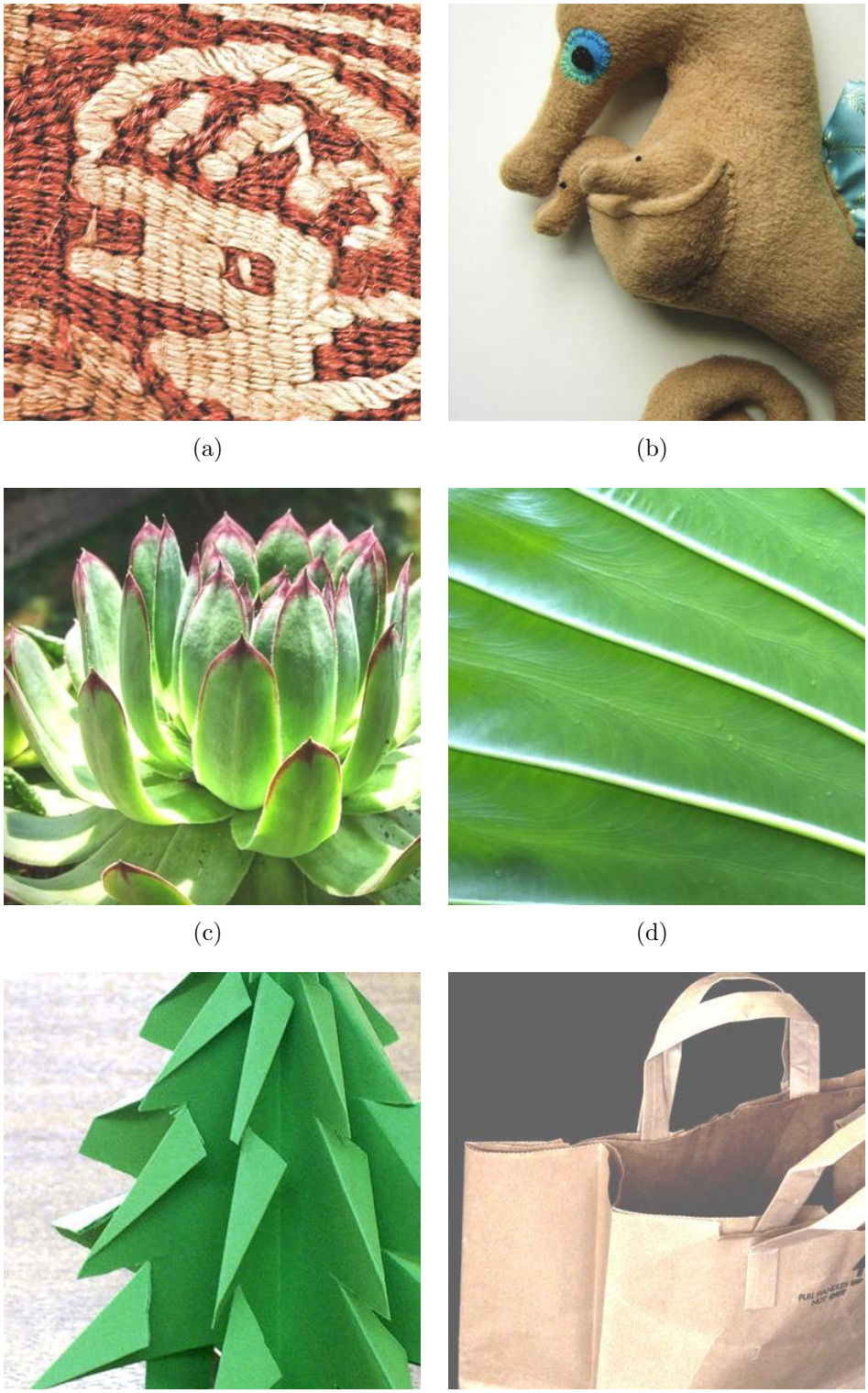

(a) (b)

(c) (d)

(e) (f)

Figure 4.6 Non-gloss images .

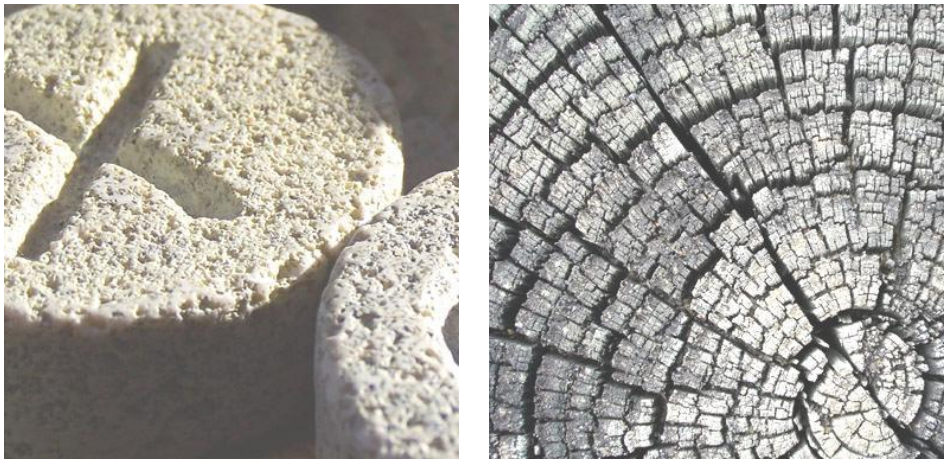

(a) (b)

Figure 4.7 Non-gloss images .

depicted in Table 4.1. The scores corresponding to the above interval are 100, 80, 60, 40, 20 and 0 respectively. Scores ranged from 100 to 0 using a continues horizontal scale, with 0 representing poor reproduction and 100 representing objects that were most similar to the original image.

Table 4.1 Rating scale used in subjective experiment.

MOS	Quality	Meaning
100-80	Excellent	Imperceptible, Fully matched with the reference
80-60	Good	Perceptible but not annoying
60-40	Fair	Slightly annoying
40-20	Poor	Annoying
20-0	Bad	Very annoying, Fully unmatched with the reference

To assess the consistency made by 5 observers measuring the same quality, calculating the interclass correlation coefficient (ICC) for the inter-observer consistency. ICC is a descriptive statistic that can be used when quantitative measurements are made on units that are organized into groups. It describes how strongly units in the same group resemble each other. Based on 100 images of each halftone, repeating the subjective experiment for each image pair with 5 observers, the data analyzed using a single-measurement, absolute-agreement, 2-way mixed-effects model. For the different halftones, ICC report is summarized as Table 4.2.

As shown in the Table 4.2, the test-retest reliability of subjective experiment is "moderate" and "good".

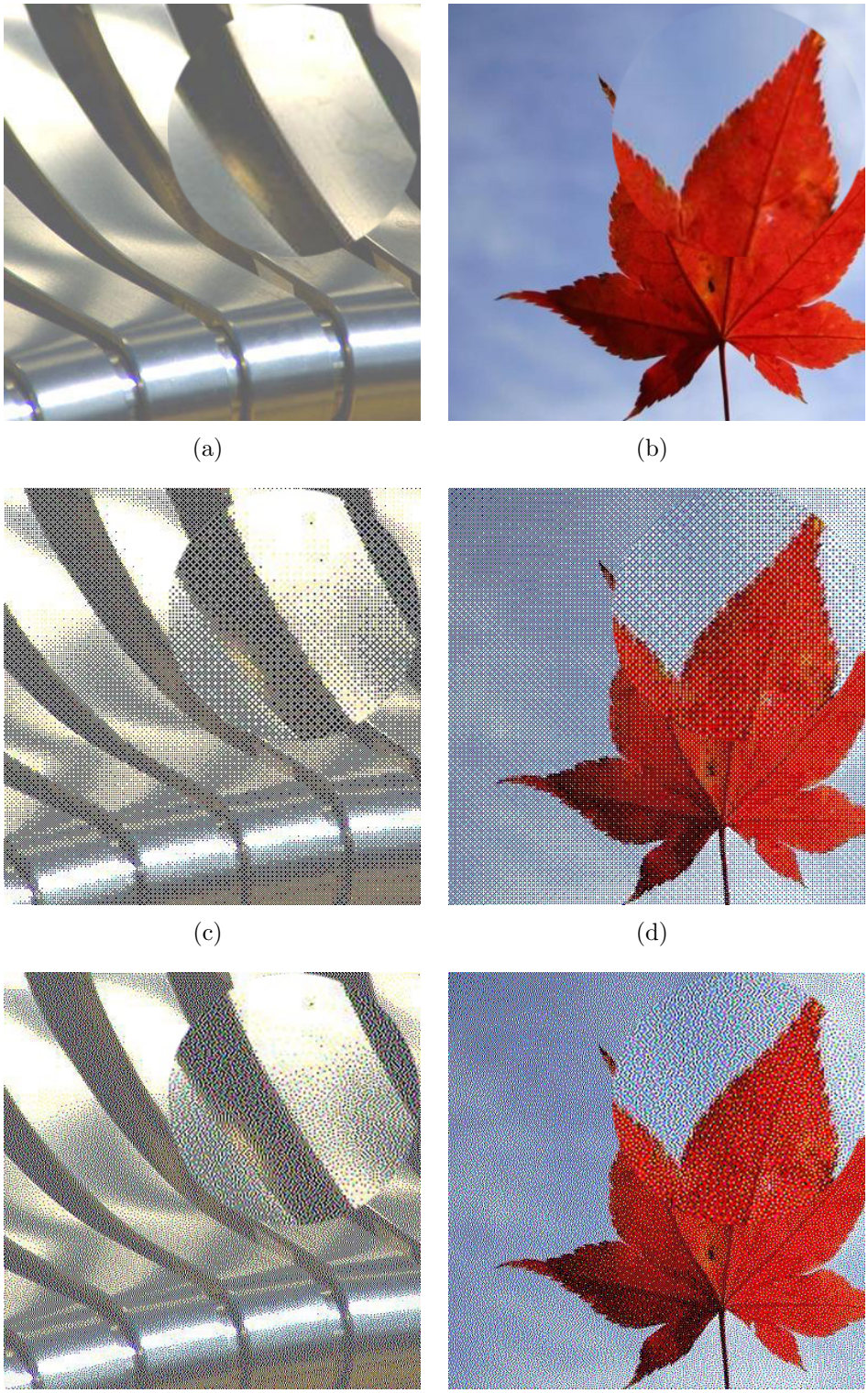

Figure 4.8 Examples of samples. Left and right images show gloss and non-gloss images, respectively: (a and b) original images, (c and d) halftone images by dithering, (e and f) halftone images by Floyd, (g and h) halftone images by DBS.

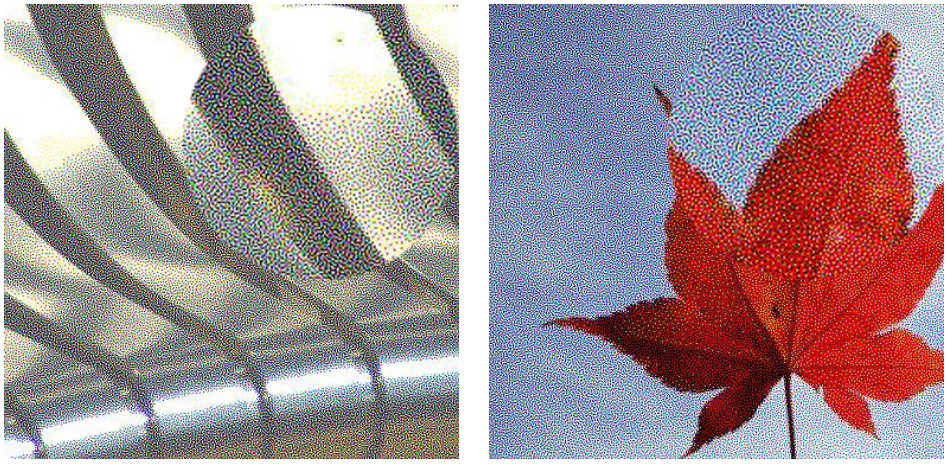

(a) (b)

Figure 4.9 Examples of samples. Left and right images show gloss and non-gloss images.

Table 4.2 ICC and 95% confident interval for different halftone.

Halftone	**ICC**	**95% confident interval**
Dithering	0.78	0.72-0.84
Floyd	0.82	0.74-0.85
DBS	0.85	0.76-0.87

4.4.2 Objective Assessment

For comparison, several image were selected to evaluate algorithms for the experiments. Calculating the peak signal-to-noise ratio (PSNR), color structural similarity (CSIM) [64], MAD [59], and the proposed index to compare the correlation between the results of each index and the subjective observer score. The normalized index values for MAD and the proposed method because the indexes belonged to $[0, \infty]$.

4.4.3 Results and Discussion

The Pearson correlation coefficient (PCC) was the most common measure of predictive performance. Here, using PCC to calculate the correlation between the observer scores and objective index values. To distinguish the effects of metrics on glossy and non-glossy images, sorting the subjective data in descending order, and the objective data were sorted accordingly. The first 50 images of the arranged data were classified as non-glossy images, and the rest were classified as glossy images. The former was represented by red points, the latter by blue dots. Figure 4.10, 4.11 and 4.12 are the scatter plot based on the dither, Floyd and DBS halftone, the vertical axis represents the subjective ratings of the perceived distortions, and the horizontal axis represents

the metrics. In all graphs, each point represented a test image. Figure 4.13 shows the error bar of subjective score based on Floyd form 5 observers. As the Figures show, the proposed index evaluated the glossiness correctly compared to other indices. Comparable results were obtained for the other halftone methods.

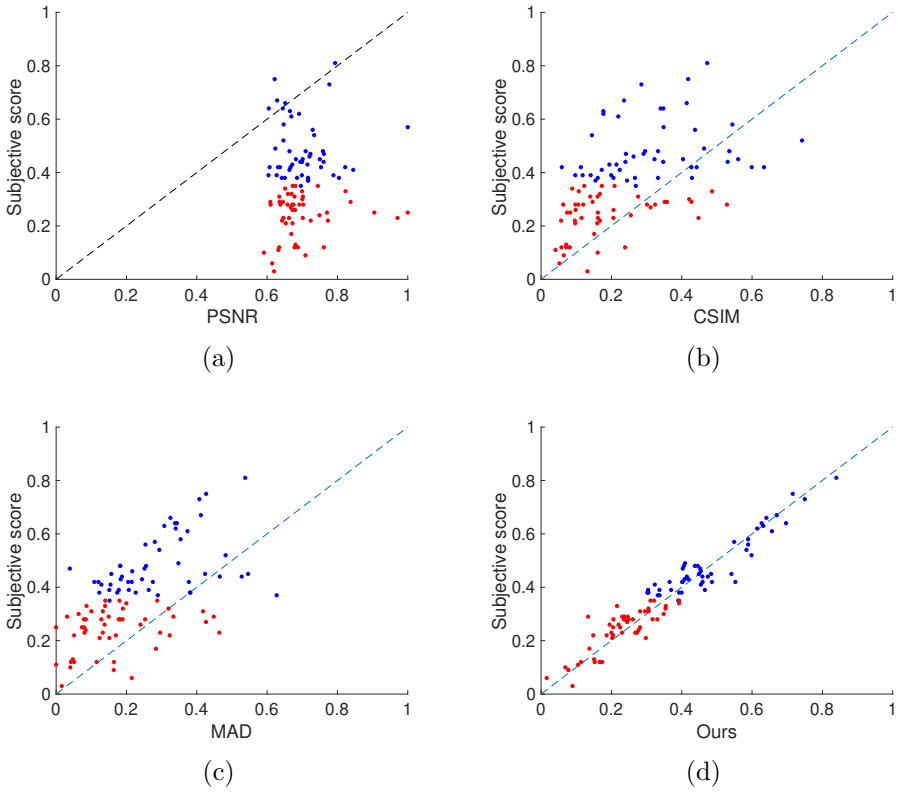

Figure 4.10 Scatter plots of the PSNR, CSIM, MAD and proposed metric for test samples halftoned by dither: (a) PSNR, (b) CSIM, (c) MAD, (d) Ours.

Table 4.3, 4.4 and 4.5 show the PCC between four kinds of different metrics and subjective observer scores based on three different halftoning algorithms (dither, Floyd and DBS). The correlation coefficients of glossy, non-glossy, and 100 image were calculated. Based on different distortion types, the PCC of glossy images, non-glossy images, and 100 images were calculated. The proposed index was consistent with the subjective evaluation regardless of the glossiness of the object.

4.5 Conclusion

This chapter proposed an effective index that explicitly separated structure detection and appearance for the glossiness of objects in halftone images. For structure detection, the SDISM algorithm was developed, which worked effectively for structural

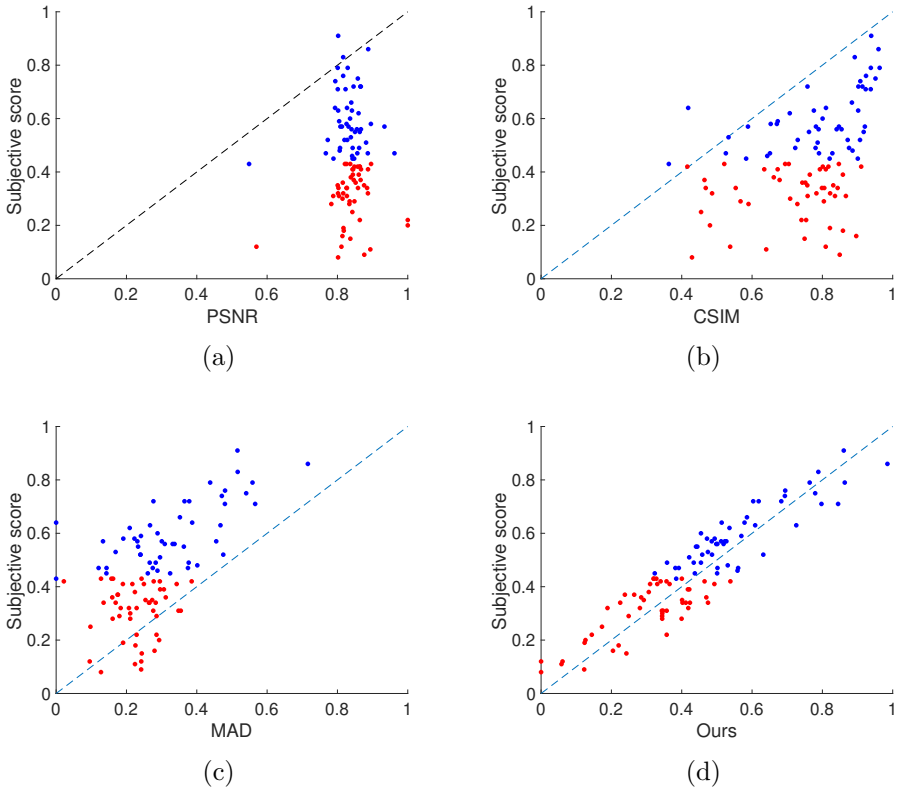

Figure 4.11 Scatter plots of the PSNR, CSIM, MAD and proposed metric for test samples halftoned by Floyd: (a) PSNR, (b) CSIM, (c) MAD, (d) Ours.

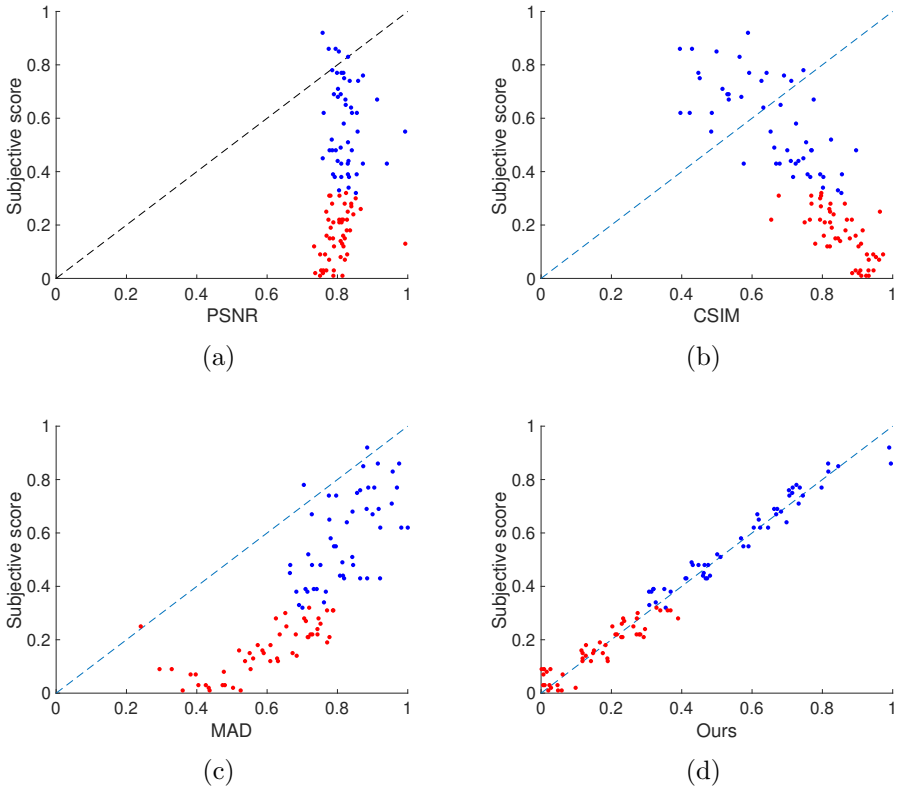

Figure 4.12 Scatter plots of the PSNR, CSIM, MAD and proposed metric for test samples halftoned by DBS: (a) PSNR, (b) CSIM, (c) MAD, (d) Ours.

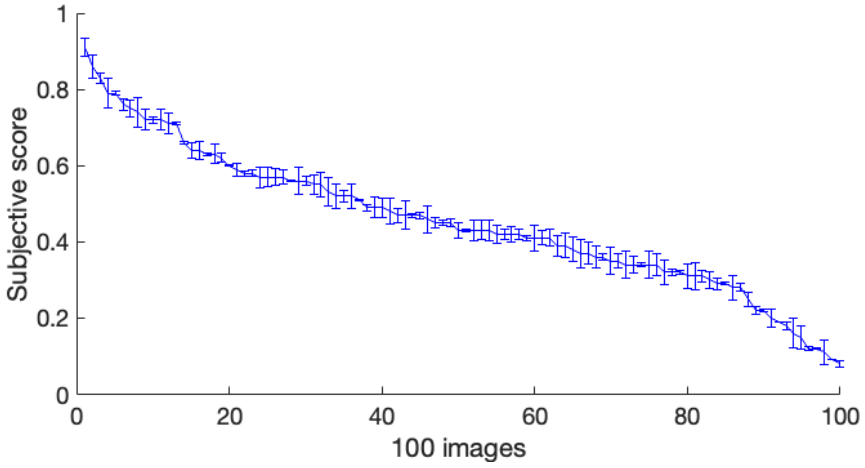

Figure 4.13 Subjective scores with error bars based on Floyd from 5 observers.

Table 4.3 Pearson correlation coefficient for PSNR, CSIM, MAD and Ours based on dithering.

Index	Glossiness images	Non-glossiness images	All 100 images
PSNR	0.2275	0.2375	0.102
CSIM	0.1944	-0.1492	0.0038
MAD	0.2566	-0.0244	0.0355
Ours	0.7563	0.7707	0.9066

Table 4.4 Pearson correlation coefficient for PSNR, CSIM, MAD and Ours based on Floyd.

Index	Glossiness images	Non-glossiness images	All 100 images
PSNR	0.1595	0.0626	0.0029
CSIM	0.0668	0.5067	0.4053
MAD	0.0896	0.6542	0.5788
Ours	0.7662	0.8716	0.9131

distortion. Two important HVS characteristics, i.e., CSF and contrast masking, were incorporated into the metric to better simulate HVS responses to visual inputs. This chapter proposed two simple quality measures, SDSIM and appearance perception, which were responsible for correlating structure, skewness, and standard deviation. Through experiments using 300 test halftone images from 100 images in FMD, the experiment demonstrated the effectiveness of the proposed index, which was consistent with the subjective evaluation scores regardless of the glossiness of the object.

The research will continue to investigate effective indices for other appearances of objects, such as perceptual transparency. The future research will consider more advanced color spaces, such as S-CIELAB and iCAM. New material perception models will also provide potential research possibilities, such as the new material perception model proposed in paper [75]. Also, the further research will verify the effectiveness of the proposed index in the actual printing with different papers and lighting environments.

Table 4.5 Pearson correlation coefficient for PSNR, CSIM, MAD and Ours based on DBS.

Index	**Glossiness images**	**Non-glossiness images**	**All 100 images**
PSNR	-0.0954	-0.2506	-0.2509
CSIM	0.6294	0.5453	0.7132
MAD	0.5735	0.6154	0.7045
Ours	0.7311	0.8881	0.9101

Chapter 5

Appearance Assessment of Halftone Images

This chapter is based upon the published journal papers of [A1] and [A2] in Appendix A. The contents of this chapter are shown in Computational Color Imaging Workshop (CCIW2022), 9-10, June, 2022

This chapter further verifies the index proposed in paper [A2] in Appendix A "Glossiness Index of Objects in Halftone Color Images Based on Structure and Appearance Distortion". Firstly, in order to verify the robustness of the proposed index to different kinds of halftones, binary and multi-level halftone comparison are added in the experiment of this chapter. The MOS data of subjective evaluation experiment are compared, and the results are obtained. The above data is based on the natural image database FMD. These images are obtained under natural illumination. Secondly, in order to verify the effect of texture perception error diffusion proposed in paper [A1] in Appendix A "Texture-aware error diffusion algorithm for multi-level digital halftoning", an objective experiment is carried out using the proposed index based on the image database selected under specific illumination. Finally, the results based on two different databases are compared. The results show that the proposed gloss perception index can also show the same results in the characteristic illumination database as in the natural illumination database. It is proved that the proposed glossiness index can play a certain role in the appearance perception of halftone image.

5.1 Experimental Results & Discussion

In this section, the glossiness index of the proposed halftone image is verified on a variety of halftones. The halftone mainly includes two types: the first is binary halftone and the second is multi-level halftone. The natural image database used is consistent with the database in paper [A2], including 50 glossy and 50 non-glossy images, which are all from the FMD database. As a comparison, assuming that the proposed glossiness perception index can still be valid in specific illumination databases, that

is, it can measure the glossiness perception of different halftone algorithms, then the halftone algorithms based on these two different databases should have the same objective index ranking, therefore, it is finally proved which halftone algorithms have better glossiness reproduction effect. The images of specific illumination used include 50 images from the database obtained under specific illumination, including images containing texture information such as gloss and non-gloss. The binary halftone algorithms used include Floyd, Shau, TAED, DBS and Ulichney (clustered dot and dispersed dot) as shown in Figure 5.1, Figure 5.2, Figure 5.3 and Figure 5.4. The 2bit result are shown in Figure 5.5, Figure 5.6, Figure 5.7 and Figure 5.8. In addition to the above algorithms, the multi-level halftone used also includes the proposed halftone algorithm MTAED for horizontal texture perception. The subjective observation test adopts the same observation environment and conditions as in Chapter 4. The gloss are classified as 6 different kinds (specular gloss, sheen gloss, contrast gloss, distinctness of reflected image gloss, absence of bloom gloss and absence of surface texture gloss) by Hunter according to different physical properties of gloss [76]. In the verification experiment, the proposed index performance of the database based on complex natural light and the database based on specific light was verified, so the robustness of the index under different physical conditions was verified to a certain extent. Therefore, it can be inferred that based on 6 different glosses, the proposed index can still correctly calculate the distortion in halftone images.

5.1.1 Results of Subjective Assessment for Natural Images: Mean Opinion Score (MOS)

In the subjective experiment of obtaining MOS score, each image of 100 images (50 gloss and 50 non-gloss images) was scored by 5 observers, and then the average score was used to replace the score of this image. These images come from FMD database and are mainly divided into two categories. The first category is gloss image, which contains obvious objects, and obvious gloss can be observed on the surface of the object, such as metal, water surface and smooth plastic. These images containing glossy objects are taken in the natural environment, and their surfaces contain complex light reflection information. The second type is non-gloss image, which contains obvious objects without surface reflection, that is, fabrics, stones and paper with rich texture information. The reflected natural light cannot be observed on the surface of the object contained in these non-gloss images. Based on these selected data, seven different halftone algorithms are used to obtain the halftone images used in the experiment. Including the classic error diffusion Floyd Steinberg, which adopts snake scanning. Shiau Fan error diffusion, TAED, DBS and Dithering error diffusion. Dithering error diffusion algorithms are divided into cluster dot 4×4, cluster dot 8×8 and dispersed dot. In Chapter 4, the proposed index used to evaluate the glossiness of objects in the image is used as the index of objective evaluation.

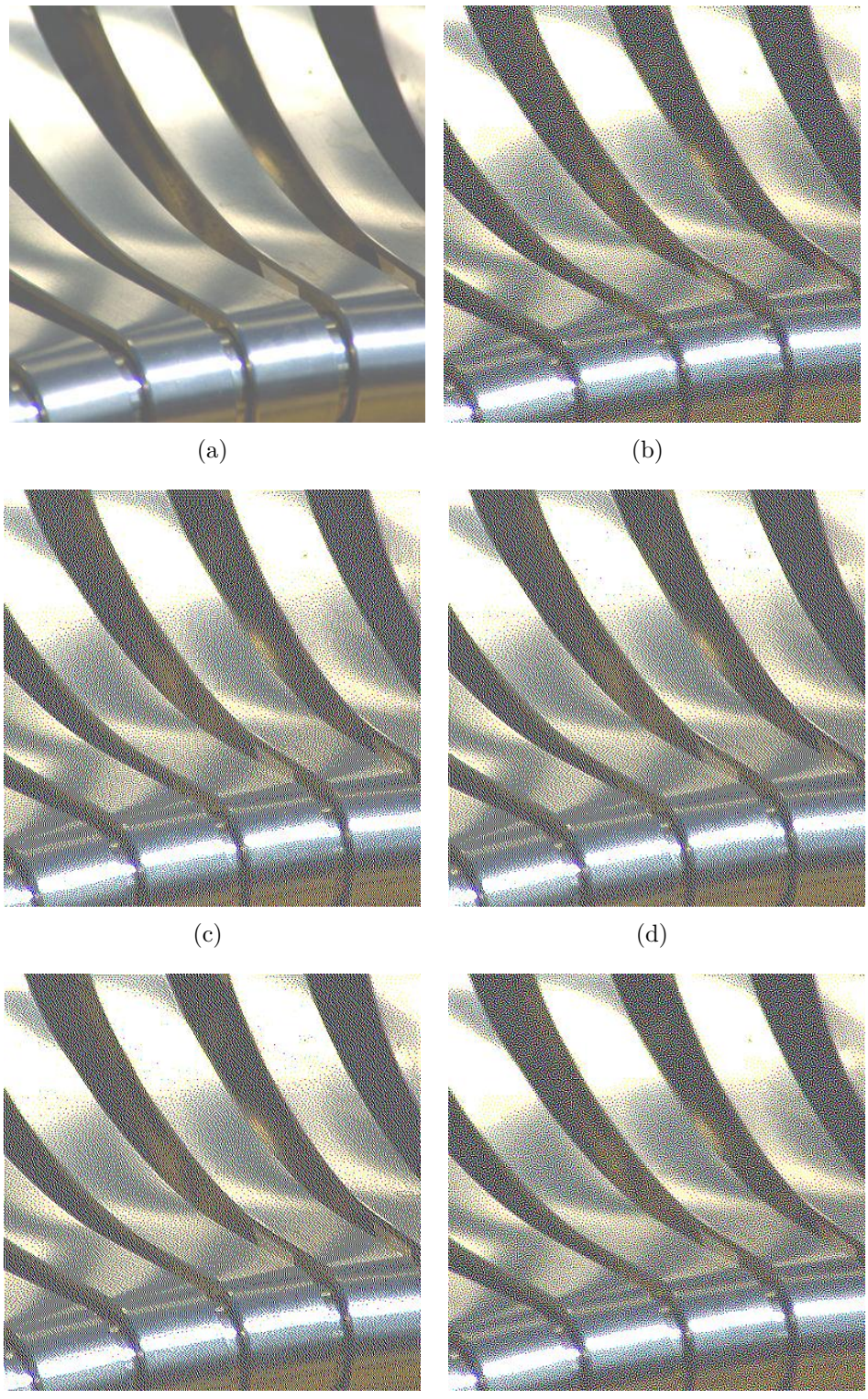

(a) (b)

(c) (d)

(e) (f)

Figure 5.1 The gloss images. (a) original image, (b) Proposed (1bit), (c) Floyd (1bit), (d) Shau (1bit), (e) TAED (1bit), (f) DBS (1bit).

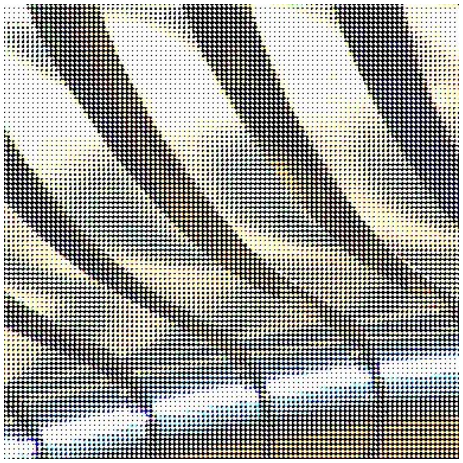

(a)

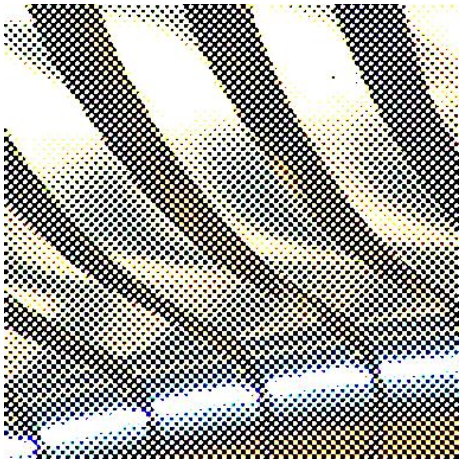

(b)

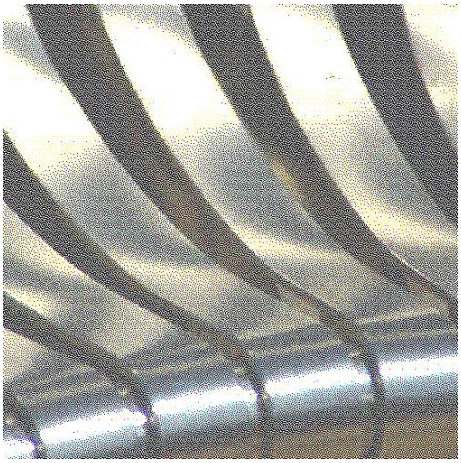

(c)

Figure 5.2 The gloss images. (a) Ulichney (clustered dot 4×4), (b) Ulichney (clustered dot 8×8), (c) Ulichney (dispersed dot).

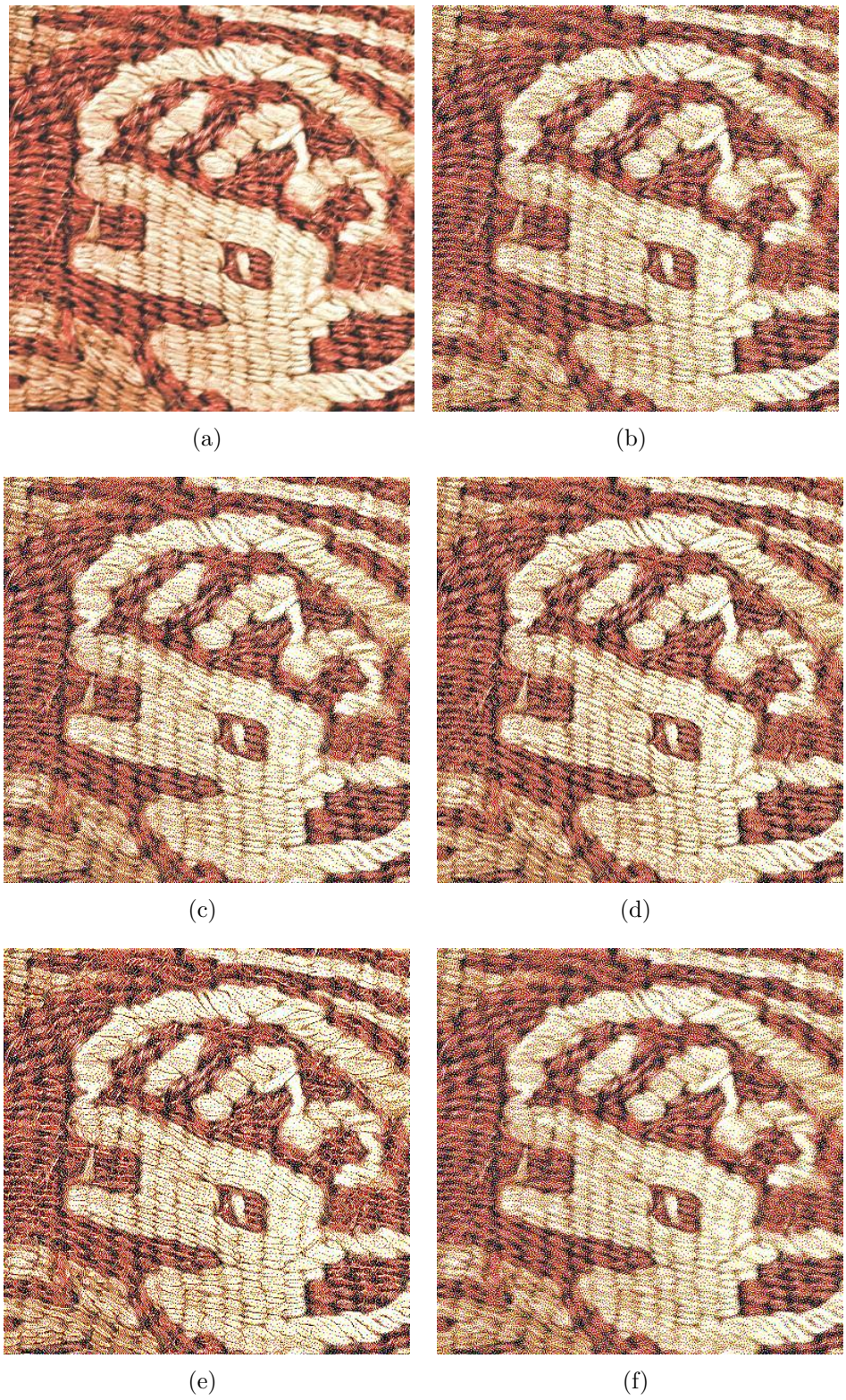

(a) (b)

(c) (d)

(e) (f)

Figure 5.3 The non-gloss image. (a) original image, (b) Proposed (1bit), (c) Floyd (1bit), (d) Shau (1bit), (e) TAED (1bit), (f) DBS (1bit).

(a)

(b)

(c)

Figure 5.4 The non-gloss image. (a) Ulichney (clustered dot 4×4), (b) Ulichney (clustered dot 8×8), (c) Ulichney (dispersed dot).

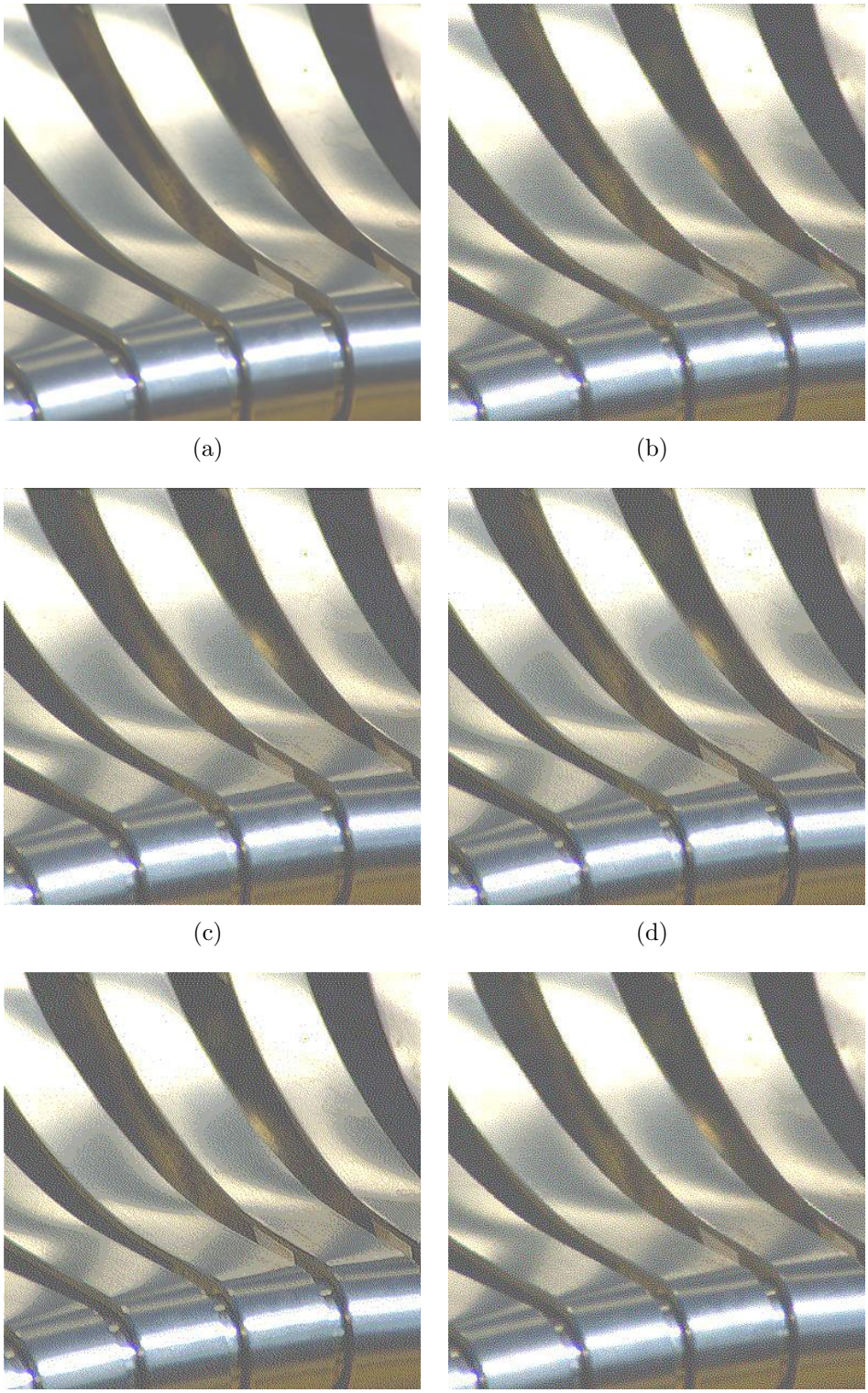

(a) (b) (c) (d) (e) (f)

Figure 5.5 The gloss images. (a) original image, (b) Proposed (2bit), (c) Floyd (2bit), (d) Shau (2bit), (e) TAED (2bit), (f) DBS (2bit).

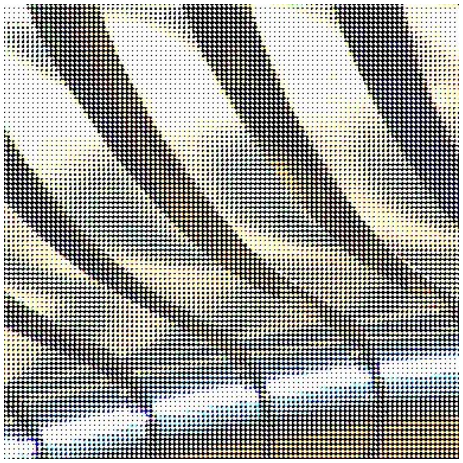

(a)

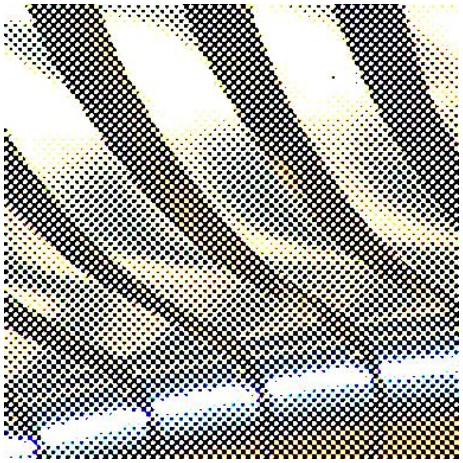

(b)

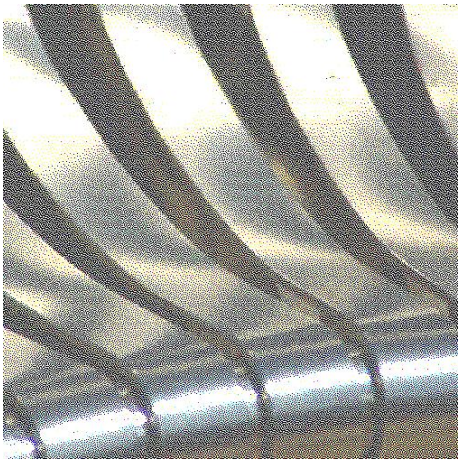

(c)

Figure 5.6 The gloss images. (a) Ulichney (clustered dot 4×4, 2bit), (b) Ulichney (clustered dot 8×8, 2bit), (c) Ulichney (dispersed dot, 2bit).

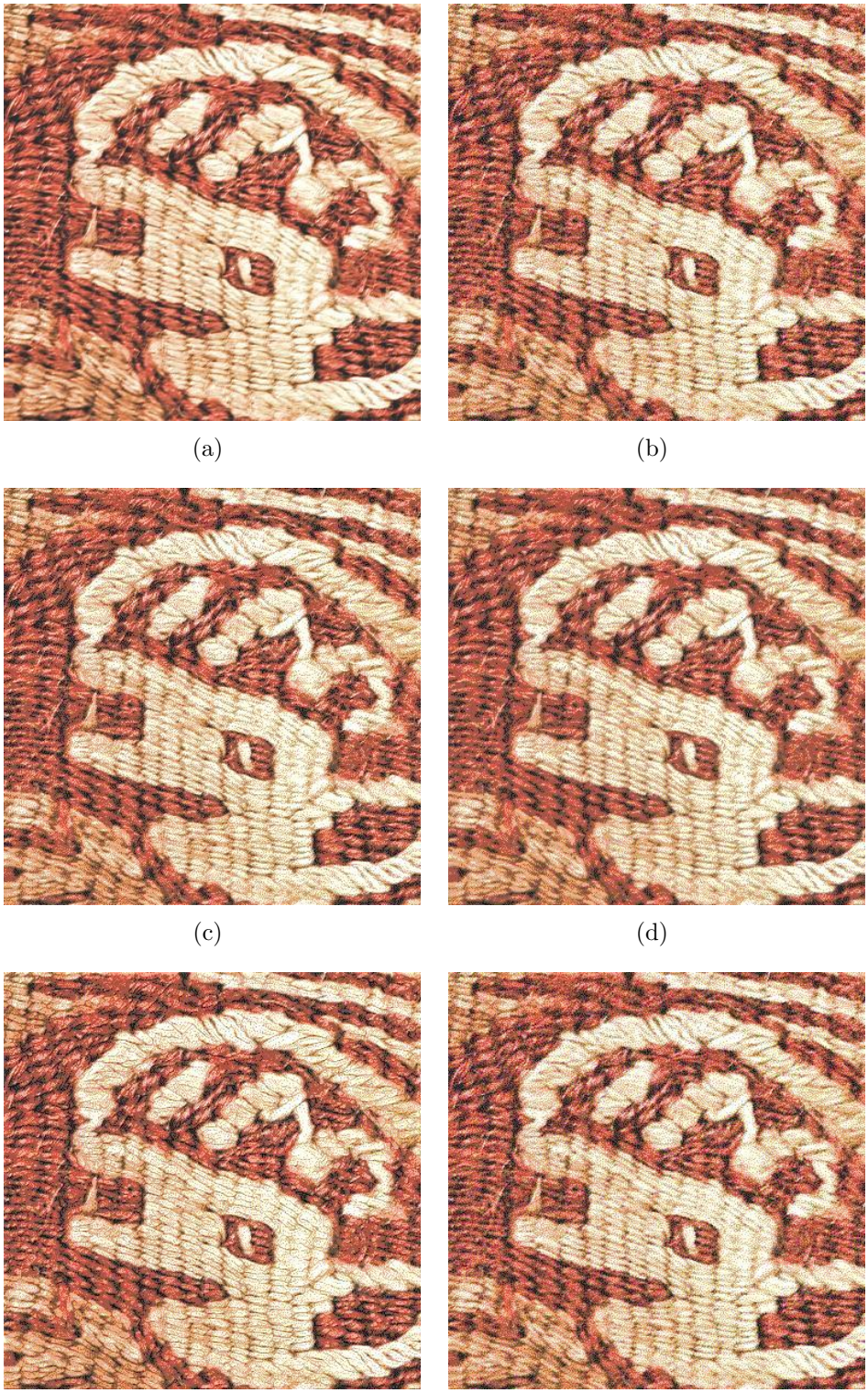

(a) (b)

(c) (d)

(e) (f)

Figure 5.7 The non-gloss image. (a) original image, (b) Proposed (2bit), (c) Floyd (2bit), (d) Shau (2bit), (e) TAED (2bit), (f) DBS (2bit).

(a)

(b)

(c)

Figure 5.8 The non-gloss image. (a) Ulichney (clustered dot 4×4, 2bit), (b) Ulichney (clustered dot 8×8, 2bit), (c) Ulichney (dispersed dot, 2bit).

Results for the natural images - Bi-level halftonings (1-bit)

Table 5.1 shows the results of subjective MOS scores of an image selected from glossy images. Each image corresponds to seven algorithms. Five observers respectively evaluate all the resulting images and give scores. In order to show which halftone algorithm has better appearance performance ability under this index, the average value of subjective scores of five observers is calculated. For an image, if the average value corresponding to a halftone algorithm is larger, the evaluation of the subjective observer is higher, and its appearance reproduction ability is stronger, so as to obtain the ranking of these algorithms. Table 5.2 shows the results of subjective evaluation scores of an image selected from the non-gloss image database, and the average values of all observers of the non-gloss image are calculated.

Table 5.1 The results of gloss image(1-bit) for Mean Opinion Score (MOS)

	Score 1	Score 2	Score 3	Score 4	Score 5	Aver.
Floyd E.D.	61	74	72	74	69	70
Shiau Fan E.D.	64	71	73	70	75	70.6
TAED	79	84	80	88	81	82.4
DBS	78	82	84	87	79	82
Dither (cluster dot 4×4)	32	43	40	41	45	40.2
Dither (cluster dot 8×8)	30	41	41	31	44	30
Dither (dispersed dot)	40	47	48	50	57	48.4

Table 5.2 The results of non-gloss image(1-bit) for Mean Opinion Score (MOS)

	Score 1	Score 2	Score 3	Score 4	Score 5	Aver.
Floyd E.D.	60	71	75	69	73	69.6
Shiau Fan E.D.	61	77	72	74	76	72
TAED	76	81	79	82	89	81.4
DBS	71	83	80	84	73	78.2
Dither (cluster dot 4×4)	31	44	47	45	49	43.2
Dither (cluster dot 8×8)	30	41	41	31	45	37.6
Dither (dispersed dot)	39	51	42	49	56	47.4

Results for the Natural Images - Multi-level halftonings (2-bit)

Table 5.3 and Table 5.4 show the subjective evaluation results of multi-level halftone of glossy image and non-glossy image respectively, in which the multi-level error diffusion is 4-value halftone (2-bit), The average value corresponding to the image is calculated, which is also used to evaluate the appearance performance of the halftone algorithm in multi-level halftones.

Table 5.3 The results of gloss image(2-bit) for Mean Opinion Score (MOS)

	Score 1	Score 2	Score 3	Score 4	Score 5	Aver.
Floyd E.D.	63	76	71	79	77	73.2
Shiau Fan E.D.	68	72	76	74	72	72.4
TAED	80	86	85	84	81	83.2
DBS	85	87	89	90	85	87.2
Dither (cluster dot 4×4)	40	47	50	53	64	50.8
Dither (cluster dot 8×8)	36	40	42	37	49	40.8
Dither (dispersed dot)	56	53	62	57	63	58.2
Proposed	87	84	94	85	89	87.8

Table 5.4 The results of non-gloss image(2-bit) for Mean Opinion Score (MOS)

	Score 1	Score 2	Score 3	Score 4	Score 5	Aver.
Floyd E.D.	71	69	74	81	80	75
Shiau Fan E.D.	65	75	76	80	73	73.8
TAED	74	82	84	80	79	79.8
DBS	82	81	84	89	84	84
Dither (cluster dot 4×4)	40	47	50	53	64	50.8
Dither (cluster dot 8×8)	36	40	42	37	49	40.8
Dither (dispersed dot)	56	53	62	57	63	58.2
Proposed	89	86	85	87	83	86

5.1.2 Results of Objective Assessment

The subjective experiment is mainly to verify whether the gloss perception targets proposed in Chapter 4 have consistent evaluation results based on different types of databases. Because the texture perception halftone related to the reproduction of the appearance of the printed image is assumed to affect the expressive ability of the appearance of the object in the image. Therefore, it is necessary to verify the error diffusion algorithm based on different database designs. Secondly, in order to verify the effectiveness of the texture aware halftone technology proposed in Chapter 3. The verification method is based on the proposed index to calculate whether the proposed texture aware halftone algorithm has less loss in appearance and structure similarity.

One of the purposes of this study is to design an index to quantitatively evaluate the appearance of halftone image, so as to simplify the cumbersome procedure of halftone image evaluation in industry. Therefore, when verifying whether the proposed halftone index can accurately predict the reproduction of halftone image appearance, this experiment only conducted objective evaluation tests, and compared it with the index ranking of subjective and objective tests based on different databases. This experiment compared the performance ability of the proposed index for 15 different

halftones (7 kinds of halftones based on 1-bit and 8 kinds of halftones based on 2-bit) under the two databases, and then briefly explained the effectiveness of the proposed index. The following are the objective evaluation data of FMD database obtained under natural scenes and database obtained under specific lighting conditions.

Results for Natural Image

The results of glossiness indicators color texture and appearance measure (CSAM) from 15 different halftones are shown in Table 5.5 and Table 5.6. Including Floyd (1-bit, 2-bit), TAED (1-bit, 2-bit), Shau (1-bit, 2-bit), dither (1-bit, 2-bit) and DBS (1-bit, 2-bit). Dither contains three halftone algorithms, namely clustered dot 4×4, clustered dot 8 and dispersed dot. Among them, there are 7 kinds of 1-bit halftone algorithm and 8 kinds of 2-bit halftones. These images are from the FMD database, which contains glossy and non-glossy images in natural scenes.

Table 5.5 Normalized data (1-bit): Floyd E.D., Shiau Fan E.D., TAED E.D., Ulichney1 E.D. clustered dot 4×4, Ulichney2 E.D. clustered dot 8×8, Ulichney3 E.D. dispersed dot, DBS E.D.

Image	F.S.	S.F.	TAED	Ulichney1	Ulichney2	Ulichney3	DBS
1	0.84957	0.61303	0.60464	0.73191	0.77211	0.92	0.7552
2	0.7432	0.64471	0.64101	0.66179	0.72997	0.91658	0.6584
3	0.46016	0.72672	0.72221	0.47668	0.56423	0.64924	0.76728
4	0.79177	0.6798	0.68278	0.7622	0.80067	0.7791	0.75203
5	0.88672	0.71459	0.7145	0.6113	0.76976	0.68777	0.79576
6	0.72525	0.62098	0.61729	0.6583	0.7599	0.76572	0.69026
7	0.94212	0.80455	0.81055	0.90545	0.92793	0.8643	0.62361
8	0.78176	0.72611	0.72809	0.8592	0.85066	0.74201	0.78955
9	0.70862	0.63281	0.62923	0.67471	0.67826	0.62634	0.71791
10	0.81341	0.63105	0.63036	0.64338	0.79783	0.6747	0.75728
11	0.79142	0.71294	0.7224	0.63064	0.66575	0.6929	0.71309
12	0.66134	0.66572	0.66159	0.57553	0.7161	0.75669	0.66099
13	0.70812	0.70349	0.69967	0.73482	0.87272	0.8222	0.68382
14	0.82151	0.7896	0.79507	0.69021	0.76435	0.70111	0.77393
15	0.89626	0.61815	0.61471	0.57706	0.71071	0.72852	0.82451
16	0.91459	0.70014	0.69291	0.64302	0.70309	0.8253	0.87543
17	0.98224	0.76941	0.76306	0.60317	0.77255	0.76294	0.9592
18	0.66187	0.80016	0.8	0.58516	0.66301	0.72294	0.62893
19	0.83623	0.96117	0.95938	0.6274	0.74998	0.73872	0.79849
20	0.93464	0.64687	0.64512	0.58131	0.74084	0.64108	0.90105
21	0.80933	0.69222	0.69132	0.63203	0.79689	0.74733	0.74954
22	0.76857	0.75267	0.74765	0.66252	0.91957	0.80951	0.70899
23	0.78081	0.78309	0.80259	0.61519	0.65244	0.65674	0.73737

Continued on next page

Table 5.5 – continued from previous page

Image	F.S.	S.F.	TAED	Ulichney1	Ulichney2	Ulichney3	DBS
24	0.84194	0.9177	0.91789	0.51923	0.70421	0.60877	0.75959
25	0.81541	0.69048	0.68706	0.61594	0.78343	0.73108	0.78066
26	0.58517	0.68455	0.69218	0.56502	0.66554	0.68872	0.87975
27	0.94351	0.7582	0.6374	0.60262	0.79913	0.71912	0.94699
28	0.75926	0.5573	0.55661	0.59339	0.69246	0.71909	0.7348
29	0.72557	0.68014	0.67396	0.92826	0.6432	0.65418	0.70231
30	0.79016	0.74271	0.74138	0.6402	0.78952	0.77379	0.74864
31	0.89616	0.97939	0.97221	0.68057	0.68944	0.70289	0.88911
32	0.77935	0.7367	0.73686	0.66379	0.69203	0.82105	0.70956
33	0.76213	0.58335	0.58182	0.58523	0.74194	0.68411	0.70939
34	0.80903	0.79679	0.78442	0.61376	0.62449	0.63113	0.82539
35	0.63336	0.5678	0.57705	0.78898	0.59778	0.5535	0.64308
36	0.6014	0.7568	0.76043	0.62963	0.62299	0.49794	0.5816
37	0.718	0.64883	0.64833	0.71052	0.64011	0.78973	0.71585
38	0.49395	0.64179	0.64122	0.8626	0.88711	0.53067	0.48644
39	0.76674	0.70575	0.70809	0.68069	0.82179	0.80902	0.72065
40	0.97636	0.77063	0.78064	0.5787	0.69948	0.65095	0.84425
41	0.70036	0.55146	0.55182	0.5113	0.60303	0.74137	0.58641
42	0.88287	0.68167	0.67476	0.64764	0.75951	0.65262	0.85912
43	0.78438	0.59743	0.61442	0.51019	0.62492	0.63266	0.70423
44	0.79846	0.66338	0.66951	0.65061	0.75453	0.86007	0.75674
45	0.78642	0.6893	0.70518	0.629	0.75751	0.75164	0.73962
46	0.77194	0.68304	0.68202	0.6093	0.71468	0.77788	0.73223
47	0.7512	0.6552	0.64982	0.58945	0.73675	0.68602	0.67519
48	0.65142	0.64456	0.63351	0.53924	0.60178	0.66177	0.57678
49	0.85982	0.67279	0.66868	0.74073	0.84917	0.81713	0.81157
50	0.79067	0.63982	0.64132	0.71298	0.77315	0.86963	0.68662
51	0.59492	0.72438	0.72348	0.83933	0.727	0.92	0.5911
52	0.75439	0.64915	0.65664	0.8039	0.84239	0.84094	0.71442
53	0.65742	0.72365	0.76499	0.55089	0.69317	0.57954	0.53682
54	0.83449	0.71947	0.72232	0.67932	0.79028	0.67732	0.70617
55	0.80428	0.68453	0.6866	0.65027	0.65892	0.7063	0.69841
56	0.68074	0.65439	0.66816	0.71654	0.72692	0.76032	0.6191
57	0.71956	0.80893	0.81453	0.87446	0.74447	0.80002	0.68739
58	0.61692	0.77014	0.76834	0.87286	0.82211	0.52238	0.58849
59	0.76379	0.6151	0.61484	0.58241	0.62847	0.696	0.64994
60	0.92121	0.6932	0.69496	0.67736	0.59481	0.69775	0.82534
61	0.74334	0.74969	0.75335	0.68931	0.70255	0.7269	0.66661
62	0.80744	0.70808	0.71003	0.69683	0.66238	0.74279	0.76742
63	0.67317	0.69916	0.70182	0.61238	0.76391	0.59181	0.59723
64	0.74556	0.81094	0.82014	0.82323	0.93361	0.5849	0.67664

Continued on next page

Table 5.5 – continued from previous page

Image	F.S.	S.F.	TAED	Ulichney1	Ulichney2	Ulichney3	DBS
65	0.68518	0.71138	0.70701	0.91525	0.89691	0.74691	0.61237
66	0.49075	0.78396	0.78373	0.63491	0.89519	0.59298	0.42764
67	0.60892	0.8036	0.80585	0.52595	0.59179	0.48393	0.58172
68	0.53501	0.4982	0.6125	0.54528	0.72733	0.59419	0.50304
69	0.66628	0.74153	0.74012	0.9412	0.969	0.54607	0.61079
70	0.64258	0.67747	0.67999	0.57084	0.64397	0.50892	0.60686
71	0.52972	0.77754	0.77855	0.5496	0.69828	0.54157	0.47264
72	0.89271	0.91319	0.91742	0.68338	0.82946	0.72855	0.8335
73	0.7351	0.89043	0.89239	0.55512	0.53581	0.62395	0.7214
74	0.74074	0.78266	0.77712	0.7843	0.99068	0.59222	0.67796
75	0.77325	0.69693	0.70257	0.53914	0.66375	0.59681	0.74091
76	0.9468	0.83736	0.83607	0.76551	0.63366	0.72938	0.86689
77	0.66997	0.77364	0.77945	0.86045	0.58831	0.76153	0.66715
78	0.67153	0.83644	0.84191	0.69162	0.80973	0.47303	0.60256
79	0.69404	0.72082	0.7223	0.54563	0.61672	0.59962	0.61861
80	0.68401	0.73138	0.7258	0.46968	0.70823	0.68442	0.4982
81	0.76537	0.70787	0.70103	0.61174	0.57879	0.48916	0.68054
82	0.75998	0.82085	0.82807	0.5687	0.7198	0.70271	0.66504
83	0.7173	0.65552	0.65559	0.62092	0.67374	0.68751	0.64989
84	0.53323	0.69247	0.69047	0.94169	0.6321	0.56827	0.47538
85	0.94094	0.73052	0.72506	0.67383	0.73322	0.7997	0.65884
86	0.54254	0.69322	0.68297	0.58561	0.64913	0.72143	0.50321
87	0.6355	0.83384	0.82586	0.68748	0.70707	0.80275	0.58004
88	0.63132	0.71563	0.7147	0.55781	0.73055	0.66545	0.54786
89	0.74793	0.59693	0.59692	0.62473	0.68636	0.7615	0.63508
90	0.65189	0.52422	0.52413	0.61271	0.55716	0.59192	0.57351
91	0.67884	0.69099	0.66347	0.66567	0.72845	0.74354	0.59032
92	0.64989	0.64093	0.63406	0.70461	0.70543	0.80997	0.54758
93	0.92603	0.76725	0.76697	0.79199	0.69453	0.78612	0.83292
94	0.81876	0.77746	0.78205	0.70011	0.75411	0.7555	0.7778
95	0.66391	0.69527	0.69185	0.6826	0.69643	0.82788	0.59051
96	0.69221	0.69264	0.7001	0.55088	0.57031	0.65175	0.59439
97	0.89679	0.61991	0.6186	0.67657	0.57275	0.75117	0.71777
98	0.80128	0.67992	0.68226	0.73894	0.77274	0.76173	0.65423
99	0.60325	0.82588	0.82072	0.65917	0.67407	0.87451	0.53153
100	0.79685	0.71596	0.71334	0.66523	0.62963	0.80219	0.53677

Table 5.6 Normalized data (2-bit): Floyd E.D., Shiau Fan E.D., TAED E.D., Ulichney1 E.D. clustered dot 4×4, Ulichney2 E.D. clustered dot 8×8, Ulichney3 E.D. dispersed dot, DBS E.D., Proposed

Image	F.S.	S.F.	TAED	Ulichney1	Ulichney2	Ulichney3	DBS	Proposed
1	0.80137	0.66159	0.65977	0.73191	0.77211	0.5127	0.93225	0.77227
2	0.80766	0.66986	0.67138	0.66179	0.72997	0.99658	0.82095	0.78388
3	0.49352	0.73195	0.74106	0.47668	0.56423	0.72924	0.54131	0.85356
4	0.67419	0.70722	0.71215	0.7622	0.80067	0.8591	0.64408	0.85356
5	0.69958	0.72424	0.72757	0.6113	0.76976	0.76777	0.67075	0.84007
6	0.72943	0.6837	0.6856	0.6583	0.7599	0.84572	0.72486	0.7981
7	0.6791	0.75857	0.76517	0.90545	0.92793	0.9443	0.67848	0.87767
8	0.65717	0.81517	0.82176	0.8372	0.85066	0.82201	0.60407	0.93426
9	0.53009	0.6368	0.63876	0.67471	0.67826	0.70634	0.56356	0.75126
10	0.63877	0.65604	0.65987	0.64338	0.79783	0.7547	0.70378	0.77237
11	0.59574	0.64917	0.66306	0.63064	0.66575	0.7729	0.62105	0.77556
12	0.65262	0.70321	0.70443	0.57553	0.7161	0.83669	0.61305	0.81693
13	0.57488	0.71737	0.71825	0.73482	0.87272	0.9022	0.65727	0.83075
14	0.76237	0.74717	0.75598	0.69021	0.76435	0.78111	0.66036	0.86848
15	0.83343	0.62359	0.62756	0.57706	0.71071	0.80852	0.76482	0.74006
16	0.91295	0.71634	0.71598	0.64302	0.70309	0.9053	0.87992	0.82848
17	0.69439	0.775	0.7758	0.60317	0.77255	0.84294	0.77006	0.8883
18	0.72316	0.75852	0.76115	0.58516	0.66301	0.80294	0.6756	0.87365
19	0.7122	0.88455	0.88906	0.6274	0.74998	0.81872	0.72985	0.99156
20	0.72204	0.6551	0.65463	0.58131	0.74084	0.72108	0.65455	0.76713
21	0.66553	0.6705	0.67416	0.63203	0.79689	0.82733	0.71197	0.78666
22	0.6853	0.72388	0.72415	0.66252	0.91957	0.88951	0.99323	0.83665
23	0.58337	0.77394	0.78145	0.61519	0.65244	0.73674	0.60705	0.89395
24	0.7258	0.82377	0.83046	0.51923	0.70421	0.68877	0.65535	0.94296
25	0.63131	0.69424	0.69493	0.61594	0.78343	0.81108	0.74289	0.80743
26	0.55882	0.66276	0.66757	0.56502	0.66554	0.76872	0.70138	0.78007
27	0.90268	0.99101	0.99201	0.60262	0.79913	0.79912	0.85405	0.84451
28	0.66254	0.57221	0.57336	0.59339	0.69246	0.79909	0.60245	0.68586
29	0.80949	0.70533	0.70348	0.92826	0.7482	0.73418	0.71243	0.81598
30	0.79606	0.77166	0.77179	0.6402	0.78952	0.85379	0.95687	0.88429
31	0.73085	0.8567	0.7657	0.68057	0.68944	0.78289	0.68068	0.8782
32	0.80722	0.74158	0.7489	0.66379	0.69203	0.90105	0.69874	0.8614
33	0.74827	0.57451	0.57496	0.58523	0.74194	0.76411	0.70666	0.68746
34	0.74716	0.83902	0.84267	0.61376	0.62449	0.71113	0.67431	0.95517
35	0.81835	0.56344	0.57111	0.78898	0.59778	0.6335	0.70467	0.68361
36	0.73204	0.70545	0.71648	0.62963	0.62299	0.57794	0.61422	0.82898
37	0.85738	0.64148	0.64552	0.71052	0.64011	0.86973	0.73882	0.75802
38	0.53126	0.63983	0.64456	0.8626	0.88711	0.61067	0.54286	0.75706

Continued on next page

Table 5.6 – continued from previous page

Image	F.S.	S.F.	TAED	Ulichney1	Ulichney2	Ulichney3	DBS	Proposed
39	0.74065	0.72011	0.72424	0.68069	0.82179	0.88902	0.82941	0.83674
40	0.77989	0.78985	0.79725	0.5787	0.69948	0.73095	0.74933	0.90975
41	0.63954	0.61538	0.62073	0.5113	0.60303	0.82137	0.71246	0.73323
42	0.68601	0.6977	0.69782	0.64764	0.75951	0.73262	0.606	0.81032
43	0.74425	0.60125	0.61329	0.51019	0.62492	0.71266	0.64623	0.72579
44	0.70857	0.66265	0.66669	0.65061	0.75453	0.94007	0.63931	0.77919
45	0.78226	0.64847	0.65724	0.629	0.75751	0.83164	0.73903	0.76974
46	0.7345	0.73801	0.73998	0.6093	0.71468	0.85788	0.80611	0.85248
47	0.68492	0.60941	0.61626	0.58945	0.73675	0.76602	0.70715	0.72876
48	0.64479	0.67541	0.68231	0.53924	0.60178	0.74177	0.64342	0.79481
49	0.74694	0.70308	0.70297	0.74073	0.84917	0.89713	0.84091	0.81547
50	0.78157	0.70723	0.70483	0.71298	0.77315	0.94963	0.6589	0.81733
51	0.86578	0.79065	0.78184	0.83933	0.727	0.6534	0.81811	0.89434
52	0.7321	0.77425	0.76433	0.8039	0.84239	0.92094	0.7584	0.87683
53	0.54468	0.77099	0.76925	0.55089	0.69317	0.65954	0.44534	0.88175
54	0.87463	0.80416	0.80287	0.67932	0.79028	0.75732	0.68431	0.91537
55	0.93118	0.72866	0.72471	0.65027	0.65892	0.7863	0.63195	0.83721
56	0.83949	0.71101	0.71383	0.71654	0.72692	0.84032	0.65132	0.82633
57	0.85503	0.84627	0.85183	0.87446	0.74447	0.88002	0.65525	0.96433
58	0.97405	0.87486	0.8688	0.87286	0.82211	0.60238	0.60749	0.9813
59	0.85006	0.67351	0.67235	0.58241	0.62847	0.776	0.5269	0.78485
60	0.89505	0.72959	0.73126	0.67736	0.59481	0.77775	0.57861	0.84376
61	0.62572	0.81712	0.82229	0.68931	0.70255	0.8069	0.71259	0.93479
62	0.75875	0.79689	0.79473	0.69683	0.66238	0.82279	0.64862	0.90723
63	0.83245	0.76962	0.76977	0.61238	0.76391	0.67181	0.54351	0.88227
64	0.89493	0.82792	0.83367	0.82323	0.93361	0.6649	0.57434	0.94617
65	0.90901	0.82403	0.81597	0.91525	0.89691	0.82691	0.66961	0.92847
66	0.96228	0.86224	0.85875	0.63491	0.89519	0.67298	0.74041	0.97125
67	0.6435	0.83178	0.83315	0.52595	0.59179	0.56393	0.42963	0.94565
68	0.47819	0.99609	0.99647	0.54528	0.72733	0.67419	0.43612	0.80897
69	0.87005	0.85419	0.85022	0.9412	0.969	0.62607	0.54701	0.96272
70	0.65878	0.78893	0.78417	0.57084	0.64397	0.58892	0.48295	0.89667
71	0.87753	0.86863	0.86153	0.5496	0.69828	0.62157	0.52066	0.97403
72	0.71599	0.8532	0.8582	0.68338	0.82946	0.80855	0.55062	0.9707
73	0.64425	0.89321	0.90386	0.55512	0.53581	0.70395	0.45705	0.81636
74	0.76137	0.8853	0.87893	0.8532	0.99068	0.67222	0.53724	0.99143
75	0.52456	0.7728	0.77253	0.53914	0.66375	0.67681	0.41153	0.88503
76	0.8572	0.90245	0.90078	0.76551	0.63366	0.80938	0.73684	0.71328
77	0.87519	0.87996	0.88064	0.86045	0.58831	0.84153	0.63258	0.99314
78	0.63058	0.8212	0.83384	0.69162	0.80973	0.55303	0.39376	0.94634
79	0.83322	0.77302	0.7791	0.54563	0.61672	0.67962	0.49562	0.8916

Continued on next page

Table 5.6 – continued from previous page

Image	F.S.	S.F.	TAED	Ulichney1	Ulichney2	Ulichney3	DBS	Proposed
80	0.92367	0.79405	0.79182	0.46968	0.70823	0.76442	0.67669	0.90432
81	0.75221	0.83714	0.84093	0.61174	0.57879	0.56916	0.42913	0.95343
82	0.75742	0.85489	0.86069	0.5687	0.7198	0.78271	0.52433	0.97319
83	0.78697	0.7623	0.75696	0.62092	0.67374	0.76751	0.51156	0.86946
84	0.54708	0.73903	0.73401	0.94169	0.6372	0.64827	0.56272	0.84651
85	0.73991	0.80371	0.79847	0.67383	0.73322	0.8797	0.7321	0.91097
86	0.64332	0.72713	0.72972	0.58561	0.64913	0.80143	0.55989	0.96968
87	0.87223	0.85744	0.85718	0.68748	0.70707	0.88275	0.79595	0.86076
88	0.54775	0.74952	0.74826	0.55781	0.73055	0.74545	0.49593	0.78025
89	0.5431	0.67529	0.66775	0.62473	0.68636	0.8415	0.73746	0.65849
90	0.78509	0.5455	0.54599	0.61271	0.55716	0.67192	0.4497	0.79726
91	0.71928	0.67858	0.68476	0.66567	0.72845	0.82354	0.76159	0.8155
92	0.7843	0.70435	0.703	0.70461	0.70543	0.88997	0.9188	0.95023
93	0.61239	0.83441	0.83773	0.79199	0.69453	0.86612	0.77204	0.95674
94	0.87454	0.84472	0.84424	0.70011	0.75411	0.8355	0.7142	0.83959
95	0.8534	0.71338	0.72709	0.6826	0.69643	0.90788	0.77965	0.82728
96	0.72145	0.71054	0.71478	0.55088	0.57031	0.73175	0.53143	0.8065
97	0.7382	0.69865	0.694	0.67657	0.57275	0.83117	0.65147	0.88445
98	0.66197	0.77586	0.77195	0.73894	0.77274	0.84173	0.7513	0.85106
99	0.73243	0.94837	0.93856	0.65917	0.67407	0.95451	0.81796	0.83943
100	0.64905	0.83459	0.82693	0.66523	0.62963	0.88219	0.80742	0.84951

comparing the data in Table 5.5(1-bit) and Table 5.6(2-bit), it can be seen that in the CSAM index value of the corresponding image, the data in table 5.6 is generally higher than that in table 5.5. The reason is that multi-valued halftone can reproduce more detailed information of the object and surface in the image. For the CSAM index with the ability to perceive the texture and gloss of the object surface, the larger the value, the better the image restoration effect. The stronger the structural information and appearance of the object that can be reproduced by halftone. When comparing the data in a single table, obvious differences can also be observed in the index values of different halftones of the same image. The largest value is MTAED and DBS proposed in Chapter 3. The reason is that MTAED has stronger texture reproduction ability, while DBS uses direct binary search for halftone, which can well avoid the influence of artifacts on the reproduced image. Therefore, in all halftone algorithms, it has a larger index value. Among them, the smallest value belongs to the clustered dot halftone in the dither halftone, and the halftone of 4×4 clustered dot is better than that of 8×8 clustered dot. The reason is that using the dithering algorithm with regular pattern for halftone will reduce the visibility of image details, but there will be no artifacts in error diffusion. The detail restoration ability of 8×8

clustered dot is lower than that of 4×4 clustered dot. The reason is that 4×4 dot only uses 4 aggregated pixels to represent a point in the halftone that needs to be printed on the paper. Therefore, more points need to be printed, which enhances the ability of image reproduction.

Results for Unnatural Images

Unnatural image refers to the image obtained under unnatural light. Printing companies usually take the printing of printing samples. These printing samples include objects with rich colors and objects under various other conditions. They are some images that try to simulate the real printing scene. These images are often taken under some specific light. In order to test whether the proposed CSAM index can also show outstanding performance in such scenes, and also to test whether MTAED proposed in Chapter 3 has the advantage of appearance reproduction compared with other classical halftone technologies, the index is applied to the selected images in these scenes without subjective observer test, which can be proved only by obtaining the results consistent with the database in natural scenes.

Table 5.7 Normalized data (1-bit): Floyd E.D., Shiau Fan E.D., TAED E.D., Ulichney1 E.D. clustered dot 4×4, Ulichney2 E.D. clustered dot 8×8, Ulichney3 E.D. dispersed dot, DBS E.D.

Image	F.S.	S.F.	TAED	Ulichney1	Ulichney2	Ulichney3	DBS
1	0.28989	0.82598	0.29989	0.63081	0.56034	0.67411	0.61847
2	0.46569	0.52175	0.46092	0.4218	0.3213	0.5642	0.25153
3	0.89504	0.6034	0.88865	0.74361	0.671	0.8018	0.8972
4	0.56391	0.57975	0.55553	0.62523	0.60742	0.66858	0.65229
5	0.72194	0.43329	0.71655	0.53909	0.5076	0.56915	0.68289
6	0.68325	0.41884	0.67615	0.6067	0.53891	0.67371	0.62351
7	0.46635	0.69196	0.46329	0.50033	0.50896	0.4958	0.55719
8	0.52098	0.53499	0.51558	0.57557	0.56852	0.61827	0.53782
9	0.661	0.6845	0.65456	0.60669	0.57376	0.63662	0.61133
10	0.5585	0.46934	0.54441	0.43443	0.39623	0.47427	0.53875
11	0.4982	0.67464	0.5846	0.50974	0.5024	0.54211	0.43483
12	0.66078	0.4076	0.65885	0.496	0.50835	0.51542	0.49075
13	0.71252	0.47444	0.71674	0.45304	0.41022	0.48767	0.56154
14	0.60283	0.8307	0.6107	0.42207	0.43279	0.42938	0.9764
15	0.52005	0.82117	0.51468	0.43173	0.40856	0.43915	0.69012
16	0.53881	0.48483	0.53521	0.52927	0.53822	0.53145	0.72252
17	0.71657	0.71568	0.7174	0.59367	0.58754	0.6145	0.67762
18	0.68	0.59585	0.67009	0.63393	0.60405	0.6925	0.62192
19	0.73015	0.64388	0.71917	0.70561	0.6772	0.75929	0.72325
20	0.70659	0.68912	0.70181	0.6371	0.5783	0.66754	0.73611

Continued on next page

Table 5.7 – continued from previous page

Image	F.S.	S.F.	TAED	Ulichney1	Ulichney2	Ulichney3	DBS
21	0.43876	0.45007	0.44213	0.47597	0.47713	0.49826	0.53873
22	0.69287	0.44069	0.68389	0.51451	0.4889	0.5289	0.63198
23	0.46946	0.75941	0.4671	0.68808	0.70588	0.80078	0.52465
24	0.81239	0.60982	0.8069	0.79372	0.70028	0.8886	0.81388
25	0.78118	0.44081	0.78723	0.57887	0.58726	0.65103	0.60437
26	0.7675	0.6534	0.76614	0.59394	0.5364	0.63963	0.6451
27	0.71809	0.84406	0.7168	0.5171	0.49194	0.56772	0.63152
28	0.64428	0.75637	0.63703	0.57881	0.55307	0.61696	0.69536
29	0.69825	0.85067	0.68971	0.64081	0.56679	0.66782	0.69063
30	0.7897	0.62621	0.78854	0.55279	0.55088	0.55239	0.73703
31	0.61446	0.74763	0.60745	0.46213	0.40511	0.50963	0.60003
32	0.79099	0.57278	0.79238	0.47183	0.44383	0.51846	0.52145
33	0.69341	0.58783	0.69985	0.56428	0.5267	0.56892	0.85346
34	0.6785	0.42214	0.67182	0.4825	0.43937	0.52337	0.57051
35	0.8527	0.36689	0.8529	0.4682	0.43424	0.49124	0.81327
36	0.50533	0.75573	0.49784	0.45786	0.43538	0.48815	0.63831
37	0.77142	0.56122	0.7686	0.50273	0.50659	0.54049	0.81495
38	0.52597	0.64852	0.52536	0.54562	0.52875	0.57666	0.74452
39	0.63569	0.7679	0.62238	0.57018	0.51201	0.62425	0.5908
40	0.65563	0.62855	0.60661	0.54808	0.53023	0.58529	0.73558
41	0.5347	0.78085	0.52265	0.54989	0.53893	0.57565	0.5438
42	0.71428	0.61305	0.70383	0.60379	0.55435	0.6604	0.66065
43	0.67611	0.54978	0.67269	0.43191	0.39639	0.45748	0.56634
44	0.70314	0.55868	0.70512	0.4501	0.46072	0.45405	0.62331
45	0.62448	0.69546	0.62481	0.3821	0.40046	0.37917	0.47347
46	0.614	0.41006	0.61458	0.34203	0.32849	0.38966	0.63451
47	0.5833	0.84869	0.57984	0.16778	0.14136	0.07582	0.59437
48	0.52513	0.73743	0.52286	0.13315	0.13191	0.084847	0.55328
49	0.43798	0.61531	0.43601	0.17903	0.19035	0.093338	0.61669
50	0.44936	0.70777	0.44535	0.12387	0.15964	0.079882	0.57735

Table 5.8 Normalized data (2-bit): Floyd E.D., Shiau Fan E.D., TAED E.D., Ulichney1 E.D. clustered dot 4×4, Ulichney2 E.D. clustered dot 8×8, Ulichney3 E.D. dispersed dot, DBS E.D., Proposed

Image	F.S.	S.F.	TAED	Ulichney1	Ulichney2	Ulichney3	DBS	Proposed
1	0.69422	0.84153	0.90372	0.12599	0.13334	0.29888	0.82672	0.92152
2	0.5432	0.73436	0.73082	0.43985	0.4385	0.37018	0.4473	0.74862

Continued on next page

Table 5.8 – continued from previous page

Image	F.S.	S.F.	TAED	Ulichney1	Ulichney2	Ulichney3	DBS	Proposed
3	0.79665	0.91063	0.89755	0.99562	0.9901	0.8321	0.9624	0.91535
4	0.67654	0.52189	0.42869	0.60761	0.60352	0.59977	0.61156	0.44649
5	0.57544	0.7582	0.91908	0.81661	0.81056	0.7908	0.8298	0.93688
6	0.67754	0.94753	0.85713	0.67051	0.66785	0.69585	0.6735	0.87493
7	0.5056	0.66456	0.72138	0.42009	0.4221	0.44667	0.40822	0.73918
8	0.6346	0.70763	0.70386	0.52429	0.52312	0.52414	0.52616	0.72166
9	0.64279	0.74641	0.75359	0.69762	0.69641	0.68366	0.70557	0.77139
10	0.47771	0.64581	0.61147	0.62528	0.62918	0.58301	0.66551	0.62927
11	0.54227	0.80355	0.90507	0.7611	0.5431	0.97964	0.95546	0.92287
12	0.53081	0.61404	0.59148	0.62282	0.63268	0.54028	0.63484	0.60928
13	0.49166	0.6881	0.67783	0.73309	0.72918	0.68399	0.74112	0.69563
14	0.4341	0.73408	0.79442	0.61681	0.61754	0.56523	0.62628	0.81222
15	0.43962	0.74235	0.75071	0.5599	0.55903	0.55334	0.56019	0.76851
16	0.54097	0.70533	0.76098	0.50578	0.50663	0.50341	0.49953	0.77878
17	0.61353	0.74857	0.75176	0.69311	0.69499	0.65713	0.70167	0.76956
18	0.70675	0.80563	0.81074	0.71308	0.716	0.69871	0.71516	0.82854
19	0.77319	0.80543	0.7804	0.75709	0.75099	0.74329	0.77299	0.7982
20	0.65766	0.98215	0.7439	0.76258	0.76353	0.77711	0.75812	0.7617
21	0.51301	0.60641	0.65655	0.38019	0.38063	0.40511	0.37198	0.67435
22	0.53352	0.75823	0.6846	0.67904	0.67907	0.71256	0.6747	0.7024
23	0.81131	0.61593	0.55828	0.50645	0.50229	0.48325	0.52049	0.57608
24	0.88932	0.84996	0.80336	0.89585	0.88648	0.9109	0.9019	0.82116
25	0.67941	0.57603	0.63532	0.78507	0.78736	0.75701	0.75374	0.65312
26	0.64306	0.81644	0.74465	0.81554	0.81121	0.80176	0.82568	0.76245
27	0.58016	0.80201	0.8252	0.71072	0.70819	0.70111	0.70877	0.843
28	0.62443	0.85284	0.96416	0.66955	0.65804	0.72035	0.67132	0.98196
29	0.67969	0.77134	0.86807	0.76433	0.75808	0.76393	0.76844	0.88587
30	0.55985	0.6429	0.78267	0.80741	0.82875	0.76413	0.83735	0.80047
31	0.51534	0.79325	0.62423	0.68219	0.67693	0.72052	0.69635	0.64203
32	0.52667	0.64485	0.66167	0.67158	0.66839	0.69608	0.66853	0.67947
33	0.57296	0.60828	0.78682	0.62644	0.62607	0.66093	0.6102	0.80462
34	0.52887	0.62342	0.59594	0.63976	0.64009	0.63109	0.63808	0.61374
35	0.49267	0.6236	0.69979	0.79173	0.79647	0.79777	0.7869	0.71759
36	0.49257	0.68996	0.7254	0.5255	0.51927	0.52711	0.53432	0.71759
37	0.55411	0.47316	0.47767	0.71789	0.71715	0.72533	0.68534	0.7432
38	0.58787	0.78032	0.78988	0.54102	0.54099	0.54042	0.54831	0.49547
39	0.62482	0.83423	0.81529	0.67484	0.67444	0.64814	0.6865	0.80768
40	0.59169	0.70373	0.66602	0.63094	0.63326	0.65514	0.63193	0.83309
41	0.58107	0.7745	0.81201	0.53379	0.53221	0.53665	0.53589	0.68382
42	0.66835	0.82532	0.81079	0.74041	0.73552	0.74618	0.7426	0.82981
43	0.46107	0.77995	0.76137	0.62813	0.61925	0.65437	0.61585	0.82859

Continued on next page

Table 5.8 – continued from previous page

Image	F.S.	S.F.	TAED	Ulichney1	Ulichney2	Ulichney3	DBS	Proposed
44	0.48426	0.6288	0.63049	0.61949	0.61742	0.5877	0.62698	0.77917
45	0.38869	0.6632	0.73355	0.58912	0.59299	0.56888	0.59476	0.64829
46	0.39625	0.56452	0.61086	0.52074	0.52912	0.56727	0.51304	0.75135
47	0.071611	0.73444	0.77875	0.61978	0.61436	0.62721	0.60886	0.62866
48	0.071519	0.6639	0.7234	0.49433	0.4853	0.48585	0.50755	0.79655
49	0.062538	0.68806	0.74175	0.43499	0.43267	0.43094	0.43721	0.7412
50	0.092116	0.81391	0.90488	0.48913	0.484	0.46129	0.49191	0.75955

Table 5.7 and Table 5.8 show the objective index values calculated by CSAM index based on 15 halftone algorithms. By comparing the data of the two tables, it can be seen that the CSAM index of the corresponding image in Table 5.8 based on multi-level halftone is higher than that in Table 5.7 based on binary halftone. The reason is that multi-level halftone can reproduce more details of the original image, make the structure and appearance of the halftone image closer to the original image, and then have higher appearance reproduction quality. At the same time, by comparing the data in each table, it can be seen that for the data in Table 5.7 of 1-bit, the largest CSAM index belongs to TAED, and the DBS is slightly smaller than TAED. The halftone algorithm with the worst performance, that is, the dither halftone algorithm with the smallest CSAM value, including clustered dot 4×4, clustered dot 8×8 and dispersed dot. Due to the inherent characteristics of dithering algorithm, although it reduces the artifacts and other shortcomings in error diffusion halftone algorithm to a certain extent, However, due to its weak detail reproduction ability, it can not produce a high CSAM index value.

Results Comparison for Unnatural Images

For two different kinds of databases, the average CSAM index of the total images corresponding to each algorithm was calculated, and each algorithm was ranked according to the average score. Among the 1-bit and 2-bit results for the FMD database, the ones with the largest mean values are TAED and the proposed MTAED, respectively. The test results of the selected 50 images in unnatural scenes are found to be consistent with the results of the FMD database, thus proving the effectiveness of the proposed algorithm CSAM, and at the same time proving the proposed texture-aware error diffusion compared with the classical algorithm, the algorithm has higher advantages.

5.2 Conclusion

In this chapter, appearance reproduction related to texture perception is proved. That is, CSAM based on the proposed gloss perception can effectively evaluate the results of texture perception of halftone, which proves that there is a certain positive relationship between gloss perception and texture perception in halftone. In Chapter 4, the gloss evaluation index based on FMD database is applied to the image database obtained under unnatural gloss conditions. In the evaluation process, the algorithm of texture sensing halftone is introduced to verify whether the proposed MTAED has advantages compared with the classical halftone algorithm. Secondly, it is also proved that the CASM index value of this algorithm is greater than other classical halftone algorithms and binary halftone algorithm TAED. It is proved that MTAED algorithm has stronger appearance reproduction ability than TAED and classical halftone algorithm. The effectiveness of the proposed algorithm is proved.

Chapter 6

General Conclusions

Starting from the two objectives of designing and developing halftone technology related to texture perception and its quantitative evaluation, this research determines the research for the purpose of accurate appearance reproduction by studying the traditional halftone technology and combined with the development direction of halftone technology in recent years. The purpose is to obtain the halftone technology with higher reproduction quality and more in line with human visual perception. At the same time, to some extent, the new texture perception halftone technology is evaluated, the index based on image structure and appearance distortion evaluation is designed, and subjective and objective experiments are carried out. The results show that the proposed texture perception related halftone technology cannot only improve the appearance reproduction of printed images, but also improve the reproduction ability such as the luster of objects in images. The proposed gloss evaluation index can also objectively and correctly evaluate the halftone technology.

The main contribution of this research is that the combination of classical error diffusion theory and modern texture editing technology of image processing produces a halftone technology with higher performance, which can better meet the pursuit of image reproduction appearance in modern printing industry. It is an innovative attempt. In addition, because the classical image quality evaluation algorithm is not applicable or cannot be directly used in the evaluation process of halftone image, based on the perceptual characteristics of human visual system and combined with the classical image evaluation index, designing a new index to evaluate the appearance perception of halftone, and realize the evaluation of color halftone image. This research combines the needs of real industry and strictly analyzes the research needs. In this process, new concepts and theories are produced, which contribute to the actual printing and the objective evaluation of image quality in printing.

This dissertation starts with the introduction of the error diffusion halftone technology often used in the printing industry, introduces the technology often used in texture sensing halftone from the technical point of view, analyzes the shortcomings of this halftone technology, and puts forward a new goal to further improve and improve the texture sensing halftone technology. Furthermore, based on the proposed

multi-level halftone, the binary halftone characteristics are guaranteed not to be destroyed, so that the proposed error diffusion technology further continues and extends the characteristics of the classical halftone technology. As a result of this research, the existing texture perception error diffusion algorithm was extended, which not only adopts the method of directly expanding from binary halftone to multi-level error diffusion, but also solves the problems in this process. The proposed algorithm mated adopts the way of nonlinear transformation to realize the method of gradual error diffusion, which not only retains the excellent reproduction ability of the binary halftone algorithm, but also eliminates the problem that multi-level halftones are prone to artifacts. Secondly, an index for evaluating the gloss of halftone image considering human visual characteristics is also proposed. This index can correctly measure the restoration degree of shiny objects in halftone image, and give the corresponding score in line with human subjective observer. Finally, in order to further verify whether the perception of gloss is related to texture perception, verification experiments based on different databases are carried out. The experimental results determine that the halftone technology of texture perception has greater advantages than other classical halftones in texture presentation.

Although this research has made some achievements in research, there are also deficiencies. The author would like to mention here some problems and solutions that may be designed for future research:

- In the proposed process of expanding from binary halftone to multi-level error diffusion, nonlinear transformation is used. In this research, multi-level halftone refers to the halftone containing only four gray levels. Therefore, the image of a channel only needs to undergo two transformations to realize the transition from binary to multi-level halftone. However, in the actual industrial printing environment, the printing of more than 4 inks has been practiced. Therefore, based on the proposed nonlinear transformation, it is necessary to realize more transformations and synthesize halftone images with higher gray level. Therefore, how to reasonably control the nonlinear transformation process of image will become the key of multi-level error diffusion algorithm with higher gray level.

- In the proposed glossiness index, the structural similarity information of the image and the standard deviation and skewness related to the appearance perception are used to measure the distortion between the halftone image and the original image. As we all know, the appearance of the image is a complex perception process, and glossiness is only an attribute of the image appearance. How to correctly perceive the appearance of the object under the influence of color, shooting environment, etc, It will need more in-depth research to complete. For example, perceptual transparency in images will be a more challenging research work because there is little information such as available structure. Therefore, the glossiness perception index based on structural information proposed in this research may give the wrong objective index value.

- Due to the limitation of actual hardware, the subjective observer test in this research does not fully consider the evaluation of printed matter in industry. For example, although the display can simulate the display of printed images to a certain extent and correctly perceive the changes of reproduced images caused by the changes of image texture, it fails to fully consider all influencing factors as much as possible. For example, in the actual printing, the gloss of paper will affect the customer's perception of the gloss of printed matter. In different environments, due to the different printing paper, the intensity of gloss perception will be different. Therefore, different observers may give different subjective evaluation scores, resulting in the irrationality and failure of the subjective test. Therefore, it is necessary to strengthen and improve the environment of subjective evaluation test, and fully consider the impact of the actual printing environment on the final printed matter as much as possible.

From the above point of view, it can be seen that halftone technology is becoming more and more demanding with the continuous improvement of digital image processing means. The reproduction of halftone image appearance will become a key to improve the printing image technology.

List of Figures

List of Tables

ACKNOWLEDGEMENTS

I would like to express my heartfelt thanks to all the people who have given me the opportunity to complete this dissertation.

Most of all, I would like to express my sincere thanks to my supervisor Professor Takahiko Horiuchi for his help, enlightening suggestions and encouragement in the whole process of my research and writing this dissertation. I am also very grateful to Assistant Professor Midori Tanaka. During the discussion, I got a lot of useful help. I can't find any language to express their selfless help to me, their comments on my course work, and even their personal problems during all research periods.

I would also like to thank Mr. Kaku Shigeta from Think Laboratory Co., Ltd. for his useful discussion. Thanks to his help, this dissertation can obtain the printed matter for algorithm verification.

I am also very grateful to the late Associate Professor Keita Hirai for his help and for the research equipment and software he provided at the beginning of my PhD. I also thank him very much for his teaching of imaging system, which gave me a deeper understanding of my major. Although he had left us forever, but I will always remember his help in my heart.

I would like to deeply appreciate to Prof. Yoko Mizokami, Prof. Norimichi Tsumura and Prof. Yoshitsugu Manabe from the Chiba University, for their valuable comments, stimulating suggestions over the entire dissertation. Without their considerable review comments, I could not complete this dissertation finally.

Finally, I would like to thank my parents for their support, understanding and tolerance, so that I can have the ability and dedication to complete this job.

Chiba, August 2022

Bibliography

[1] J.-H. Lee, J.-W. Kweon, W.-S. Cho, J.-H. Kim, K.-T. Hwang, H.-J. Hwang, and K.-S. Han, "Formulation and characterization of black ceramic ink for a digital ink-jet printing," *Ceramics International*, vol. 44, no. 12, pp. 14 151–14 157, 2018.

[2] F. Loffredo, A. D. G. Del Mauro, G. Burrasca, V. La Ferrara, L. Quercia, E. Massera, G. Di Francia, and D. Della Sala, "Ink-jet printing technique in polymer/carbon black sensing device fabrication," *Sensors and Actuators B: Chemical*, vol. 143, no. 1, pp. 421–429, 2009.

[3] O. Nechyporchuk, J. Yu, V. A. Nierstrasz, and R. Bordes, "Cellulose nanofibril-based coatings of woven cotton fabrics for improved inkjet printing with a potential in e-textile manufacturing," *ACS Sustainable Chemistry & Engineering*, vol. 5, no. 6, pp. 4793–4801, 2017.

[4] K. Knowlton and L. Harmon, "Computer-produced grey scales," *Computer Graphics and Image Processing*, vol. 1, no. 1, pp. 1–20, 1972.

[5] C. Judice, "Digital video: A buffer-controlled dither processor for animated images," *IEEE Transactions on Communications*, vol. 25, no. 11, pp. 1433–1440, 1977.

[6] J. Allebach and Q. Lin, "Fm screen design using dbs algorithm," *Proceedings of 3rd IEEE International Conference on Image Processing*, vol. 1, pp. 549–552, 1996.

[7] R. Ulichney, M. Gaubatz, and S. Simske, "Encoding information in clustered-dot halftones," *NIP & Digital Fabrication Conference*, vol. 2010, no. 2, pp. 602–605, 2010.

[8] Z. Wang, A. C. Bovik, H. R. Sheikh, and E. P. Simoncelli, "Image quality assessment: from error visibility to structural similarity," *IEEE transactions on image processing*, vol. 13, no. 4, pp. 600–612, 2004.

[9] J.-H. Lee, T. Horiuchi, and R. Saito, "Confined-error-diffusion algorithm for flat-panel display," *Journal of the Society for Information Display*, vol. 15, no. 7, pp. 507–518, 2007.

[10] M. P. Eckert and A. P. Bradley, "Perceptual quality metrics applied to still image compression," *Signal processing*, vol. 70, no. 3, pp. 177–200, 1998.

[11] R. W. Fleming and H. H. Bülthoff, "Low-level image cues in the perception of translucent materials," *ACM Transactions on Applied Perception (TAP)*, vol. 2, no. 3, pp. 346–382, 2005.

[12] M. Tanaka and T. Horiuchi, "Investigating perceptual qualities of static surface appearance using real materials and displayed images," *Vision research*, vol. 115, pp. 246–258, 2015.

[13] D. Shaked, N. Arad, A. E. Fitzhugh, and I. E. Sobel, "Color diffusion: error diffusion for color halftones," *Color Imaging: Device-Independent Color, Color Hardcopy, and Graphic Arts IV*, vol. 3648, pp. 459–465, 1998.

[14] C. Tomasi and R. Manduchi, "Bilateral filtering for gray and color images," *Sixth international conference on computer vision (IEEE Cat. No. 98CH36271)*, pp. 839–846, 1998.

[15] K. He, J. Sun, and X. Tang, "Guided image filtering," *IEEE transactions on pattern analysis and machine intelligence*, vol. 35, no. 6, pp. 1397–1409, 2012.

[16] M. Aubry, S. Paris, S. W. Hasinoff, J. Kautz, and F. Durand, "Fast local laplacian filters: Theory and applications," *ACM Transactions on Graphics (TOG)*, vol. 33, no. 5, pp. 1–14, 2014.

[17] H. Kong, H. C. Akakin, and S. E. Sarma, "A generalized laplacian of gaussian filter for blob detection and its applications," *IEEE transactions on cybernetics*, vol. 43, no. 6, pp. 1719–1733, 2013.

[18] K. E. Ferguson and P. Turnbull, "Oh, say, can you see?: The semiotics of the military in hawaii," vol. 10, 1999.

[19] A. I. D.Shaked, N.Arad, "Hp labs technical reports," 1999.

[20] J. Canny, "A computational approach to edge detection," *IEEE Transactions on pattern analysis and machine intelligence*, no. 6, pp. 679–698, 1986.

[21] S. M. Smith and J. M. Brady, "Susan—a new approach to low level image processing," *International journal of computer vision*, vol. 23, no. 1, pp. 45–78, 1997.

[22] L. Sharan, R. Rosenholtz, and E. Adelson, "Material perception: What can you see in a brief glance?" *Journal of Vision*, vol. 9, no. 8, pp. 784–784, 2009.

[23] E. A. Khan, E. Reinhard, R. W. Fleming, and H. H. Bülthoff, "Image-based material editing," *ACM Transactions on Graphics (TOG)*, vol. 25, no. 3, pp. 654–663, 2006.

[24] L. Sharan, Y. Li, I. Motoyoshi, S. Nishida, and E. H. Adelson, "Image statistics for surface reflectance perception," *JOSA A*, vol. 25, no. 4, pp. 846–865, 2008.

[25] R. Mantiuk, K. Myszkowski, and H.-P. Seidel, "A perceptual framework for contrast processing of high dynamic range images," *ACM Transactions on Applied Perception (TAP)*, vol. 3, no. 3, pp. 286–308, 2006.

[26] R. Floyd, "An adaptive algorithm for spatial grey scale," *SID'75, Digest*, pp. 36–37, 1975.

[27] Floyd, "An adaptive algorithm for spatial grey scale," *Proc.Soc.Inf.Display*, no. 17, pp. 75–77, 1976.

[28] J.-N. Shiau and Z. Fan, "Set of easily implementable coefficients in error diffusion with reduced worm artifacts," *Color Imaging: Device-Independent Color, Color Hard Copy, and Graphic Arts*, vol. 2658, pp. 222–225, 1996.

[29] R. A. Ulichney, "Dithering with blue noise," *Proceedings of the IEEE*, vol. 76, no. 1, pp. 56–79, 1988.

[30] I. H. Witten and R. M. Neal, "Using peano curves for bilevel display of continuous-tone images," *IEEE Computer Graphics and applications*, vol. 2, no. 03, pp. 47–52, 1982.

[31] G. Sarailidis and I. Katsavounidis, "A multiscale error diffusion technique for digital multitoning," *IEEE transactions on image processing*, vol. 21, no. 5, pp. 2693–2705, 2012.

[32] H. Kotera, H. Motomura, and T. Fumoto, "Color dithering back to the roberts' modulation," *Color and Imaging Conference*, vol. 1995, no. 1, pp. 86–89, 1995.

[33] Y.-H. Fung and Y.-H. Chan, "Edge preserving multiscale error diffusion algorithm for green noise digital halftoning," *2010 IEEE International Conference on Image Processing*, pp. 557–560, 2010.

[34] X. Li, "Edge-directed error diffusion halftoning," *IEEE Signal Processing Letters*, vol. 13, no. 11, pp. 688–690, 2006.

[35] B.-W. Hwang, T.-H. Kang, and T.-S. Lee, "Distortion-free of general information with edge enhanced error diffusion halftoning," *International Conference on Computational Science and Its Applications*, pp. 281–290, 2004.

[36] N.-J. Kwak, S.-P. Ryu, and J.-H. Ahn, "Edge-enhanced error diffusion halftoning using human visual properties," *2006 International Conference on Hybrid Information Technology*, vol. 1, pp. 499–504, 2006.

[37] H. Li and D. Mould, "Contrast-aware halftoning," *Computer Graphics Forum*, vol. 29, no. 2, pp. 273–280, 2010.

[38] T. Kiyotomo, K. Hoshino, Y. Tsukano, H. Kibushi, and T. Horiuchi, "Edge-preserving error diffusion for multi-toning based on dual quantization," *Electronic Imaging*, vol. 2017, no. 18, pp. 123–129, 2017.

[39] W.-M. Pang, Y. Qu, T.-T. Wong, D. Cohen-Or, and P.-A. Heng, "Structure-aware halftoning," *ACM SIGGRAPH 2008 papers*, pp. 1–8, 2008.

[40] L. Liu, W. Chen, W. Zheng, and W. Geng, "Structure-aware error-diffusion approach using entropy-constrained threshold modulation," *The Visual Computer*, vol. 30, no. 10, pp. 1145–1156, 2014.

[41] H.-S. Lee, K.-K. Kong, and K.-S. Hong, "Laplacian based structure-aware error diffusion," *2010 IEEE International Conference on Image Processing*, pp. 525–528, 2010.

[42] X. Shi and X. Li, "An improved error diffusion algorithm based on visual difference," *2014 IEEE International Conference on Image Processing (ICIP)*, pp. 2619–2623, 2014.

[43] J.-M. Guo, J.-Y. Chang, Y.-F. Liu, G.-H. Lai, and J.-D. Lee, "Tone-replacement error diffusion for multitoning," *IEEE Transactions on Image Processing*, vol. 24, no. 11, pp. 4312–4321, 2015.

[44] T. N. Pappas, J. P. Allebach, and D. Neuhoff, "Model-based digital halftoning," *IEEE Signal processing magazine*, vol. 20, no. 4, pp. 14–27, 2003.

[45] J.-H. Lee and J. P. Allebach, "Inkjet printer model-based halftoning," *IEEE transactions on image processing*, vol. 14, no. 5, pp. 674–689, 2005.

[46] J. Z. Lai and C.-C. Chen, "Color image halftoning with the dot overlap printer model," *Proceedings 1999 International Conference on Image Processing (Cat. 99CH36348)*, vol. 4, pp. 333–337, 1999.

[47] R. Yampolskiy, P. Anderson, J. Arney, V. Misic, and T. Clarke, "Printer model integrating genetic algorithm for improvement of halftone patterns." Citeseer, 2004.

[48] H.-W. Chang, H. Yang, Y. Gan, and M.-H. Wang, "Sparse feature fidelity for perceptual image quality assessment," *IEEE Transactions on Image Processing*, vol. 22, no. 10, pp. 4007–4018, 2013.

[49] N. Damera-Venkata and B. L. Evans, "Adaptive threshold modulation for error diffusion halftoning," *IEEE Transactions on Image Processing*, vol. 10, no. 1, pp. 104–116, 2001.

[50] V. Monga and B. L. Evans, "Tone dependent color error diffusion," *2004 IEEE International Conference on Acoustics, Speech, and Signal Processing*, vol. 3, pp. iii–101, 2004.

[51] L. Akarun, Y. Yardunci, and A. E. Cetin, "Adaptive methods for dithering color images," *IEEE transactions on image processing*, vol. 6, no. 7, pp. 950–955, 1997.

[52] M. Xia, W. Hu, X. Liu, and T.-T. Wong, "Deep halftoning with reversible binary pattern," *Proceedings of the IEEE/CVF International Conference on Computer Vision*, pp. 14 000–14 009, 2021.

[53] F. B. Leloup, J. Audenaert, and P. Hanselaer, "Development of an image-based gloss measurement instrument," *Journal of Coatings Technology and Research*, vol. 16, no. 4, pp. 913–921, 2019.

[54] B. L. Anderson and J. Kim, "Image statistics do not explain the perception of gloss and lightness," *Journal of vision*, vol. 9, no. 11, pp. 10–10, 2009.

[55] D. Li, T. Kiyotomo, T. Horiuchi, M. Tanaka, and K. Shigeta, "Texture-aware error diffusion algorithm for multi-level digital halftoning," *Journal of Imaging Science and Technology*, vol. 64, no. 5, pp. 50 410–1, 2020.

[56] W. Thompson, R. Fleming, S. Creem-Regehr, and J. K. Stefanucci, *Visual perception from a computer graphics perspective*. CRC press, 2011.

[57] C. B. Wiebel, M. Toscani, and K. R. Gegenfurtner, "Statistical correlates of perceived gloss in natural images," *Vision research*, vol. 115, pp. 175–187, 2015.

[58] S. C. Pont and J. J. Koenderink, "Reflectance from locally glossy thoroughly pitted surfaces," *Computer Vision and Image Understanding*, vol. 98, no. 2, pp. 211–222, 2005.

[59] E. C. Larson and D. M. Chandler, "Most apparent distortion: full-reference image quality assessment and the role of strategy," *Journal of electronic imaging*, vol. 19, no. 1, p. 011006, 2010.

[60] S. Li, F. Zhang, L. Ma, and K. N. Ngan, "Image quality assessment by separately evaluating detail losses and additive impairments," *IEEE Transactions on Multimedia*, vol. 13, no. 5, pp. 935–949, 2011.

[61] K. Ding, K. Ma, S. Wang, and E. P. Simoncelli, "Image quality assessment: Unifying structure and texture similarity," *arXiv preprint arXiv:2004.07728*, 2020.

[62] R. Ulichney, *Digital halftoning*. MIT press, 1987.

[63] D. L. Lau and G. R. Arce, "Modern digital halftoning," vol. 1, 2018.

[64] J. Lee and T. Horiuchi, "Image quality assessment for color halftone images based on color structural similarity," *IEICE Transactions on Fundamentals of Electronics, Communications and Computer Sciences*, vol. 91, no. 6, pp. 1392–1399, 2008.

[65] J. Mannos and D. Sakrison, "The effects of a visual fidelity criterion of the encoding of images," *IEEE transactions on Information Theory*, vol. 20, no. 4, pp. 525–536, 1974.

[66] S. Winkler, "Visual quality assessment using a contrast gain control model," *1999 IEEE Third Workshop on Multimedia Signal Processing (Cat. No. 99TH8451)*, pp. 527–532, 1999.

[67] W. Osberger, N. Bergmann, and A. Maeder, "An automatic image quality assessment technique incorporating higher level perceptual factors," *Proceedings 1998 International Conference on Image Processing. ICIP98 (Cat. No. 98CB36269)*, pp. 414–418, 1998.

[68] R. Näsänen, "Visibility of halftone dot textures," *IEEE transactions on systems, man, and cybernetics*, no. 6, pp. 920–924, 1984.

[69] N. Damera-Venkata, T. D. Kite, W. S. Geisler, B. L. Evans, and A. C. Bovik, "Image quality assessment based on a degradation model," *IEEE transactions on image processing*, vol. 9, no. 4, pp. 636–650, 2000.

[70] T. J. Flohr, B. W. Kolpatzik, R. Balasubramanian, D. A. Carrara, C. A. Bouman, and J. P. Allebach, "Model-based color image quantization," *Human Vision, Visual Processing, and Digital Display IV*, vol. 1913, pp. 270–281, 1993.

[71] K. T. Mullen, "The contrast sensitivity of human colour vision to red-green and blue-yellow chromatic gratings." *The Journal of physiology*, vol. 359, no. 1, pp. 381–400, 1985.

[72] D. M. Chandler and S. S. Hemami, "Vsnr: A wavelet-based visual signal-to-noise ratio for natural images," *IEEE transactions on image processing*, vol. 16, no. 9, pp. 2284–2298, 2007.

[73] . R. R. E. H. Lavanya Sharan1, Ce Liu1, "Flickr material database," https://people.csail.mit.edu/lavanya/fmd.html.

[74] M. Analoui and J. P. Allebach, "Model-based halftoning using direct binary search," *Human Vision, Visual Processing, and Digital Display III*, vol. 1666, pp. 96–108, 1992.

[75] A. Serrano, B. Chen, C. Wang, M. Piovarči, H.-P. Seidel, P. Didyk, and K. Myszkowski, "The effect of shape and illumination on material perception: model and applications," *ACM Transactions on Graphics (TOG)*, vol. 40, no. 4, pp. 1–16, 2021.

[76] R. S. Hunter, "Methods of determining gloss," *Journal of Research of the National Bureau of Standards*, vol. 18, no. 1, pp. 19–41, 1937.

Appendix A

Published Papers and Conferences

Papers in Journal

[A1] D.Li, T.Kiyotomo, M.Tanaka, T.Horiuchi and K.Shigeta, "Texture-Aware Error Diffusion Algorithm for Multi-Level Digital Halftoning", Journal of Imaging Science and Technology, Vol.64, Issue 5, pp.050410-1-050410-9, 2020.
[A2] D.Li, M.Tanaka and T.Horiuchi, "Glossiness Index of Objects in Halftone Color Images Based on Structure and Appearance Distortions", Journal of Imaging, Vol.8, No.3, 59, 15 pages, 2022.

International Conferences

[A3] D.Li, T.Kiyotomo, M.Tanaka, T.Horiuchi and K.Shigeta, Twenty-eighth Color and Imaging Conference (CIC28 ONLINE), "Journal of Imaging Science and Technology"-Society for Imaging Science and Technology, 4-19, November, 2020.
[A4] D.Li, M.Tanaka and T.Horiuchi, "Verification of Gloss Representation in Printing using Texture-Aware Error Diffusion Algorithm", Computational Color Imaging Workshop, (received special honors), online, June 2022.

Patents

[A5] T.Horiuchi, M.Tanaka, K.Shigeta and D.Li, "Image processing apparatus, image processing method and program," Japan Patent (P2021-106335A), Publication date: July 26, 2021.
[A6] T.Horiuchi, M.Tanaka, K.Shigeta and D.Li, "Image processing apparatus, image processing method and program," Japan Patent (P2021-106364A), Publication date: July 26, 2021.

Appendix B

Experiment Datas

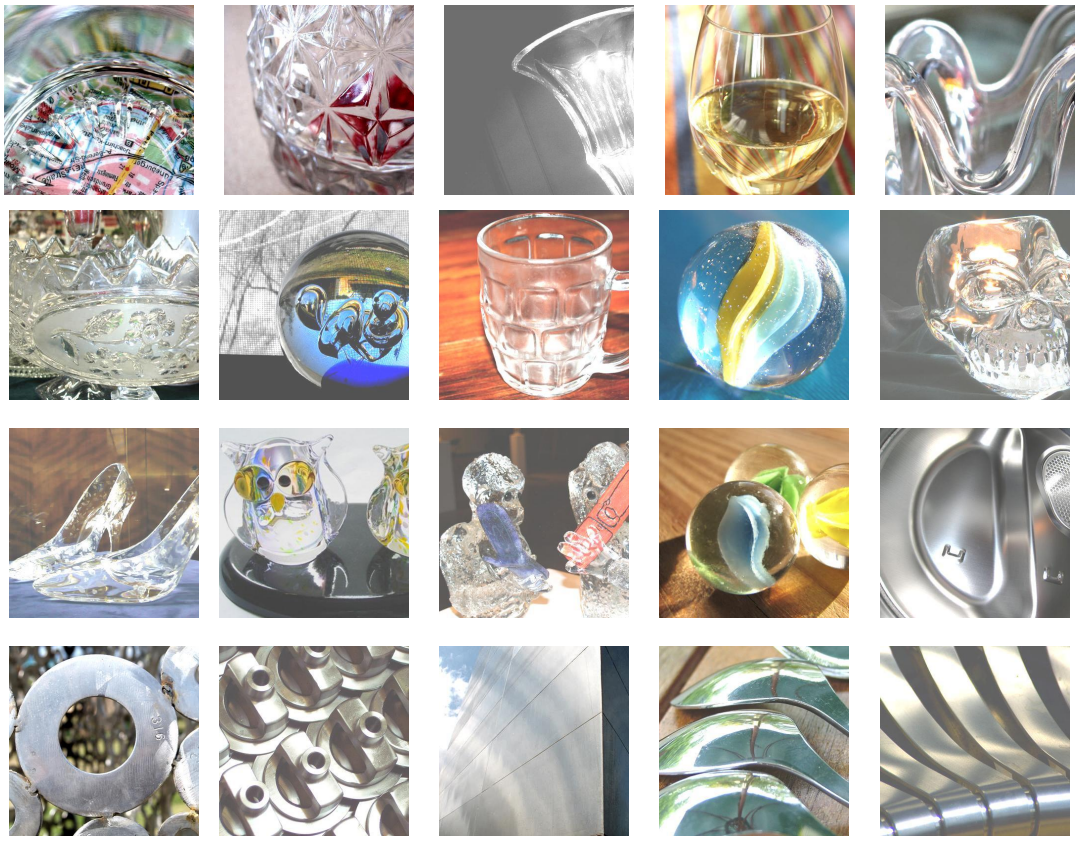


CAUTION

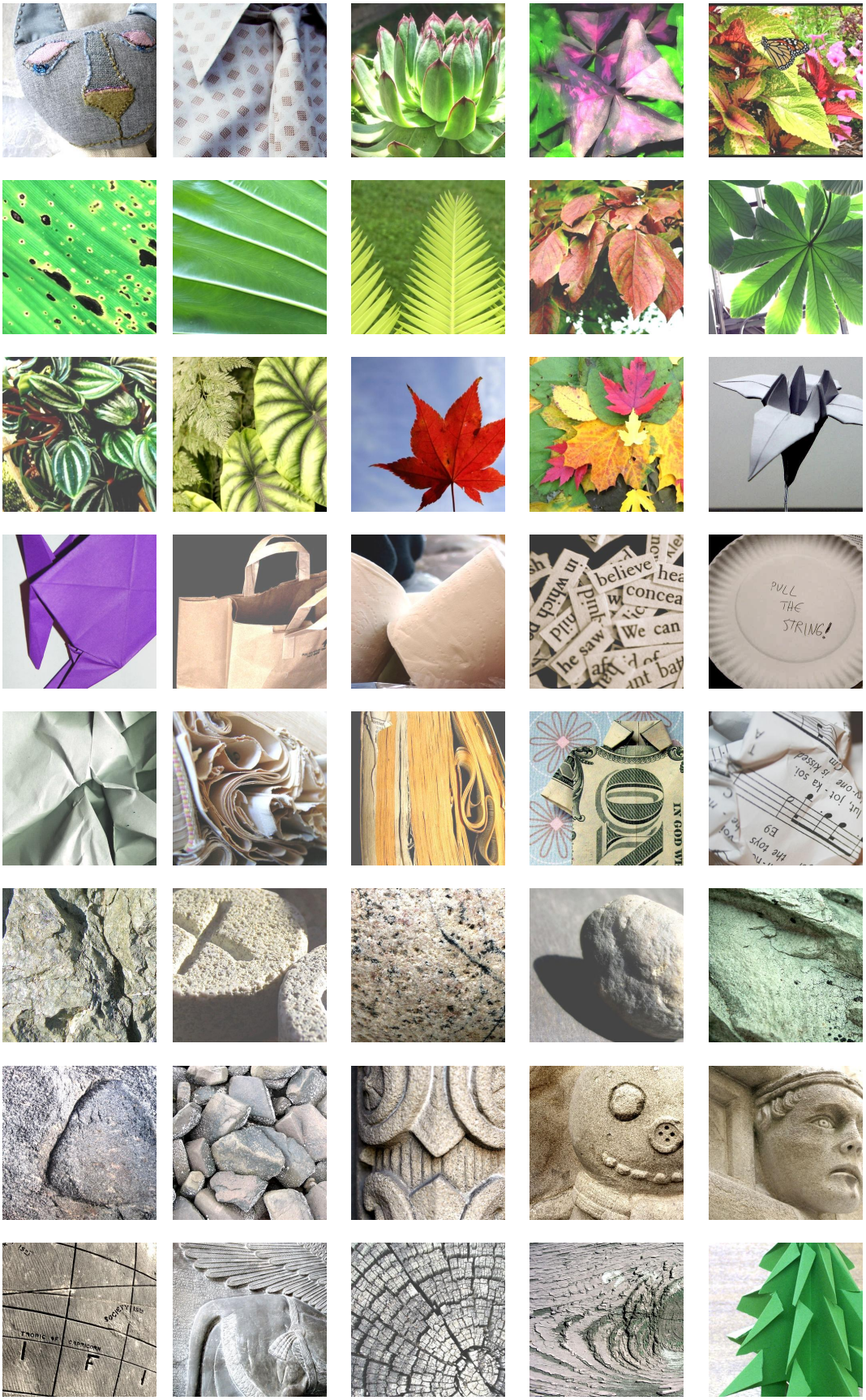
believe
We can
PULL
THE
STRING!

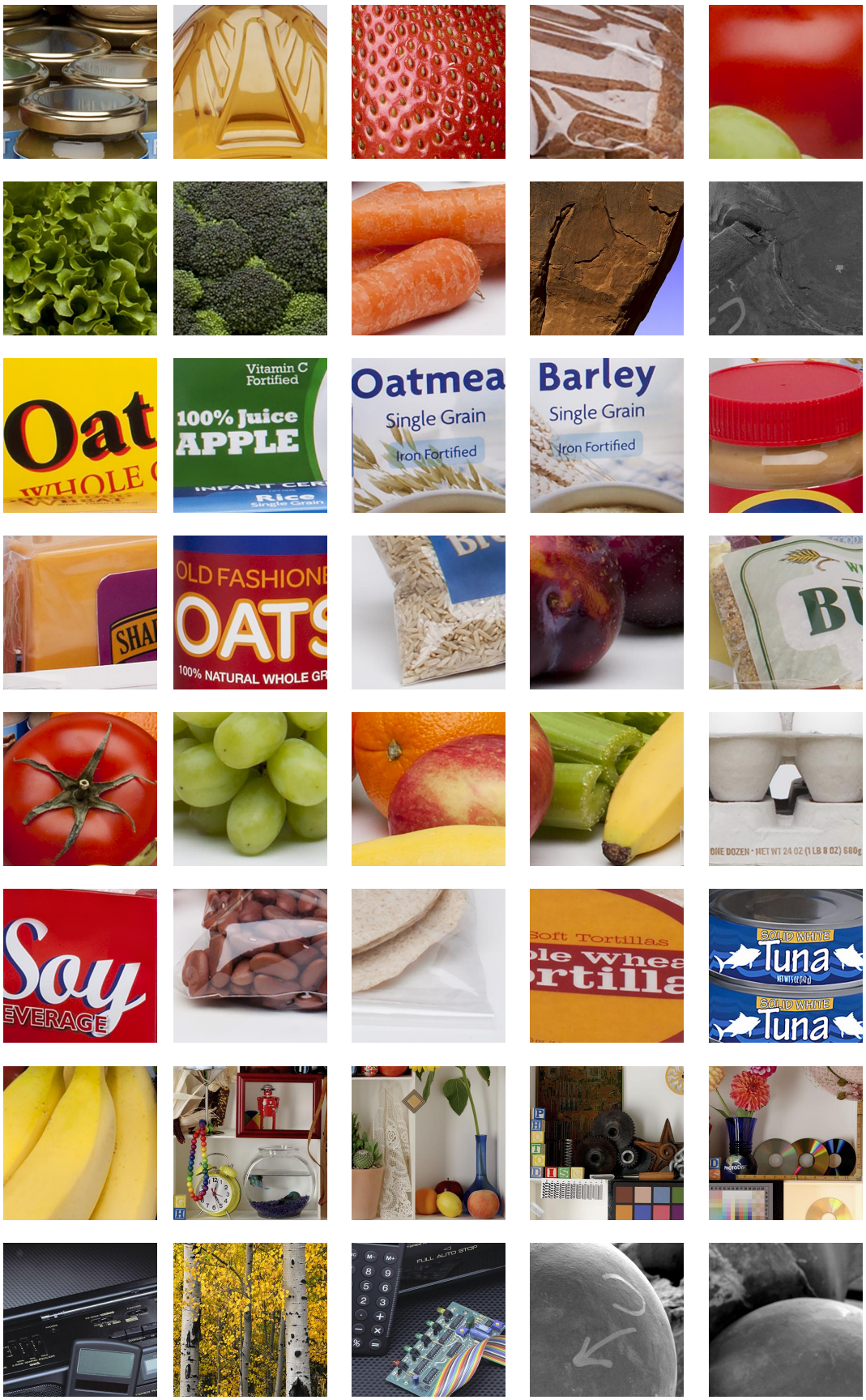
Oat
WHOLE
Vitamin C
Fortified
100% Juice
APPLE
Oatmea
Single Grain
Iron Fortified
Barley
Single Grain
Iron Fortified
OLD FASHIONE
OATS
100% NATURAL WHOLE GR
Soy
EVERAGE
Soft Tortillas
SOLID WHITE
Tuna
SOLID WHITE
Tuna

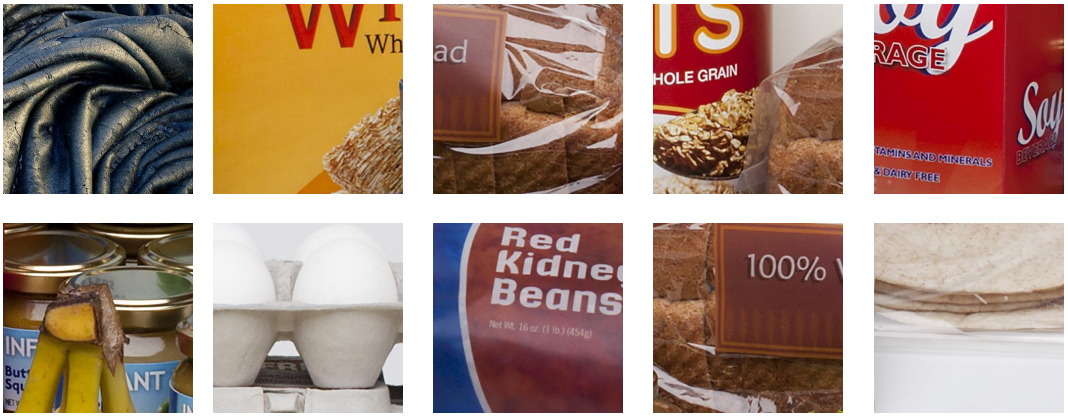
Wh
ad
HOLE GRAIN
RAGE
TAMINS AND MINERALS
& DAIRY FREE
Red
Kidne
Beans
100%